Ph.D. in Electronic and Computer Engineering
Dept. of Electrical and Electronic Engineering
University of Cagliari

Realisation and Characterisation of Organic Electronic Devices for E – textiles applications

Giorgio Mattana

Advisor: Prof.ssa Annalisa Bonfiglio
Curriculum: ING-INF/01 Electronics

XXIII Cycle
March 2011

Ph.D. in Electronic and Computer Engineering
Dept. of Electrical and Electronic Engineering
University of Cagliari

Realisation and Characterisation of Organic Electronic Devices for E – textiles applications

Giorgio Mattana

Advisor: Prof.ssa Annalisa Bonfiglio
Curriculum: ING-INF/01 Electronics

XXIII Cycle
March 2011

Dedicated to Valentina, Alessandra and Mattia.

Contents

List of Figures

Thesis abstract.

This Ph.D. Thesis is essentially concerned with the realisation and characterisation of organic electronic devices for applications in the textile field.

It is structured as follows:

- *Motivation*: an introduction chapter explaining briefly the field in which the present Ph.D. research may be situated and the reasons why this work may pave the way for future interesting applications, both in the industrial and research fields;
- *Chapter 1*: an introduction to the most important concepts of Organic Electronics (physical and chemical properties of the materials used and models commonly employed to describe the electrical behaviour of the devices);
- *Chapter 2*: an overview on the field of Wearable Electronics, in which some useful definitions are provided as well as a review on the present state-of-the-art of organic devices and for textile applications;
- *Chapter 3*: a detailed discussion on the materials, deposition techniques, devices assembly and characterisation techniques utilised in the course of my research activity;
- *Chapter 4*: a presentation concerning the results obtained;
- *Conclusion*: a summary of the main goals achieved and prospectives for future research.

Keywords: Organic Electronics, Wearable Electronics, electronics on cotton fibres, OFET, OECT.

Thesis motivation.

According to modern Sociology, clothing is one of man's basic needs [1]. Throughout history, the members of every human community have shown the necessity to wear something in order to cover their body, or at least parts of it. At the very early stages of human history, the function of clothing was essentially to protect the body from natural elements. This function is still preserved today, but with the progress of human civilisation and the development of broader and more complex interconnections between human beings, new functionalities have emerged.

Nowadays, sociologists attribute four different functions to clothing [2]:

1. Body protection from the environment (against the weather - cold, sun, wind, rain, snow - as well as against the attack of wild animals and parasites);

2. Maintenance of decency: in the majority of human societies it is not considered socially acceptable for men and women to show their naked body; clothes then allow people to interact one another without violating their ethical code;

3. Social differentiations: clothing is a means used in order to express the differences between the sexual genders, or the social and religious status of a member within a certain community;

4. Self expression and fashion: people use their clothes in order to communicate their status, feelings, identity or to express their connection with a specific group, culture or idea.

The importance of clothing in human life is also reflected by the considerable development of the Textile and Apparel industry. In agreement with the data provided by the World Trade Organisation (WTO) [3], the Textile and Apparel industry has an annual sales volume of about $ 400 billion and, notwithstanding the global economic crisis of these last years, the textile sector has grown of about the 25% from 2002 to 2010.

What are the present tendencies in the textile field? What can we expect from our clothes in the near future?

As reported by different sources [7][5][6], the reply to these questions seems to be univocal: 'smart textiles'. The expression 'smart textiles' usually refers to

"[...] textiles that are able to sense stimuli from the environment, to react to them and adapt to them by integration of functionalities in the textile structure. The stimulus as well as the response can have an electrical, thermal, chemical, magnetic or other origin. [...]" [7]

The concept of smart textiles is strictly connected to the concept of 'smart materials', that is chemical compounds able to change significantly and in a controlled way, by the application of external stimuli. From this point of view, smart textiles may be (oversimply) defined as textiles treated with smart materials [8]. Many of these smart materials are organic molecules, that is carbon - based compounds, and may be used to build electronic devices.

The overlap existing between smart textiles and smart materials is the context in which my PhD Thesis may be situated.

This work represents my personal contribution to the field of smart textiles. During my doctorate, I studied and tested several organic materials with the aim to realise cylindrical,

'yarn - like' electronic devices, starting from common metal substrates and going through more 'familiar' materials, such as cotton.

As I will show in the following chapters of this thesis, cotton is characterised by some important properties that make it the most used material for the production of clothes; any specialist working in the field of smart textiles has to face, sooner or later in their job, the possibility to integrate their systems into a cotton matrix or to build them directly on a cotton substrate.

At the moment, much work still has to be done in order to combine the functionalities of organic materials with the mechanical properties and the natural comfort offered by cotton fibres; with this thesis I tried to partially fill this scientific gap.

In the following pages, I will describe the way I realised and characterised the behaviour of my electronic devices on both substrates (metallic and cellulosic).

Though not an exhaustive treatise on this topic, I strongly believe that my work describes a very original approach to design the most basic devices from which to start to develop a brand new cotton - based smart textiles technology.

Bibliography

[1] J.J. Macionis, K. Plummer, *Sociology: A global introduction*, Pearson Education, **2008**. ISBN: 97802051583.

[2] P. Corrigan, *The dressed society: clothing, the body and some meanings of the world*, SAGE Publications, **2008**. ISBN: 0761952063.

[3] www.WTO.org

[4] X. Tao, *Smart fibres, fabrics and clothing*, Woodhead Publishing, **2001**. ISBN: 1855735466.

[5] A. Lymeris, D. De Rossi, *Wearable health systems for personalised health management: state of the art and future challenges*, IOS Press, **2004**. ISBN: 1586034499.

[6] G. Cho, *Smart Clothing: Technology and Applications, Taylor and Francis*, **2009**. ISBN: 1420088521.

[7] P. Kiekens, L. Van Langenhoven, C. Heertleer, *Int. J. of Clothing Sci. and Technol.*, **2009**, 16*(1/2)*, 63 - 72.

[8] M. C. Petty, *Molecular electronics: from principles to practice*, Wiley - Interscience, **2007**. ISBN: 9780470013076.

1

This chapter is intended to provide a general introduction to the field of Organic Electronics.

After a short historical outline describing the development of this relatively new scientific sector, some chemical and physical concepts will be introduced in order to understand the basic electrical properties of the materials and structures which are the object of this research.

In particular, a short overview on conjugated and aromatic polymers (at present, the most important materials used in Organic Electronics) will be provided, with specific reference to those aspects connected to conduction mechanisms.

At the end of the chapter, two important organic electronic devices, namely field effect and electrochemical transistors, will be presented and a qualitative description of their working principles and a short description of the mathematical models commonly used in order to describe their electrical output characteristics will be also given.

1.1 Historical outline of organic electronics.

It is usually recognised [1] that the history of organic electronics began in 1977, when Heeger, MacDiarmid and Shirakawa of University of Pennsylvania published a renowned paper about the doping of polyacetylene [2].

However, a careful look at scientific literature shows that the interest of scientists towards what we now call "conductive polymers" had begun at least one century earlier. Indeed, in 1862 Dr. H. Letheby of the College of London Hospital was able to produce green and blue pigments (polyanilines) starting from aniline salts treated with sulphuric acid and electrically oxidised. Surprisingly, while the reactants were markedly electrically insulating, the obtained pigments were characterised by a partly metallic behaviour, being able to conduct electricity [3]. The results obtained by Letheby were revolutionary: before these experiments were carried out, all polymers had been considered intrinsically insulating.

Even so, these important achievements were not followed by further analyses and in-depth examinations, probably because of the rudimentary analytical techniques of that period [1].

It was only in the Sixties of the last century that the physical and chemical details of Letheby's experiments were finally understood and explained by Yu and co-workers [4]. In this paper, the Authors described the linear, polymeric structure of the chemical products; moreover, they also provided a possible mechanism to explain the conductivity of the polymer. The paper of Yu *et al.* is also very important because, starting from this publication, it became routine for chemists, physicists and engineers to characterise polymers and other organic materials from an electrical point of view, performing resistance and conductivity measurements [1].

The study of conductive polymers continued throughout the Sixties and the Seventies, until in 1974 McGinness and co-workers of University of Texas realised a dynamic switch based on chemically synthesised melanin (a biological, pigmented polymer) doped with iodine [5]. This switch prototype (Fig. 1.1) is now displayed at the "Smithsonian Chips" collection of the American Museum of History and is usually considered the first example of organic electronic device [6][7].

It was eventually in 1977 that the so called "Pennsylvania group", composed by H. Shirakawa, A. G. MacDiarmid, A. J. Heeger and their co-workers, published their well-known paper describing the electrical properties of polyacetilene, the prototype of all conjugated polymers. This paper illustrated a process to increase in a controlled fashion the conductivity of this conjugated polymer by means of chemical doping [2]. It is worth noting that the three Authors were awarded the Nobel Prize in 2000 for their important, pioneering work.

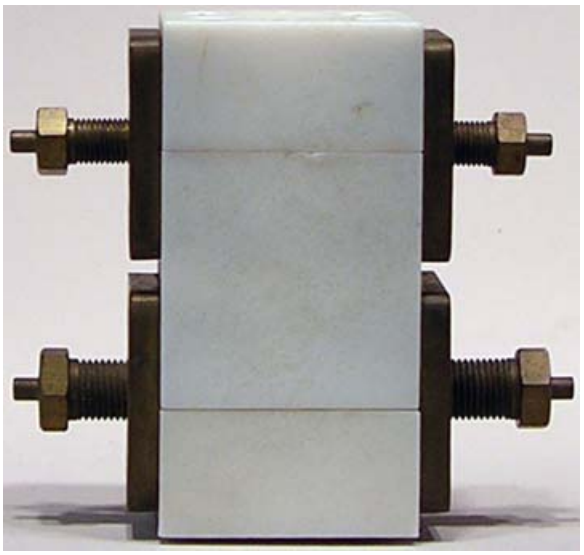

Figure 1.1: Melanin switch realised by McGinness *et al.*

A couple of years later, MacDiarmid and Heeger also presented a mathematical model obtained by applying, for the first time, the concepts of quantum mechanics to an organic polymer [8]; this model showed that, under proper conditions, the semiconductive/conductive behaviour of organic polymers could be explained in terms of band-like diagrams representing thus an extremely important connection bridge between the theory of inorganic semiconductors and that of organic materials.

During the Eighties and the early Nineties, new materials were synthesised and analysed; among them, it is worth mentioning the synthesis of a water-soluble compound belonging to the family of polythiophenes [9], namely PEDOT:PSS, nowadays one of the most important and utilised organic semiconductors.

In the same period, the very first examples of organic semiconductor-based electronic devices were built and studied, such as Field Effect Transistors [10], Electrochemical Transistors [11], Light Emitting Diodes [12] and photovoltaic cells [13]. It is in these years that the expression *organic electronics* started to be used in scientific publications to indicate those devices whose active materials are organic compounds, especially in contrast to 'traditional', inorganic semiconductor-based electronics.

These last ten years were characterised by the synthesis of new materials as well as new processing and deposition techniques. Perhaps, one of the most important features of organic materials is that they are usually solution processable which means that they can be easily processed at ambient temperature and deposited (or even printed) on large areas forming lightweight, thin films which often exhibit interesting mechanical properties such as elasticity and flexibility [11].

According to a recent market analysis [15], organic electronics is destined to become one of the most important sectors in the field of electronics, with a manufacturing capacity expected almost to double growing from $23 million in 2011 to $43 million in 2014. The synthesis of new materials and the development of applications (especially in the field of sensoristics) will probably be the 'hottest' research topics of the very next years.

1.2 The carbon atom.

The adjective *organic* used in the expression *organic electronics* refers to the fact that, in this branch of electronics, the active materials used for the fabrication of devices are organic compounds.

Although the distinction between 'organic' and 'inorganic' compounds is not always straightforward, an organic molecule is usually defined as a chemical compound containing carbon [16]. For historical reasons, this definition does not include a few types of carbon-containing compounds (such as carbonates, simple oxides of carbon and cyanides, as well as the allotropes of carbon such as diamond and graphite) which are therefore considered inorganic.

Consequently, in order to explain and understand the electrical properties of organic compounds it is necessary to describe the electronic configuration of the carbon atom and the way it forms chemical bonds with other atoms (of the same type or belonging to different chemical species).

Electronic configuration of carbon.

Carbon is an element belonging to the Group 14 of the periodic table. The members of this group are characterised by the fact that they have four electrons in the outer energy level.

There are three naturally occurring isotopes of carbon: carbon-12, carbon-13 and carbon-14 (the number following the element name indicates the total number of neutrons and protons contained into the atom nucleus). Carbon-12 (whose nucleus is formed by six neutrons and six protons) is the most stable of all three isotopes and is also the most abundant, accounting for the 98.89 % of carbon [17]. In this thesis, whenever the name 'carbon' is used, the isotope carbon-12 will always be implicitly referred to.

In order to understand the electronic properties of organic compounds it is essential to describe the way carbon electrons are distributed in space and the way they are bonded to the nuclei. In other words, it is necessary to introduce the concepts of *atomic orbital* and *orbital hybridisation*.

According to quantum mechanics [18], the wave-like behaviour of an electron may be described by a complex wave function depending on both position and time $\Psi(r,t)$; the square modulus $|\Psi|^2$ is equal to a probability density: the integral of the square modulus over a certain volume V gives the probability of finding, at a certain instant t, the electron in that volume.

Let us consider now the following equation:

$$\int_{\Omega} |\Psi(r,t)|^2 \, \mathrm{d}x\mathrm{d}y\mathrm{d}z \geq 0.9 \tag{1.1}$$

Equation 1.1 defines a volume Ω in which the probability to find an electron (described by $\Psi(r,t)$) is at least the 90%; such a region in space is called *atomic orbital* and its shape depends on how Ψ is mathematically defined.

Each orbital is defined by a different set of quantum numbers and contains a maximum of two electrons. Fig. 1.2 illustrates the shape of the first five orbitals:

The first two orbitals on top of Fig. 1.2 are respectively the orbitals 1s and 2s; they are shaped as spheres centred in correspondence with the atom nucleus. The three orbitals on the bottom are the 2p orbitals; each one of them is shaped as a couple of ellipsoids with a point of tangency in correspondence with the atom nucleus. The three p orbitals are reciprocally orthogonal: if we consider a cartesian coordinate system centred in the nucleus, these orbitals appear aligned along the three axes and are therefore called $2p_x$, $2p_y$ and $2p_z$ orbitals.

As mentioned previously, carbon belongs to the Group 14 of the periodic table. It is actually the simplest element of its group, having just six electrons: two of them are contained into

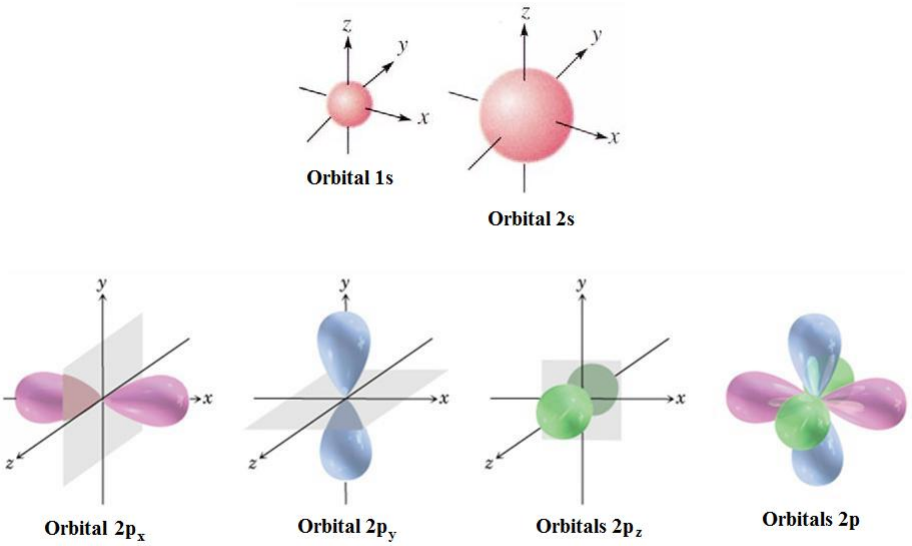

Figure 1.2: Shape of the first five orbitals.

the 1s orbital, while the other four are hosted by the second electron shell. When carbon is in its ground state (that is lowest energy state) two of the outer electrons are placed into the 2s orbital while the two remaining electrons are located in two of the 2p orbitals (let us assume, for instance, in $2p_x$ and $2p_y$). According to the standard rules set by IUPAC [19], the ground-state electron configuration of carbon may be expressed by the following notation: $1s^2 2s^2 2p_x^1 2p_y^1$ or, in a more compact fashion, $1s^2 2s^2 2p^2$.

Orbital hybridisation.

Chemical elements interact with one another through the formation of chemical bonds. From the point of view of organic chemistry, the most important chemical bond is the *covalent bond*.

A covalent bond occurs when two atoms share a pair of electrons; this bond forms when the bonded atoms have a lower total energy than that of widely separated atoms [20].

The formation of a covalent bond requires the partial overlap of two atomic orbitals; the shared electrons have a higher probability to be located in the area between the two atoms nuclei, where the overlap is maximum (see Fig. 1.3, depicting the formation of a covalent bond in the hydrogen molecule).

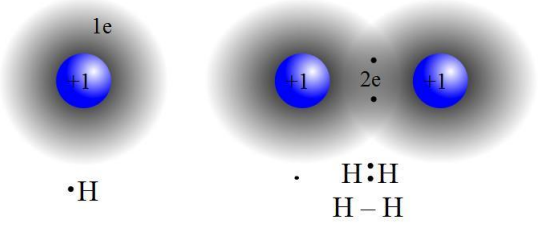

Figure 1.3: Covalent bond in a hydrogen molecule.

In certain cases, however, the structure of a molecule may not be explained if one considers the orbital shapes previously described. Let us examine, for instance, the simplest organic molecule, namely methane, CH_4 (Fig. 1.4):

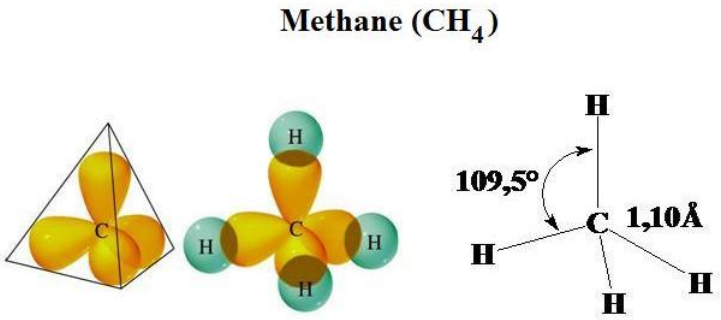

Figure 1.4: Methane molecule.

As can be seen from Fig. 1.4, methane is characterised by a tetrahedral geometry, in which the carbon atom occupies the tetrahedron centre while the four hydrogen atoms are placed in correspondence with the four tetrahedron corners.

This geometry is not compatible with the orbitals depicted in Fig. 1.3; in particular, the three 2p orbitals cannot be geometrically arranged to fit a tetrahedral structure.

This problem was solved in 1931 by Linus Pauling, in a famous paper [21] in which the theory of *orbital hybridisation* was described for the first time.

The concept of orbital hybridisation can be explained as follows [22]. Let us take n different orbitals, each one described by its own wavefunction $\Psi_i(r,t)$; when hybridisation occurs, these orbitals are linearly combined in order to form n new hybridised orbitals, each one corresponding to its own wavefunction $\Phi_j(r,t)$ as shown in the following formula:

$$\Phi_j(r,t) = \sum_{i=1}^{n} c_{ij}\Psi_i(r,t) \tag{1.2}$$

The coefficients c_{ij} are usually determined according to the following rules:

1. the wavefunctions describing the hybridised orbitals must be normalised (that is: the integral over all space of their square modulus must be equal to 1);

2. all hybridised orbitals must have the same energy (isoenergetic orbitals).

From a qualitative point of view, hybridisation may be thought of as a 'mix' of an atom orbitals which results in the formation of new, isoenergetic orbitals more suitable for the description of a specific molecule structure.

That being said, the particular structure of methane may be explained if one considers the hybridisation of carbon outer orbitals (namely, 2s and the three 2p orbitals) which results in the formation of four sp^3 orbitals, as shown in Fig. 1.5:

The four sp^3 orbitals of carbon partially overlap with the 1s orbitals of hydrogen atoms, giving rise to four covalent bonds which are usually indicated as σ-bonds.

Other organic molecules show geometrical characteristics which can be explained only considering other forms of hybridisation. Let us take, for instance, the ethylene molecule, $CH_2{=}CH_2$ (Fig. 1.6):

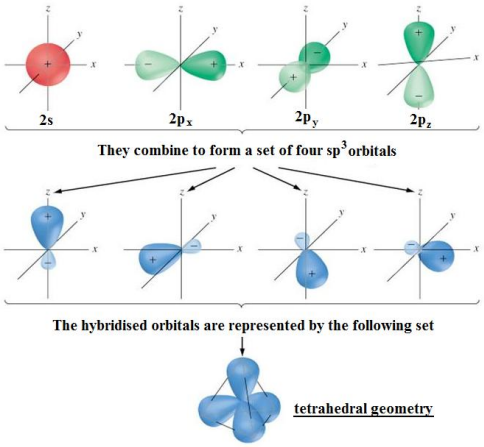

Figure 1.5: Sp^3 hybridisation.

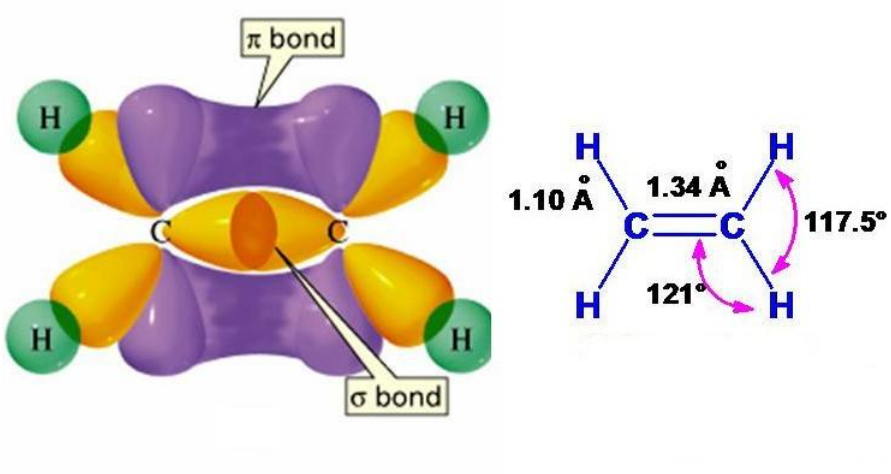

Figure 1.6: Ethylene molecule.

Ethylene is a planar molecule whose structure cannot be explained if one considers the original set of carbon orbitals or an sp^3 hybridisation.

Indeed, the carbon atoms of ethylene (as well as of all other compounds where a double C = C bond is present) are characterised by another form of orbital hybridisation, called sp^2 hybridisation, depicted in Fig. 1.7:

In this case, the 2s orbital and two 2p orbitals (let us assume 2p$_x$ and 2p$_y$) hybridise and form a set of three sp^2 orbitals which lie on the XY plane and are located in correspondence with the corners of an equilateral triangle.

The fourth, unhybridised 2p$_z$ orbital lies along a direction which is perpendicular to the plane containing the hybridised sp^2 orbitals.

When two sp^2-hybridised carbon atoms come into close contact in order to form a chemical bond, the orbitals overlap occurs at two different levels. On one hand, one can notice the formation of a covalent σ-bond resulting from the intersection between two sp^2 orbitals along the line joining the two carbon atoms' nuclei. The other two sp^2 orbitals overlap with the hydrogen atoms' 1s orbitals and form two other covalent σ-bonds. When the two carbon atoms come into contact, a partial overlap between the two unhybridised 2p$_z$ orbitals occurs. This

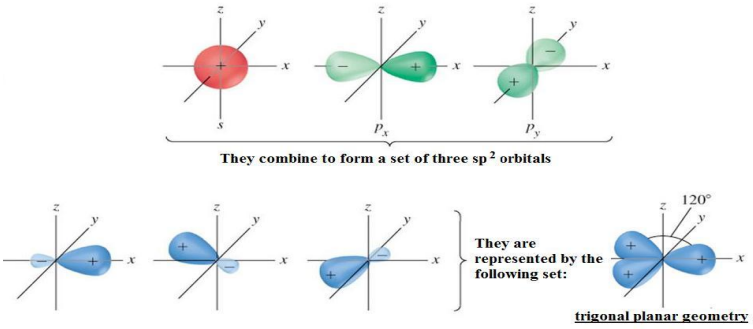

Figure 1.7: Sp^2 hybridisation.

overlap is responsible for the formation of a second covalent bond between the carbon atoms, called π bond. These two types of covalent bond are shown in the following picture (Fig. 1.8, but see also Fig. 1.7):

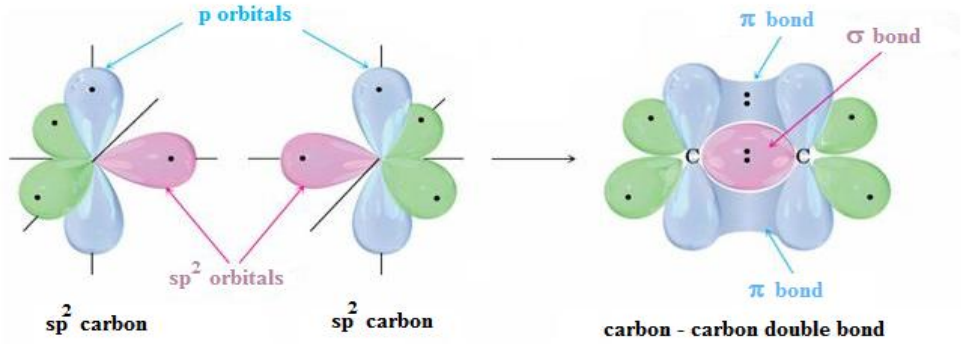

double bond.jpg

Figure 1.8: Formation of carbon-carbon double bond.

It should be noted that π bonds are less energetic than σ bonds (about 65 kcal/mol versus 80 kcal/mol) [23]. This is essentially due to the fact that, geometrically speaking, a σ bond is characterised by a much larger overlap volume, which causes a stronger constructive interference between the orbitals responsible for the formation of the bond.

This phenomenon has very important consequences for the electrical behaviour of the molecule: while σ electrons are strictly confined into the small volume between the two carbon atoms' nuclei, π electrons are able to move into a larger volume and their interaction with the nuclei is relatively weak.

It is also important to notice that two sp^3-hybridised carbon atoms (therefore connected by a single bond) are able to rotate around the bond axis, while in the case of two sp^2-hybridised carbon atoms (therefore connected by a double bond) this rotation is not allowed. [1]

[1] Carbon also shows a third type or orbital hybridisation called *sp hybridisation* which leads to the formation of carbon-carbon triple bonds (one σ bond together with two π bonds). From our point of view, this hybridisation is not particularly relevant and therefore will not be described or mentioned in the rest of the thesis.

Polymers.

Carbon is a chemical element showing an ability which is almost unique: the capability to form covalent bonds with other carbon atoms and create macromolecules represented by very long chains or more complex structures such as nets. This property is called *catenation*.

Since many organic compounds used in organic electronics are *polymers*, which are macromolecules obtained through this catenation process, in order to understand the behaviour of organic electronic devices it is necessary to define exactly what polymers are and examine shortly their properties.

According to the definition provided by IUPAC [19], a polymer may be defined as a molecule of high relative molecular mass, composed of repeating structural units called *monomers*, characterised by a low relative molecular mass. Monomers are interconnected typically (but not exclusively) by means of covalent bonds. Polymers containing a small number of monomers are usually called *oligomers* or *small molecules* [19]; the maximum number of monomers that can be used in order to distinguish an oligomer from a polymer is actually a matter of debate. The organic molecule used to produce the monomer is usually named *precursor*. The following picture (Fig. 1.9) illustrates these concepts using a very simple molecule as example: polyethylene (PE):

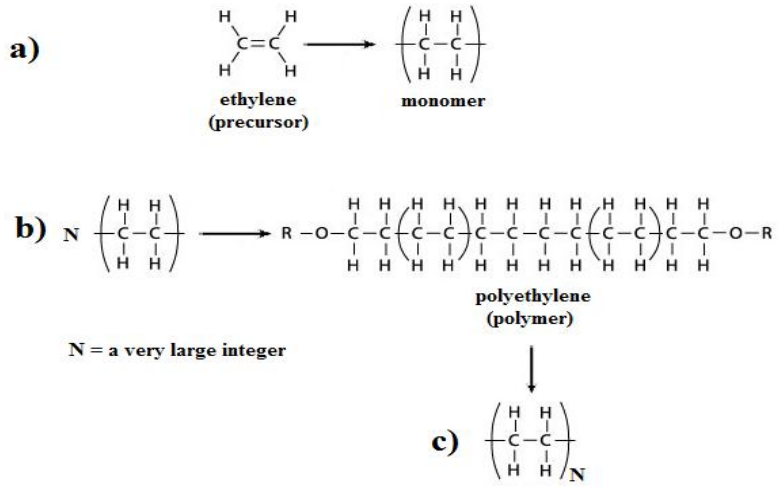

Figure 1.9: Synthesis of polyethylene.

Fig. 1.9 depicts the synthesis of polyethylene. Ethylene is used as a precursor and is chemically treated in order to obtain a monomer (Fig. 1.9a). When a very large number of monomers is synthesised, another reaction (*polymerisation*) occurs and covalent bonds between the monomers are formed (Fig.1.9b). The polymer is usually represented by drawing the monomer in round brackets and adding a subscript indicating that the molecule is actually composed of a large number of monomers (Fig. 1.9c).

It is not at all easy to provide general guidelines for the characterisation of a polymer, considering the enormous number of chemical compounds that have been synthesised. However, some classification parameters do exist [24]:

- the chemical characteristics of the composing monomer(s);
- the morphology of the single polymer molecule, that is the geometrical structure formed by the monomers connection (for instance, linear versus branched chain);

- the average molecular weight of a single polymer molecule;
- tacticity (the spatial orientation of the chain's side groups);
- the polymer morphology (the way polymer molecules are spatially arranged in a film or solid);

This last point is extremely important because many electrical transport properties are strictly connected to the morphological features of the polymeric layer. We will discuss about this topic in the next paragraph.

Polymer solid structures.

Polymer chains are normally very long so that intermolecular cohesion forces are usually extremely high. Moreover, when heated over a critical temperature, polymers are often degraded and decomposed into their monomers. As a consequence, polymers do not exist in the gaseous state [26].

Polymers liquid phase is also very particular: because of the high cohesion forces and the friction between molecules, polymeric liquids exhibit unusual properties (they are typically strongly non Newtonian fluids).

From the point of view of Organic Electronics, it is very important to discuss the properties of the so-called *polymeric solids*. Polymeric solids are usually defined as rigid bodies, resistant to changes of shape and volume, whose molecules are represented by polymer chains [27]. Different types of polymeric solids may be defined, according to their degree of crystallinity. Usually, crystallinity of polymeric solids is defined as the weight (or the volume) ratio between the weight (or volume) of the crystalline portion of the solid and its whole weight (or volume). Theoretically speaking, this ratio may vary from zero (completely amorphous solid) to one (perfectly crystalline solid), but in concrete terms polymer chains are so long and tangled that polymeric solids are never completely crystalline [28].

Three different types of polymeric solids may be distinguished, according to their crystallinity ratio:

- Highly crystalline polymeric solids (crystallinity > 0.9): in this case, polymer chains are usually arranged to form lamellar crystals with a thickness of 10 to 20 nm in which the parallel chains are perpendicular to the face of the crystals;
- Semi-crystalline polymeric solids ($0.3 <$ crystallinity < 0.9): these polymers are characterised by the presence of crystalline regions (called *crystallites*) in which the molecules are tidily packed together; crystallites are surrounded by amorphous regions, in which the molecules are oriented randomly and are intertwined. These solids are also called *polycrystalline solids*;
- Amorphous polymeric solids (crystallinity < 0.3): the molecules of these solids are randomly coiled and entangled.

These differences are shown in a schematic way in Fig. 1.10:

Several factors affect the degree of crystallinity of a polymeric solid. Some of them are related to the intrinsic characteristics of the molecule: molecules with large side groups or branches usually generate amorphous or low crystallinity solids because, due to their conformation, it is almost impossible for these molecules to pack in an ordered fashion. Other factors are connected to the process used in order to deposit the polymer on its substrate [29], which means that varying the deposition conditions, the same polymer may exhibit different crystallinity.

The deposition parameters which most influence the degree of crystallinity are the following:

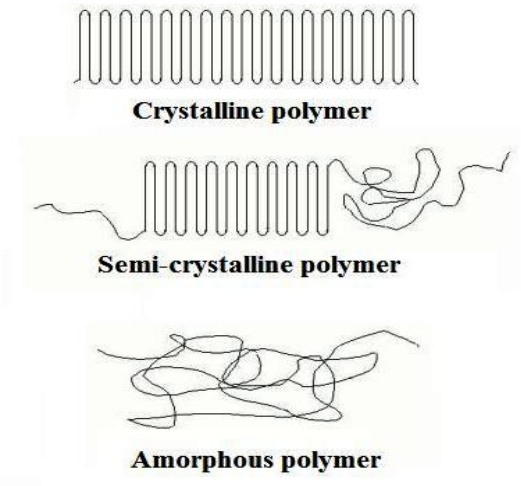

Figure 1.10: Different degrees of crystallinity in polymeric solids.

- polymer purity;
- deposition temperature;
- deposition pressure;
- deposition rate.

Though it is not possible to provide universal criteria applicable to all polymers, generally speaking it has been noticed that polymers with high levels of purity, deposited at low pressures and low rates tend to show higher degrees of crystallinity [29].

The crystallinity of a polymeric solid is actually a very important parameter because, as will be shown in the following paragraphs, the conduction behaviour of a polymer is strictly connected to its morphology.

1.3 Conductive phenomena in organic polymers

Electronics may be defined as that branch of Physics which studies electronic phenomena occurring within closed paths (*electric circuits*) designed to carry, manipulate or control electron flow for some purpose [51].

In order to understand how organic devices work it is therefore essential to have a clear picture of the conduction mechanisms in organic conductors and semiconductors.

Conductive polymers

Conductive polymers are usually defined as organic polymers able to conduct electricity, exhibiting a conductive or a semiconductive behaviour [31]. Several different types of conductive polymers have been synthesised, however they can be roughly grouped into three different categories:

- conjugated polymers;
- polymers containing aromatic cycles;

- conjugated polymers containing aromatic cycles.

In the following paragraphs, the most important theories describing conduction mechanisms in polymers will be briefly described.

Conjugated polymers

According to IUPAC Gold Book [19], a conjugated polymer is a molecule characterised by the alternation of single and multiple bonds (usually, double bonds). The simplest conjugated polymer is polyacetylene described in Fig. 1.11:

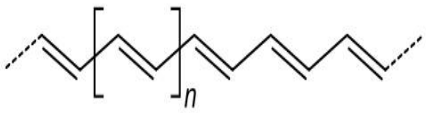

Figure 1.11: Polyacetylene, the simplest example of conjugated molecule.

As can be clearly seen from the picture above, the chain structure of molecules like polyacetylene may be thought of as a sequence of carbon atoms in which sp^3-hybridised carbon atoms are alternated with sp^2-hybridised carbon atoms. In paragraph 1.2.2, it has been shown that each sp^2-hybridised carbon atom exhibits a non-hybridised p-orbital lying perpendicularly to the polymer plane; the proximity of sp^2-hybridised carbon atoms is responsible for the formation of a continuous overlap of all unhybridised p-orbitals, as depicted in Fig. 1.12:

Thanks to this continuous orbital overlap, π electrons (which are loosely bound to the atoms' nuclei) are able to flow along the polymer chain when a voltage is applied to the molecule's extremities, thus enabling the polymer itself to conduct electricity.

A quantitative description of conductivity phenomena in conjugated polymers may be provided through the theory of Molecular Orbitals (MOs). According to this theory, the orbital of a complex molecule (MO) may be expressed starting from the wave functions describing the orbitals of the atoms (AOs) which compose the molecule [32]. From a mathematical point of view, this is usually done by expressing the MO as a linear combination of the AOs; this approach is known through the acronym LCAO (*Linear Combination of Atomic Orbitals*).

Let us apply the theory of Molecular Orbitals to a very simple molecule, namely molecular hydrogen. This molecule is composed of two hydrogen atoms; each one of them contains just a single electron into the 1s orbital.

Let ϕ_1 be the wave function describing the 1s orbital of the first hydrogen atom and ϕ_2 the wave function describing the 1s orbital of the second hydrogen atom; conforming to the LCAO approach, the MO Ψ of the hydrogen molecule may be defined as follows:

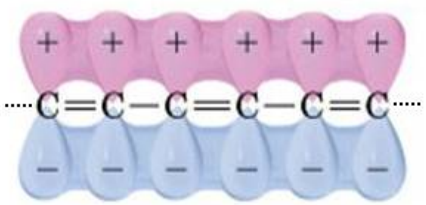

Figure 1.12: Overlap of p-orbitals in conjugated polymers.

$$\Psi = c_1\phi_1 + c_2\phi_2 \tag{1.3}$$

where *c1* and *c2* are the coefficients of the linear combination. Physically speaking, these two coefficients are a measure of the contribution that each single AO is making to the MO.

Being ϕ_1 and ϕ_2 wave functions, they satisfy Schrödinger's equation, as shown below:

$$H\phi_1 = E\phi_1 \tag{1.4}$$

$$H\phi_2 = E\phi_2 \tag{1.5}$$

where H represents the hamiltonian operator and E is the energy level associated to the AOs; it is worth noting that, since the two AOs describe the same atomic species, then the corresponding energy is the same. The MO itself, defined in equation 1.3, must satisfy Schrödinger's equation:

$$H\Psi = E^*\Psi \tag{1.6}$$

Equation 1.6 refers to a molecule, not a single hydrogen atom, therefore the energy associated to the wave function is different. We can now obtain two more equations, starting from 1.6, by multiplying for each AO wave function:

$$\begin{cases} \phi_1(H\Psi) = \phi_1(E^*\Psi) \\ \phi_2(H\Psi) = \phi_2(E^*\Psi) \end{cases} \tag{1.7}$$

If we insert in 1.7 the definition provided with 1.3 and use the linearity of hamiltonian operator, we get the following equations system:

$$\begin{cases} c_1\phi_1 H\phi_1 + c_2\phi_1 H\phi_2 = E^* c_1\phi_1^2 + E^* c_2\phi_1\phi_2 \\ c_1\phi_2 H\phi_1 + c_2\phi_2 H\phi_2 = E^* c_1\phi_1\phi_2 + E^* c_2\phi_2^2 \end{cases} \tag{1.8}$$

Now we can integrate both equations in the whole space; 1.8 then becomes:

$$\begin{cases} c_1\alpha + c_2\beta = E^* c_1 \\ c_1\beta + c_2\alpha = E^* c_2 \end{cases} \tag{1.9}$$

where the orthogonality condition (see paragraph 1.2.1) has been used and the following symbols have been introduced:

$$\int_V \phi_1 H(\Phi_1)\,\mathrm{d}x\mathrm{d}y\mathrm{d}z = \int_V \phi_2 H(\Phi_2)\,\mathrm{d}x\mathrm{d}y\mathrm{d}z = \alpha \tag{1.10}$$

$$\int_V \phi_1 H(\Phi_2)\,\mathrm{d}x\mathrm{d}y\mathrm{d}z = \int_V \phi_2 H(\Phi_1)\,\mathrm{d}x\mathrm{d}y\mathrm{d}z = \beta \tag{1.11}$$

The quantities defined above, α and β, are called respectively *Coulomb Integral* and *Exchange Integral*; α describes the electrostatic interaction between an electron and a proton belonging to the same atom, it roughly corresponds to the energy associated to the single hydrogen atom. On the other hand, β describes the electrostatic interaction between an electron and a proton belonging to two different atoms.

Equations in 1.9 may be rewritten the following way:

$$\begin{cases} c_1(\alpha - E^*) + c_2\beta = 0 \\ c_1\beta + c_2(\alpha - E^*) = 0 \end{cases} \tag{1.12}$$

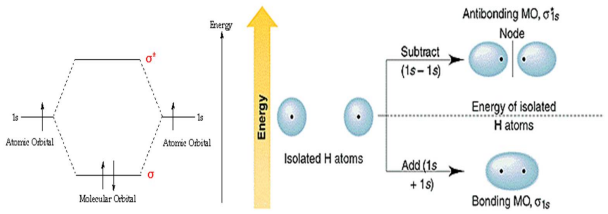

Figure 1.13: Bonding and antibonding MOs of the hydrogen molecule.

The equations above are usually known as *secular equations*. This homogeneous system admits a non-trivial solution if, and only if, its determinant is equal to zero, which requires that:

$$(\alpha - E^*)^2 - \beta^2 = 0 \tag{1.13}$$

This condition actually leads to *two* different solutions for system 1.12:

$$E_1^* = \alpha - \beta \qquad \text{and} \qquad E_2^* = \alpha + \beta \tag{1.14}$$

The linear combination of the two hydrogen atoms orbitals may therefore generate two different MOs:

- a *bonding* σ orbital with energy α - β (lower than that of each single atom);
- an *antibonding* σ orbital (usually written as σ^*) with energy $\alpha + \beta$ (higher than that of each single atom);

Since the purpose of each chemical bond is to allow the bonding atoms to decrease the total amount of energy, the electron pair shared by the hydrogen atoms will occupy the bonding MO. The antibonding MO, though a proper mathematical solution to the secular equation, is characterised by a level of energy *higher* than that of the two single atoms; therefore, it will not contain any electrons.

The formation of a MO may be graphically described by means of an energy diagram in which the three energy levels (energy of single atoms, energy of bonding MO and energy of antibonding MO are reported). Fig. 1.13 is an example of such a diagram referred to molecular hydrogen:

It is important to notice that, as previously stated, the bonding electrons will occupy only the bonding MO, while the antibonding MO will be empty. For this reason, the bonding MO is usually indicated as *Highest Occupied Molecular Orbital - HOMO*, while the antibonding MO is generally called *Lowest Unoccupied Molecular Orbital - LUMO*.

What happens when we consider larger molecules? For the sake of simplicity, let us analyse for the moment a hypothetical "hydrogen polymer" [32], made of a large sequence of equally-spaced hydrogen atoms (see Fig. 1.14):

Using the same LCAO approach, the k-th MO of this chain may be defined as follows:

$$\Psi_k = \sum_{r=0} c_{rk}\phi_r \tag{1.15}$$

where, as usual, ϕ_r wave functions describe the single AOs.

In this case, the structure periodicity may help us find a convenient expression for the linear combination coefficients. Using Bloch's theorem, indeed, the coefficients may be expressed as complex exponentials so that equation 1.15 may be rewritten as follows:

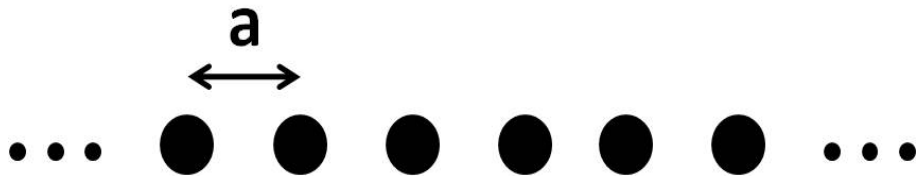

Figure 1.14: Linear sequence of hydrogen atoms.

$$\Psi_k = \sum_r \exp(jkra)\phi_r \tag{1.16}$$

where j is the imaginary unit and a is the chain period. Let us now apply cyclic boundary conditions (we can think of the atoms chain as ring-shaped) so that the coefficient c_{0k} must be equal to the coefficient c_{Nk}:

$$c_{0k} = c_{Nk} \implies \exp(0) = \exp(jkNa) \implies j2\pi q = jkNa \tag{1.17}$$

where q is an integer. From equation 1.17 we can draw that:

$$2\pi q = kNa \implies k = q\,2\pi/Na \tag{1.18}$$

This result is incredibly important, because it shows that k is *quantised* and that the spacing between two consecutive values of k decreases as N increases. The parameter k is usually interpreted as a wave vector; considering the periodicity of the chain, it is immediate to notice that adding (or subtracting) the quantity 2π/a to k the value of c_{rk} coefficients remains unchanged. Therefore, it is sufficient to restrict the k values to an interval whose width is 2π/a; the standard choice is to centre this interval in k = 0 and consider - π/a and + π/a as endpoints. In analogy to inorganic semiconductors, this interval is called *first Brillouin zone*.

Let us consider now the wave functions in correspondence with two specific values of k:

$$k = 0 \implies \Psi_0 = \sum_r \phi_r \tag{1.19}$$

In this case, the MO is simply the sum of all AOs; from a chemical point of view, this condition corresponds to the most bonding wave function: all AOs interfere constructively (this situation is analogous to the σ bond case of the hydrogen molecule) and the energy of the molecule is at its minimum.

The opposite case occurs when we take k = π/a:

$$k = \pi/a \implies \Psi_{\pi/a} = \sum_r (-1)^r \phi_r \tag{1.20}$$

In this last case, the sum becomes an alternating series, meaning that two consecutive AOs are *always* in phase opposition. This condition corresponds to the most antibonding wave function: all AOs interfere destructively (this situation is analogous to the σ^* bond case of the hydrogen molecule) and the molecule energy reaches its maximum.

Starting from k = 0 and moving towards k = π/a, the MO loses its bonding character and becomes more and more antibonding; at the same time, its energy also increases.

For very large values of N, the values of k may be considered continuous and it is therefore possible to plot a graph (called *dispersion curve*) of E as a function of k; it is possible, therefore,

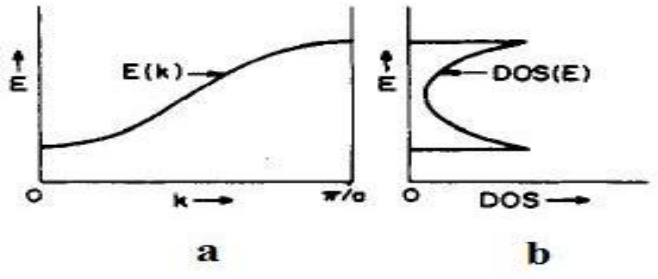

Figure 1.15: Dispersion curve (a), DOS (b) of a linear hydrogen chain.

to describe the conduction properties of organic materials by means of band-like structures, as usually done in the case of inorganic semiconductors.

Another important parameter we need in order to fully understand the conduction mechanisms of organic molecules is the *Density Of States - DOS*. The DOS may be simply defined as the number of energetic levels (*states*) contained into an infinitesimal interval of energy dE located between E and E + dE in the energy scale. Fig. 1.15 provides a graphical representation of both the dispersion curve and DOS in the case of the hydrogen chain described above.

The mathematical approach used above in order to obtain a band diagram of a hypothetical hydrogen polymer may be successfully employed also in the case of more complicated molecules, such as conjugated polymers [33] .

Let us go back, therefore, to the molecule we started with, namely polyacetylene. This case is actually much more complex than the one just described, for several different reasons:

- polyacetylene is composed of carbon atoms, therefore 2s, $2p_x$, $2p_y$ and $2p_z$ are also involved in the formation of the band structure;
- the interaction between two different chemical species (namely hydrogen and carbon) and all their orbitals must be taken into account;
- the carbon atoms composing the molecule chain are not equally spaced, because of the alternation of single and double bonds: two different periodicities must be considered.

It is impossible to report here the whole mathematical description of this molecule; in the following lines, just the main results will be highlighted. Polyacetylene, as other conjugated polymers, is characterised by three different chemical bonds: σ bond between hydrogen and carbon atoms, σ bonds between adjacent carbon atoms and alternate π bonds between carbon atoms. For each of these bonds, it is possible to build a separate MO, taking into account the proper AOs. In order to explain the conductive properties of polyacetylene, we are especially interested in the description of π bonds; in this case, we have to consider the overlap of unhybridised $2p_z$ AOs. Using the LCAO method previously illustrated and expressing the linear combination coefficients as Bloch functions, for large values of N it is possible to obtain the dispersion relationship depicted in Fig. 1.16.

The most important aspect shown in Fig. 1.16 is represented by the large energy gap ($\sim$ 2 eV) occurring at the edge of the first Brillouin zone; this band diagram, demonstrating the existence of an energy range in which no electron state may exist, constitutes the analytical proof of the semiconductive behaviour of polyacetylene. This result has been widely confirmed experimentally by conductivity measurements, which established that undoped polyacetylene, at room temperature, exhibits a conductivity of about 10^{-5} S cm^{-1} [34].

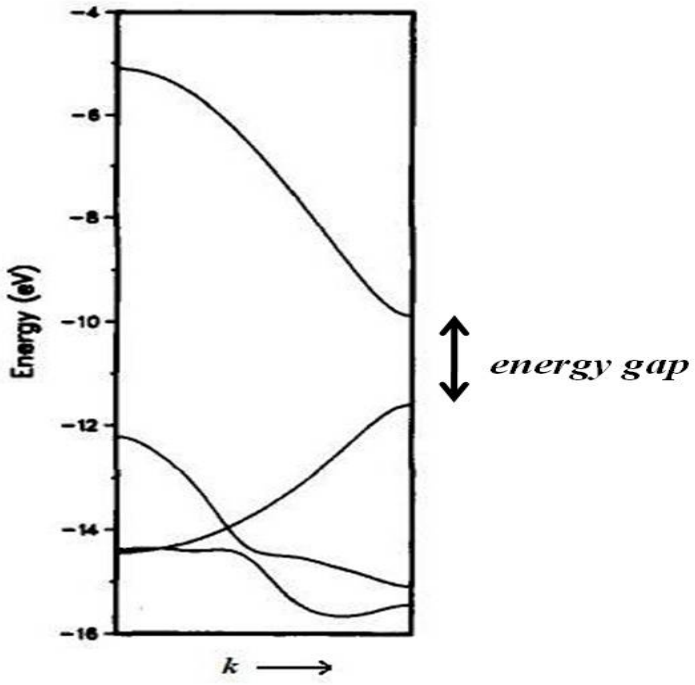

Figure 1.16: Dispersion curve of π molecular orbital in polyacetylene.

Curiously enough, when Prof. Hideki Shirakawa and his students developed a method to synthesise polyacetylene films (by accidentally using a catalyst concentration one thousand times higher than the required amount), they obtained a film with metallic conductivity. It was later found out that such films had been unintentionally oxidised by some of the chemicals composing the catalyst.

It was later discovered that polyacetylene, as well as other common conjugated polymers, can be doped in a controlled fashion in order to increase its conductivity up to eleven orders of magnitude [35] and transform it from a semiconductive to a conductive polymer.

Today, it is known that conjugated polymers can be doped by means of oxidation-reduction reactions. Dopants can be roughly grouped into two different categories [36]:

- strong electron-accepting chemical species (such as halogens); these dopants are able to remove electrons from the polymer chain thus creating positive charges (*p-doping*);
- strong electron-donating chemical species (such as alkali metals); these dopants donate electrons to the polymer chain increasing the number of negative charges (*n-doping*);

The effects on dopants on conductivity may be explained in terms of *solitons* [37]. Although no universally accepted definitions have been provided yet, solitons are usually defined [38] as travelling waves that may occur in non-linear systems and, therefore, do not obey the superposition principle. Their most interesting property is that they are able to travel along the medium at a constant speed, without losing their original shape. For this reason, they are usually called *non-dispersive* or *self-reinforcing* waves.

In the case of conjugated polymers, solitons are generally represented by "defects" (i.e. abrupt interruptions) in conjugation symmetry *solitons* [37] caused by a chemical reaction occurred between the polymer and a dopant; these defects may be electrically neuter or charged (positively

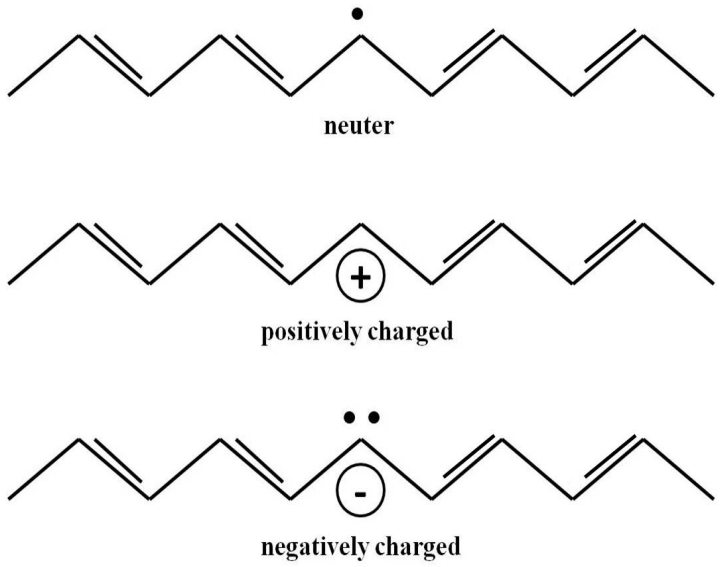

Figure 1.17: Neuter and charged solitons in polyacetylene.

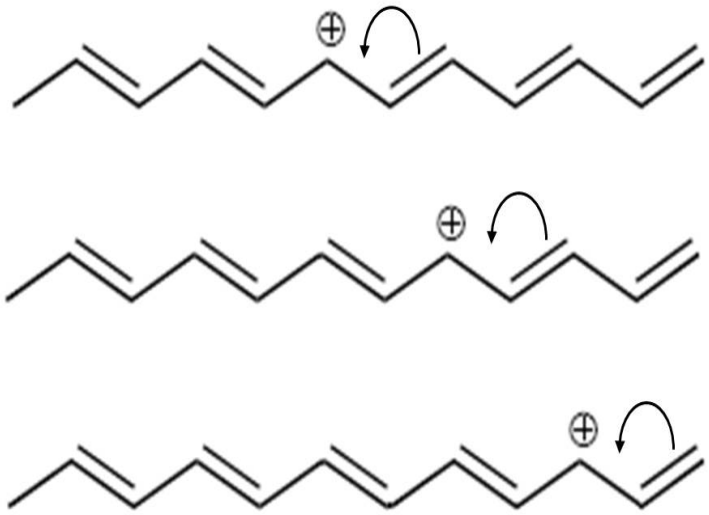

Figure 1.18: Movement of a positively charged soliton along a polyacetylene chain.

or negatively, depending on the type of polymer doping). These three typologies of solitons are schematically illustrated in Fig. 1.17.

Being travelling waves, solitons can propagate along the polymer chain. When the soliton is charged, the corresponding charge also flows through the molecule (Fig. 1.18).

Why are solitons, generated by doping, responsible for the conductivity increase? On one hand, charged solitons cause an increment of the number of mobile charges available for conduction; on the other hand, it has been shown [33] that solitons are associated to energy states that localise within the band gap thus reducing the energy required by electrons in order to cross the gap, which results in a conductivity increment.

Polymers containing aromatic cycles.

In order to understand the electrical properties of this polymers it is essential, first of all, to define the concept of *aromaticity*. In the history of Organic Chemistry, the adjective "aromatic" was initially used to indicate a class of organic compounds showing a characteristic aroma [39].

Today, this adjective is employed in order to describe the particular chemical and physical properties of molecules such as benzene, its derivatives and a small group of other compounds [40], characterised by great stability and marked chemical inertia (these molecules are not normally attacked by strong acids and bases and tend to react by substitution mechanisms rather than addition mechanism which are preferred by non-aromatic unsaturated hydrocarbons).

In more detail, an organic molecule is said to be aromatic if the following conditions are satisfied [41]:

- the molecule must be cyclic, i.e. its atoms must be located around a ring;
- the molecule must be planar or approximately planar;
- the atoms composing the ring must show an arrangement of alternating single and double bonds (*conjugation*);
- the total number N_Π of π electrons must satisfy *Hückel's Rule*

$$N_\Pi = 4n + 2 \quad \text{where n is a non-negative integer} \tag{1.21}$$

When all these conditions but Hückel's Rule are satisfied, the organic molecule is called *antiaromatic* and is very reactive and unstable.

Let us analyse the physical meaning of the conditions stated above. As discussed in the previous paragraphs, conjugation allows the overlap of unhybridised p-orbitals and, when the molecule is planar and ring shaped, this overlap generates a circular π orbital which extends above and below the plane of the molecule (see Fig. 1.19, representing a typical example of aromatic molecule, i.e. benzene).

The presence of such a delocalised π orbital enables the π electrons to flow around the ring, this phenomenon is usually known as *ring current*.

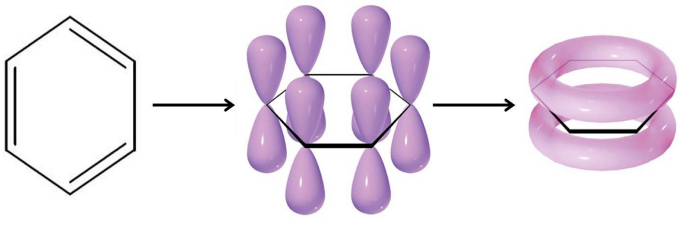

Figure 1.19: Delocalisation of π electrons in benzene.

The demonstration of Hückel's Rule is more complex because it derives from a particular application of the LCAO method [42] whose explanation requires an advanced mathematical formulation which goes beyond the purposes of this thesis; we will therefore assume its validity without further justification.

Aromatic rings may be used in the synthesis of aromatic macromolecules. In some cases, it is possible to fuse these rings in order to synthesise small molecules (or olygomers); a typical example is represented by *polyacenes*, a class of organic compounds made up of n linearly fused benzene rings. When $n = 5$, we obtain a small molecule called *pentacene* (see Fig. 1.20a), one

of the best known and important chemicals employed in Organic Electronics. Aromatic rings may be also connected by means of covalent bonds; in this case, long polymer chains may be synthesised such as, for instance, *polyphenylene* (see Fig. 1.20b).

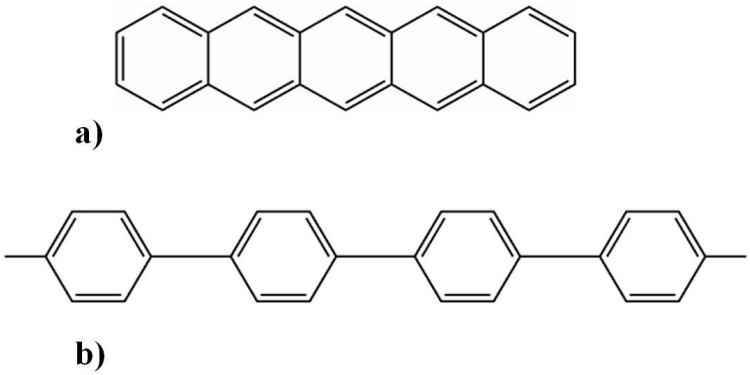

Figure 1.20: a) Pentacene b) Polyphenylene.

The conduction mechanisms in aromatic polymers may be explained using arguments similar to those described for conjugated polymers in paragraph 1.3.2 [43].

In both cases, indeed, conduction is related to delocalisation of π electrons and structural periodicity: undoped aromatic polymers therefore behave as semiconductors. An important difference [34], however, is related to the different behaviour of solitons generated by doping. In conjugated polymers, solitons are (relatively) able to move along the polymer chain while in aromatic polymers they are usually pushed towards the chain ends, where they are kept by lattice forces *solitons confinement*. This is due to the fact that in conjugated polymers, solitons occur between two identical, isoenergetic fragments of the polymer chain while in aromatic polymers solitons usually separate two very different parts of the polymer chain: a low-energy aromatic part and a high-energy quinoid non aromatic part (see Fig. 1.21).

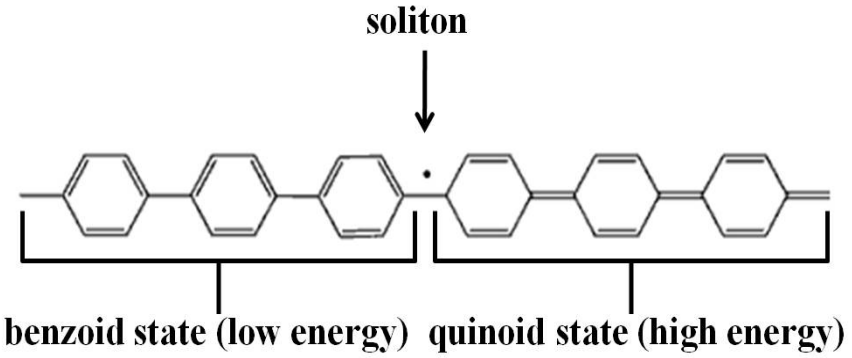

Figure 1.21: Soliton in polyphenylene.

Once a soliton has been created, the molecule needs to minimise the length of the quinoid portion, in order to reach energetic stability. This is usually done by coupling a pair of solitons, which are pushed towards each other so that the quinoid region is reduced to a single ring. This pair of coupled solitons is usually known as *polaron*; the most common type of polaron is represented by a neuter and a positive soliton (see Fig. 1.22). Other types of polarons (negative and positive solitons or negative and neuter solitons) are not stable and tend to recombine or repulse.

Figure 1.22: Polaron in polyphenylene.

In analogy with solitons in conjugated polymers, polarons are associated to energy states located within the forbidden band that decrease the width of the band gap thus increasing the polymer conductivity.

Conjugated polymers containing aromatic cycles (CPCACs).

These polymers may be thought of as a sort of hybrid of the two classes described above. In this case, the monomers from which polymers are synthesised contain an aromatic ring; monomers are then connected by means of alternating single and double bonds. A classical example is poly(phenylene vinylene), shown in Fig. 1.23.

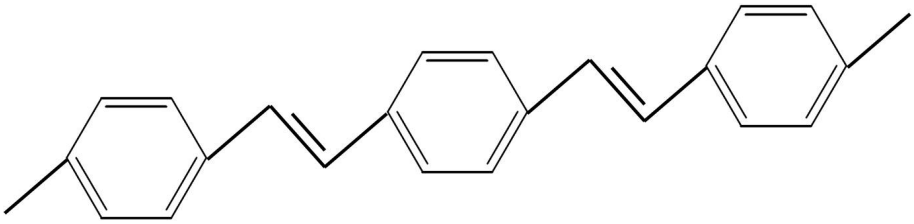

Figure 1.23: Polyphenylene vinylene.

CPCACs conductive behaviour is very similar to that of aromatic polymers. At room temperature they behave as semiconductors, but doping with strong electron donors/acceptors may increase conductivity up to 16 orders of magnitude[44]; this increment is attributed to the doping-induced formation of polarons [34].

1.4 Charge carrier transport.

In section 1.3 we described an analytical model able to explain the semiconductive behaviour of certain classes of organic materials. We have shown that if we hypothesise an ordered, periodic structure, then the electronic properties *of the single polymer chain* may be illustrated through a band diagram showing a band gap in which a conduction and valence bands may be clearly identified.

However, as stated in paragraph 1.2.4, when polymer molecules aggregate, the resulting polymeric solids exhibit different crystallinity degree, varying from almost perfect crystals to amorphous solids. As a consequence, charge carrier transport in such solids varies in a range delimited by two extreme cases: band transport and hopping [45].

Band transport is normally observed only in pure, single organic crystals [46]. In such materials, charge mobility depends on temperature according to the following power law:

$$\mu \propto T^{(-n)} \qquad \text{with n} \in [1 - 3] \tag{1.22}$$

In highly disordered polymeric solids, such as amorphous solids, transport usually proceeds via *hopping* and is thermally activated [47]. In amorphous solids, molecules are arranged in a random, disordered way. Therefore, energy states are not organised in continuous bands separated by an energy gap but instead localised energy states (i.e. existing only for discrete values of the wave number k)occur [45]. The density of these states is usually described using a couple of Gaussian distributions, the Gaussian functions being centred in correspondence with the energy level where the majority of levels appear [45] [47]. The functions peaks may be interpreted as analogous to conduction and valence bands in crystalline semiconductors (see Fig. 1.24).

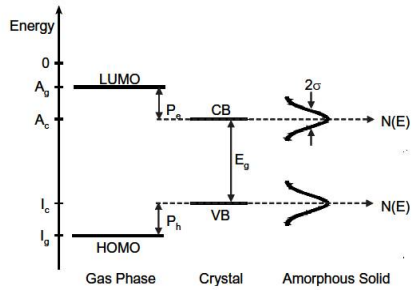

Figure 1.24: Energy diagrams in different types of organic semiconductors.

In amorphous solids, charge flow takes place when electrons start moving (*hopping*) from lower energy levels to higher energy levels. This flow is due to an increment in electrons energy which may be caused both by temperature or the application of an external electric field [48].

A simple model frequently used in order to express mathematically the mobility dependence on the factors cited above is the following:

$$\mu(F,T) \propto \exp\left(-\frac{\Delta E}{kT}\right) \exp\left(\frac{\beta\sqrt{F}}{kT}\right) \tag{1.23}$$

where ΔE is a parameter called *activation energy* (i.e. the minimum amount of energy to be provided in order to start conduction) and F represents the applied electric field.

The case of semicrystalline polymeric solids is perhaps the most complicated, from an analytical point of view. These solids usually assume a polycrystalline structure, in other words they may be thought of as many crystalline grains immersed into an amorphous matrix. While within the grains charges move thanks to band transport, the problem arises in correspondence with the grain boundaries. Here, mobile charges are temporarily immobilised (*trapping*) thus creating a potential barrier which electrostatically repels same sign charges [49]; as a consequence, charge mobility is greatly decreased. A simple expression utilised in order to express mobility in polycrystalline semiconductors is given by the following:

$$\mu \propto \mu_0 \exp\left(-\frac{E_B}{kT}\right) \tag{1.24}$$

In formula 1.24, μ_0 is the mobility in crystalline grains (it linearly increases with grain size) and E_B is the height of potential barrier.

1.5 Organic transistors.

The organic semiconductors described in the previous sections are commonly used for the realisation of organic electronic devices [50] [11], such as transistors, diodes and light emitting diodes,

and sensors.

In organic transistors, the active layer is a thin film made of organic semiconductors. In the following paragraphs,two types of organic semiconductors will be illustrated, namely the organic field effect transistor (OFET) and the organic electrochemical transistor (OECT).

Organic Field Effect Transistors (OFETs).

The first example of organic field effect transistor was provided in 1986 by Tsumura and co-workers [51] using a thin film of polythiophene as active layer.

In these twenty-five years, performances of OFETs have improved tremendously and mobilities up to 20 cm^2/Vs have been reported in transistors based on purified rubrene single crystals [52].

In OFETs, the organic semiconductor is deposited between two conductive electrodes, named *source* and *drain*, forming a region called *channel*. The channel conductivity is modulated by means of a third electrode, called *gate*, which is capacitively coupled with the channel [53].

The operating principle of OFETs may be schematically described as follows. When no voltage is applied to the gate electrode, the current flowing between source and drain is normally very low and the transistor is in its OFF state. Increasing the gate voltage, a mobile charge layer is accumulated at the interface between the semiconductor and the dielectric, so that the source-drain current becomes bigger: this is the transistor ON state.

According to the position of the semiconductive layer with respect to both the three electrodes, four different geometries are usually distinguished:

- bottom contact - bottom gate, when all the three electrodes lie under the semiconductor;
- bottom contact - top gate, when the source and drain contacts lie below the semiconductor, while the gate electrode is on the top of it;
- top contact - bottom gate, when the gate electrode lies below the semiconductor, while the source and drain contacts are on the top of it;
- top contact - top gate, when all the three electrodes are on the top of the semiconductor;

These geometries are schematically represented in Fig. 1.25.

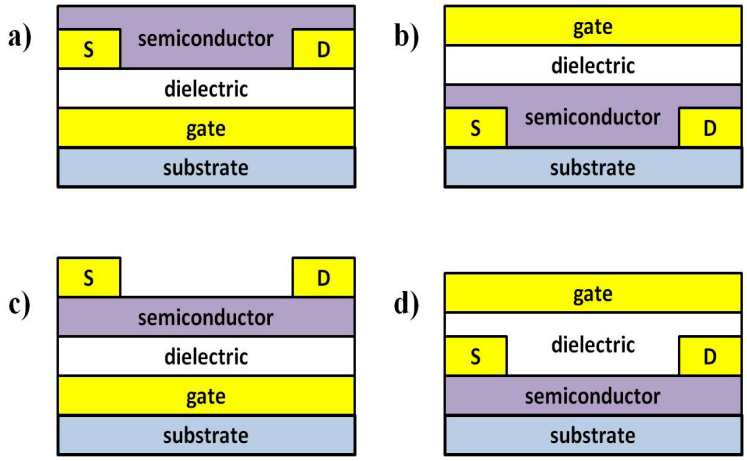

Figure 1.25: OFETs geometries: a) bottom contact - bottom gate; b) bottom contact - top gate; c) top contact - bottom gate; d) top contact - top gate.

The dielectric and metal used to complete the transistor realisation may be either inorganic (for instance, SiO_2 as dielectric and Au as metal) or organic; all polymeric OFETs have been reported in the literature since the early Nineties [54].

An interesting feature of organic materials is that, in principle, each organic semiconductor is potentially able to allow both holes and electrons conduction [55]. However, ambipolar behaviour is rarely observed in organic semiconductors: they usually exhibit only holes transport or, much more rarely, electrons transport [49].

It has been shown that an organic semiconductor category (p-type or n- type) depends on a complex set of parameters: both the work function of S-D electrodes, the dielectric properties of the insulating layer and the device geometry could influence the device operation model [57]; for this reason, it would be better to speak of *p-channel* transistor or *n-channel* referring to the device as a whole, rather than define the single semiconductor as p-type or n-type.

How can the electrical behaviour of OFETs be modelled?

Let L and W be, respectively, the channel length (that is, the distance between the source and drain electrodes) and the channel width. Let us also assume that the gate voltage V_G is high enough so that a mobile charge layer is formed at the semiconductor-dielectric interface.

Two different regimes may be identified [58] [59] .

Linear regime.

In this case, the mobile charge layer has a uniform thickness along the channel. The source drain current may be then expressed as follows:

$$I \doteq \frac{Charge}{Time} \quad \Longrightarrow I_{DS} = \frac{Q_{channel}(WL)}{t_{transit}} \tag{1.25}$$

where $Q_{channel}$ is the channel charge per unit area and $t_{transit}$ is the mean time a mobile charge requires in order to move from the source to drain electrode.

Let us now assume that mobile charges are characterised by a constant mobility μ, so that the source-drain electric field may be related to drift velocity as expressed by formula 1.26:

$$E_{DS} = \mu v_{drift} \tag{1.26}$$

Combining equations 1.25 and 1.26 we obtain the following result:

$$Time \doteq \frac{Space}{Velocity} \implies t_{transit} = \frac{L}{v_{drift}} = \frac{L}{E_{DS}\mu} = \frac{L}{\frac{-V_{DS}}{L}\mu} = -\frac{L^2}{V_{DS}\mu} \tag{1.27}$$

In 1.27, V_{DS} represents the voltage applied between source and drain.

Let us define a threshold voltage V_T as the minimum gate voltage at which a mobile charge layer forms between the semiconductor and the dielectric. The channel charge per unit area may be then defined as:

$$Q_{channel} = -C_i(V_{GS} - V_T) \tag{1.28}$$

where C_i is the dielectric capacitance (per unit area).

We can finally combine equations 1.28 and 1.25 in order to get the following result:

$$I_{DS} = \frac{-C - i(V_{GS} - V_T)(WL)}{-\frac{L^2}{V_{DS}\mu}} \implies I_{DS} = \mu C_i \frac{W}{L}(V_{GS} - V_T)V_{DS} \tag{1.29}$$

It can be clearly noticed from equation 1.29, that when the mobile charge layer has a uniform thickness along the channel then the drain current depends linearly on the drain-source voltage (hence the name *linear* regime).

Saturation regime.

When the value of V_{DS} approaches V_{GS} the hypothesis of uniformity of the mobile charge layer at the semiconductor-dielectric interface is not valid anymore and the current equation has to be remodelled.

Indeed, when $V_{DS} = V_{GS}$, the mobile charge density next to the drain electrode is zero and if one further increases V_{DS} this region empty of mobile charges starts to extend towards the source contact so that the channel length is reduced.

Let us consider a 1-dimensional model of OFET, in which an x axis runs parallel to the OFET channel (Fig. 1.).

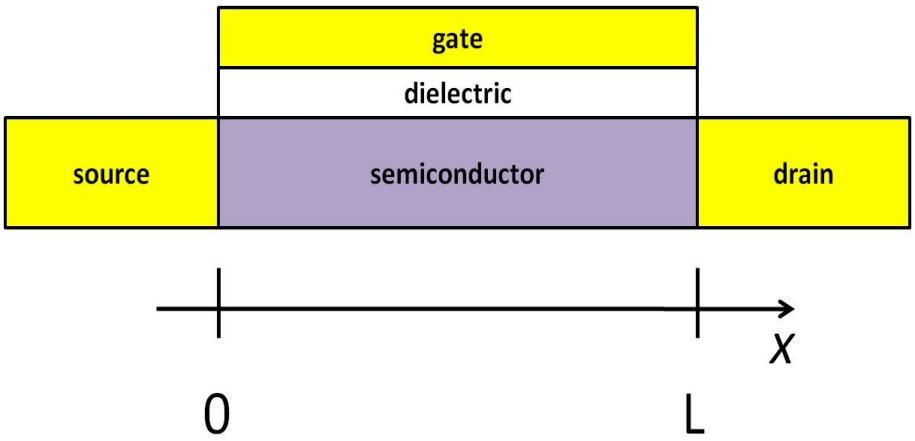

Figure 1.26: Geometry chosen to derive the saturation regime model.

Considering the non-uniform thickness of the mobile charge layer, the channel charge per unit area must be rewritten according to equation 1.30:

$$Q_{channel} = -C_i[V_{GS} - (V(x) + V_T)] \tag{1.30}$$

where *V(x)* represents the drain-source voltage drop in correspondence with the point x, so that the term *[V_{GS} - (V(x) + V_T)]* is the potential between the gate electrode and the point x (in other words, the voltage drop through the gate insulator).

Assuming that the source-drain current is mainly a drift current, the current at x can be expressed as follows:

$$I_{DS}(x) = W\mu Q_{channel}(x)E(x) = -W\mu Q_{channel}(x)\frac{dV(x)}{dx} \tag{1.31}$$

where *E(x)* is the electric field in correspondence with x. We can combine equations 1.30 and 1.31 and we get the following expression:

$$I_{DS}(x) = -W\mu C_i[V_{GS} - (V(x) + V_T)]\frac{dV(x)}{dx} \tag{1.32}$$

We can then integrate equation 1.32 between $x = 0$ and $x = \mathrm{L}$, as shown by 1.33:

$$\int_0^L I_{DS}(x)\,dx = \int_0^L I_{DS}\,dx = -W\mu C_i \int_0^{V_{DS}} [V_{GS} - V_T - V(x)]\,dV(x) \tag{1.33}$$

In 1.33, we assumed that the voltage drop between source and drain is equal to 0 for $x = 0$ and V_{DS} for $x = \mathrm{L}$. It is worth noting that since drain-source current is constant throughout the whole channel, the symbol $I_{DS}(x)$ was replaced by I_{DS}.

As previously stated, when $V_{DS} \gg V_{GS}$, a region of empty charge, characterised by a very high resistivity, is accumulated near the drain electrode, thus reducing the effective channel length to a value we call L_{eff}. This empty charge region actually limits the increment of drain-source current which becomes therefore constant. According to these considerations, equation 1.34 may be rewritten as follows:

$$\int_0^{L_{eff}} I_{DS}\,dx = -W\mu C_i \int_0^{V_{GS}} [V_{GS} - V_T - V(x)]\,dV(x) \tag{1.34}$$

Solving the integral in 1.33 leads to the following result:

$$I_{DSat} = \frac{W}{L_{eff}}\mu C_i \left[\frac{[(V_{GS} - V_T)]^2}{2}\right] \simeq \frac{W}{L}\mu C_i \left[\frac{[(V_{GS} - V_T)]^2}{2}\right] \tag{1.35}$$

where we considered the length of the empty charge region negligible with respect to the channel total length.

Expression 1.34 describes the value of the constant current in a regime which is usually called *saturation*.

A typical example of current-voltage characteristics (of an n-channel OFET) is shown in Fig. 1.27.

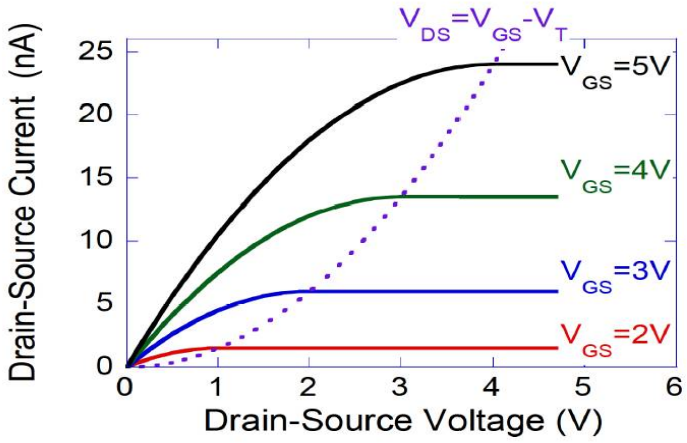

Figure 1.27: Example of an n-channel OFET current-voltage curves.

Fixing the value of V_{DS}, it is also possible to plot the graph of the I_{DS} as a function of V_{GS}. One should notice that, in the linear regime, the dependence of the current of V_{GS} is *linear* while it becomes *quadratic* in the saturation regime. A graph in which I_{DS} values are plotted as a function of V_{GS} is usually called *transcharacteristic*. Fig. 1.28 shows an example of a transcharacteristic acquired on an n-channel OFET.

Extraction of basic electrical parameters of OFETs.

In order to evaluate the electrical performance of an OFET, three physical parameters are usually considered [60]:

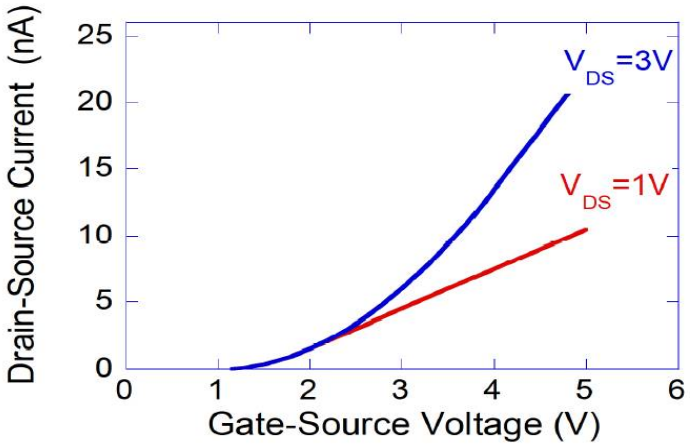

Figure 1.28: Example of an n-channel OFET transcharacteristics both in linear (red curve) and saturation (blue curve) regime.

- field effect mobility μ, describing how quickly a mobile charge can move through the organic semiconductor when pulled by the applied electric field;
- threshold voltage V_T, which may be defined as the minimum voltage value in correspondence with which the conductive layer at the semiconductor-dielectric interface is formed;
- Ion/Ioff ratio, usually defined as the ratio between the maximum and the minimum drain-source current values.

The mathematical models described in the previous paragraph, though somewhat oversimplified, are those usually used [60] [38] in order to determine those physical parameters used in order to evaluate the electrical behaviour of the tested OFETs.

According to the general habit, as it appears in the most of scientific work, and conforming to the prescriptions provided by the Institute of Electrical and Electronic Engineers [62], in this thesis the field-effect mobility will be assumed as a constant and, together with the threshold voltage, they will be determined by a simple linear fit of the square root of the transcharacteristic acquired in saturation regime, while the Ion/Ioff ratio will be calculated simply taking the ratio of the maximum and minimum I_{DS} values at a fixed V_{DS} value.

It should be however noted, for the sake of completeness, that some Authors [63] [64] have criticised the approached described above and proposed an alternative method of characterisation.

This method may be synthetically schematised as follows:

- the OFET has to be switched on and the drain-source current may be measured, in the linear regime, as a function of V_{DS};
- the slope of the curve (called *channel conductance* g_d) has to be extracted;
- the channel conductance may be expressed as described by the mathematical expression described hereafter:

$$g_d = \frac{\partial I_{DS}}{\partial V_{DS}} = \left(\frac{1}{K(V_{GS} - V_T)^{\alpha - 1}} \right) \tag{1.36}$$

- field-effect mobility is described as stated in the following formula:

$$\mu = K \left(V_{GS} - V_T \right)^{\alpha} \tag{1.37}$$

In this approach, two new constants (α and K) are introduced; these constants are typical parameters of the semiconductor used as active layer and may be calculated experimentally.

Moreover, it is worth noticing that according to this approach, the field-effect mobility is not a constant, but a parameter depending on the gate voltage.

Once one has calculated the threshold voltage, from channel conductance measurements, equation 1.36 may be eventually used in order to calculate the value of mobility.

This method, though able to provide more accurate results, is seldom used in scientific research and, for this reason, it will be not employed in this thesis.

As stated at the beginning of this paragraph, the IEEE standard test methods will be used instead.

Organic ElectroChemical Transistors (OECTs).

The first example of OECT was described in 1984 by White and co-workers [11], using a thin film of polypyrrole as active layer.

An OECT is made up of two electrodes, source and drain, connected by an active layer called channel realised using a semiconductive polymer which can be electrochemically doped/de-doped [38].

The channel conductivity is modulated by applying a voltage on a third electrode, the gate, immersed in an electrolyte solution in contact with the channel.

It is possible to illustrate qualitatively the behaviour of an OECT referring to one of the most commonly used organic polymers, namely PEDOT:PSS (see Chapter 2 for further details on this polymer).

Let us consider an electrochemical structure in which a thin film of PEDOT:PSS joins two electrodes (called E_1 and E_2) , while an electrolyte solution is placed on the PEDOT:PSS layer. Let us also assume that a third electrode E_3 is placed into the electrolyte solution.

When 0 V are applied to E_3, PEDOT:PSS is in its "high conductivity " state and a high current may be measured between E_1 and E_2.

When E_3 is positively addressed, the electrolyte cations M^+ are driven into the PEDOT:PSS film and react according to the following equation:

$$\mathrm{PEDOT{:}PSS} + \mathrm{M^+} + \mathrm{e^-} \iff \mathrm{PEDOT} + \mathrm{M{:}PSS} \tag{1.38}$$

In equation 1.38 e^- represents the electrons provided to PEDOT by the grounded electrode. The equation above describes the reduction of PEDOT:PSS to its neutral, low conductivity PEDOT state and is therefore responsible for a decrease in the current measured between E_1 and E_2.

This current modulation effect may be exploited in order to build organic electrochemical transistors in which PEDOT:PSS plays the role of active layer used for the transistor channel. In this case, the electrodes E_1 and E_2 are the source and drain of the OECT, while E_3 represents the gate electrode. The source is connected to the the circuit ground and both drain and gate potential drops are referred to the source.

It should be noted that, in PEDOT:PSS-based OECTs, the drain-source voltage must be negative, in order to drive holes from the source to the drain electrode. On the other hand, the gate-source voltage must be positive, so that the cations M^+ may be driven into the semiconductor film and react in accordance with the mechanism described above.

A schematic view of an OECT is presented in Fig. 1.29.

In order to model the electrical behaviour of an OECT, Bernards [65] and co-workers have recently proposed an equivalent circuit consisting of two different parts, namely an electrical and an ionic circuits.

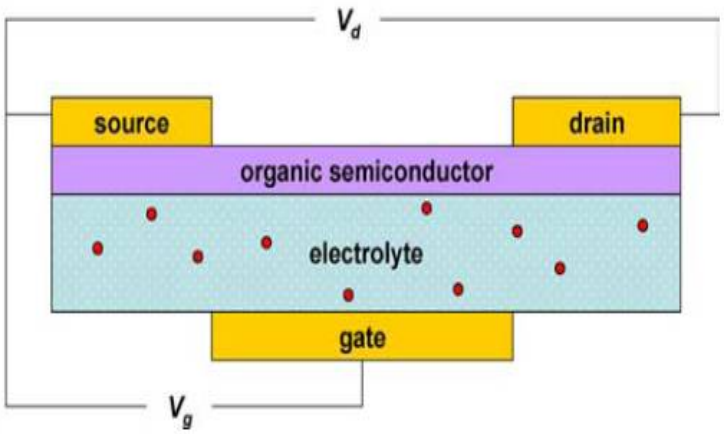

Figure 1.29: Schematic view of an OECT.

The electronic circuit describes the holes/electrons transport between the source and drain electrodes and is physically represented by the organic semiconductor film; its electrical behaviour is governed by Ohm's law.

On the other hand, the ionic circuit accounts for transport of ionic charge in the electrolyte solution.

The transport of ions from the electrolyte into the organic semiconductor film represents the physical phenomenon which is the base of the interaction of these two circuits.

According to this model, an OECT exhibits two different regimes of operation, depending on the relationship existing between the two voltages V_{DS} and V_{GS}:

- when $V_{DS} \ll V_{GS}$ then the semiconductor de-doping occurs *uniformly* along the channel and the relationship between I_{DS} and V_{DS} is approximately linear (*linear regime*);
- when $V_{DS} \simeq V_{GS}$ then the semiconductor de-doping occurs especially in correspondence with the drain electrode so that an empty charge region forms in this area; the current I_{DS} becomes constant and a saturation phenomenon occurs (*saturation regime*).

A typical example of a PEDOT:PSS-based OECT output curves is provided in Fig. 1.30.

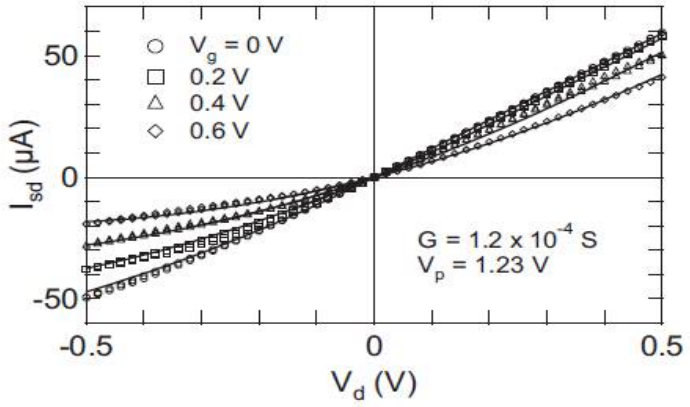

Figure 1.30: PEDOT:PSS-based OECT output curves.

Comparing the curve in Fig. 1.30 with those reported in Fig. 1.27, it can be easily noticed that OECTs usually require much lower input voltages than OFETs; this is essentially due to the different working principle (redox reaction for OECTs, charge layer accumulation for OFETs). On the other hand, it is also true that OECTs exhibit lower switching times than OFETs (seconds vs milliseconds, respectively) [66].

Bibliography

[1] J. C. Scott, *Nanostructured Conductive Polymers - Chapter 1: History of conductive polymers*, John Wiley & Sons Ltd, **2010**. ISBN: 978-0-470-74585-4.

[2] C. K. Chiang, C. R. Fincher, Y. W. Park, A. J. Heeger, H. Shirakawa, E. J. Louis, S. C. Gau, A. G. McDiarmid, *Phys. Rev. Lett.* , **1977**, 39, 1098–1101.

[3] H. Letheby, *J. Chem. Soc.*, **1862**, 15, 16-19.

[4] L. T. Yu, M. S. Borredon, M. Jozefowicz, G. Belorgey, R. Buvet, *J. Polym. Sci. Part C-Polym. Symp.*, **1967**, 16, 2931.

[5] J. McGinness, P. Corry, P. Proctor, *Science*, **1974**, 183, 853-855.

[6] D. Micha, I. Burghardt, *Quantum dynamics of complex molecular systems*, Springer, **2007**. ISBN: 978 - 3 - 540 - 34458 - 2.

[7] N. S. Hush, *Annals of the New York Academy of Sciences*, **2003**, 1006, 1-20.

[8] S. Etemad, A. J. Heeger, A. G. MacDiarmid, *Annual Rev. of Phys. Chem.*, **1982**, 33, 443-469.

[9] G. Heywang, F. Jonas, *Adv. Mater.*, **1992**, 4, 116–118.

[10] F. Ebisawa, T. Kurokawa, S. Nara, *J. Appl. Phys.*, **1983**, 54(*6*), 3255–3259.

[11] H. S. White, G. P. Kittlesen, M. S. Wrighton, *J. Am. Chem. Soc.*, **1984**, 106, 5375–5377.

[12] C. W. Tang, S. A. Vanslyke, *Appl. Phys. Lett.*, **1987**, 51(*12*), 913-915.

[13] B. R. Weinberger, M. Akhtar, S. C. Gau., *Synth. Met.*, **1982**, 4(*3*), 187-197.

[14] H. Klauk, *Organic electronics: materials, manufacturing and applications*, Wiley-VCH, **2006**. ISBN: 978 - 3 - 52731261 - 1.

[15] NanoMarkets, *The Future of Organic Electronics Manufacturing*, NanoMarkets Online Research Database, **2009**.

[16] S. L. Seager, M. R. Slabaugh, *Chemistry for Today: general, organic, and biochemistry.*, Thomson Brooks/Cole, **2004**. ISBN: 053439969X.

[17] N. E. Holden, *Handbook of Chemistry and Physics*, CRC Press, **2004**. ISBN: 978-0849304859.

[18] D. J. Griffiths, *Introduction to Quantum Mechanics*, Prentice Hall, **2004**. ISBN: 0-13-111892-7.

[19] A. D. McNaught, A. Wilkinson, *The IUPAC Compendium of Chemical Terminology*, Blackwell Science, **1997**. ISBN: 0865426848.

[20] L. Pauling, *General Chemistry*, Dover Publications, **1988**. ISBN: 0486656225.

[21] L. Pauling, *J. Am. Chem. Soc.*, **1931**, 53, p. 1367.

[22] B. Kirtman,D. M. Chipman, W. E. Palke, *J. Am. Chem. Soc.*, **1977**, 99(*5*), pp. 1305-1307.

[23] L. G. Wade Jr., *Organic Chemistry*, Prentice Hall, **1994**. ISBN: 0133016315.

[24] S. A. Baeurle, *Multiscale Modelling of Polymer Materials using Field-Theoretic Methodologies*, Habilitation Thesis, **2007**.

[25] A. Rudin, *The elements of Polymer Science and Engineering*, Academic Press, **1999**. ISBN: 0126016852.

[26] P. C. Painter, M. M. Coleman, *Essentials of polymer science and engineering*, DEStech Publications, **2009**. ISBN: 978-1-932078-75-6.

[27] I. M. Wars, J. Sweeney, *An Introduction to the Mechanical Properties of Solid Polymers*, John Wiley & Sons Ltd., **2004**. ISBN: 0-471-49626-X.

[28] L. H. Sperling, *An Introduction to Physical Polymer Science*, John Wiley & Sons Ltd., **2006**.

[29] V. R. Gowariker, N. V. Viswanathan, J. Sreedhar, *Polymer Science*, New Age International, **2003**. ISBN: 0852263074.

[30] R. L. Meade, *Foundations of Electronics*, Cengage Learning, **2002**. ISBN: 0766840271.

[31] G. Inzelt, *Conducting Polymers: a new era in Electrochemistry*, Springer, **2008**. ISBN: 978-3-540-75930-0.

[32] I. Fleming, *Molecular Orbitals and Organic Chemical Reaction: Reference Edition*, John Wiley & Sons Ltd., **2010**. ISBN: 0470746580.

[33] R. Hoffmann, C. Janiak, C. Kollmar *ACS Macromolecules*, **1991**, 51(*13*), 221-242.

[34] S. Roth, D. L. Carroll, *One-dimensional metals: conjugated polymers, organic crystals, carbon nanotubes*, Wiley VHC, **2004**. ISBN: 3527307494.

[35] C. K. Chiang, M. A. Druy, S. C. Gau, A. J. Heeger, E. J. Louis, A. G. MacDiarmid, Y. W. Park, H. Shirakawa, *J. Am. Chem. Soc.*, **1978**, 100, 1013-1015.

[36] A. R. Blythe, D. Bloor, *Electrical properties of polymers*, Cambridge University Press, **2005**. ISBN: 0521552192.

[37] A. F. Albernaz Vilela, R. Gargano, G. Magela Silva, *J. Mol. Struct.*, **2006**, 769, 33-37.

[38] P. G. Drazin, R. S. Johnson, *Solitons: An Introduction*, Cambridge University Press, **1989**. ISBN: 0521336554.

[39] G. M. Badger, *Aromatic character and aromaticity*, Cambridge University Press, **1969**.

[40] J. McMurry, *Organic Chemistry*, Thomson-Brooks Editors, **2004**. ISBN: 0534389996.

[41] J. D. Hepworth, D. R. Waring, M. J. Waring, *Aromatic Chemistry*, Royal Society of Chemistry, **2002**. ISBN: 0854046623.

[42] I. Mayer, Theor. Chem. Acc., **2010**, 123(*3*), 203-206.

[43] J. Roncali, *Chem. Rev.*, **1997**, 97, 173-305.

[44] J. R. Reynolds, F. E. Karasz, J. C. W. Chien, K. D. Gourley, C. P. Lillya, *J. Phys. III*, **1988**, 6(*44*), 693-696.

[45] W. Brütting, *Physics of Organic Semiconductors*, Wiley-VHC, **2005**. ISBN: 9783527405503.

[46] N. Karl, *Synthetic Met.*, **2003**, 133, 649-657.

[47] V. Coropceanu, J. Cornil, D. A. da Silva Filho, Y. Olivier, R. Silbey, J. Brédas, *Chem. Rev.*, **2007**, 107, 926-952.

[48] F. Torricelli, Z. M. Kovács-Vajna, L. Colalongo, *IEEE SISPAD Proc.*, **2009**.

[49] S. Verlaak, V. Arkhipov, P. Heremans, *Appl. Phys. Lett.*, **2003**, 82(*5*), 745-747.

[50] E. Katz, J. Huang, *Annu. Rev. Mater. Res.*, **2009**, 39, 71-92.

[51] A. Tsumura, H. Koezuka, T. Ando, *Appl. Phys. Lett.*, **1986**, 49(*18*), 1210-1212.

[52] J. Takeya, M. Yamagishi, Y. Tominari, R. Hirahara, Y. Nakazawa, T. Nishikawa, T. Kawase, T. Shimoda, S. Ogawa, *Appl. Phys. Lett.*, **2007**, 90(*10*), 2120-2123.

[53] G. Horowitz, F. Deloffre, F. Garnier, R. Hajlaoui, M. Hmyene, A. Yassar, *Synth. Met.*, **1993**, 54, 435-445.

[54] F. Garnier, R. Hajlaoui, A. Yassar, P. Srivastava, *Science*, 265(*5179*), 1684-1686.

[55] H. Sirringhaus, *Nat. Mater.*, **2003**, 2, 641-642.

[56] P. Cosseddu, A. Bonfiglio, *Appl. Phys. Lett.*, **2010**, 97(*20*), 3305-3308.

[57] C. Di, G. Yu, Y. Liu, D. Zhu, *J. Phys. Chem. B*, **2007**, 111, 14083-14096.

[58] Y. Sun, Y. Liu, D. Zhu, *J. Mater. Chem.*, **2005**, 15, 53-65.

[59] N. Tessler, Y. Roichman, Lectures for the Graduate Course of *Organic Semiconductor Devices*, http://webee.technion.ac.il/labs/orgelect/.

[60] D. Gamota, *Printed organic and molecular electronics*, Springer, **2004**. ISBN: 1402077076.

[61] D. A. Bernards, G. G. Malliaras, *Organic semiconductors in sensor applications*, Springer, **2008**. ISBN: 3540763139.

[62] IEEE, *Standard test methods for the characterisation of organic transistors and materials*, New York, **2008**, ISBN: 9780738160139.

[63] G. Horowitz, P.Lang, M. Mottaghi, H. Aubin, *Adv. Func. Mater.*, **2004**, 14(*11*), 1069-1074.

[64] G. Horowitx, R. Hajlaoui, R. Bourguiga, M. Hajlaoui, *Synthetic. Met.*, **1999**, 101, 401-404.

[65] D. A. Bernards, G. G. Malliaras, *Adv. Func. Mater.*, **2007**, 17, 3538-3544.

[66] J. T. Mabeck, G. G. Malliaras, *Anal. Bionala. Chem.*, **2006**, 384, 343-353.

2

This chapter represents an introduction to the field of wearable electronics.

The chapter opens providing some important definitions concerning the basic concepts of this scientific field, then the most significant applications are presented.

At the end of the chapter, the state of the art of wearable electronics is described: several different devices, realised using both inorganic and organic materials, are illustrated in order to give a synthetic but clear picture of the main technologies developed and the results obtained so far.

2.1 Wearable electronics: definitions and basic concepts.

The concept of *wearable electronics* has emerged in the last 15 years, as a direct consequence of the intensive miniaturisation of silicon technology [1].

While in the early years this expression was used in a literal sense to indicate the insertion of small electronic equipment into textile substrates, its meaning has slowly become broader and nowadays it includes any electronic device realised in a textile form [2].

The definition given above is actually very general, so that a large class of different electronic systems may be defined as "wearable".

According to Park *et al.* [9] wearable electronic devices can be grouped into different categories, on the basis of the integration level existing between the electronic device and the fabric in which it is inserted:

- *wearable computers and displays*: this class includes any portable electronic system not necessarily in direct contact with clothes (see Fig. 2.1a where a jacket containing a mobile phone and an MP3 reader is shown);
- *surface mounted electronics*: in this case, clothes merely represent a substrate to which the electronic system is attached (see Fig. 2.1b where an MP3 reader remote control is inserted into a shirt sleeve) ;
- *electronics integrated on yarn*: in this last case, the integration between electronics and textiles reaches its highest peak, since the yarn itself may act as an electrical/electronic component (see Fig. 2.1c where special yarns acting as sensors are woven into the fabric of a t-shirt).

Yarns able to exhibit electrical or electronic properties are usually known as *e-yarns*. When these yarns are woven together in order to form fabrics or clothes, so that the electric components and connections are *intrinsic* to the textile, these objects are called *e-textiles* [4].

The expression *smart clothing* is usually used in order to indicate clothes able to acquire physical signals, transform them into digital data, process them and eventually store or send them to an external reception system [5]. This last definition, therefore, considers the *functionality* of clothes rather than their structure.

The definitions provided above are those commonly accepted and used by the scientific community; however, it has been emphasised by different sources that there is no general agreement on the exact meaning of concepts related to the field of wearable electronics and expressions like *e-textiles*, *smart clothing* and even *wearable electronics* are very often used as synonyms, even within the same scientific paper or book [9] [6].

In this thesis, we will comply with the following definitions:

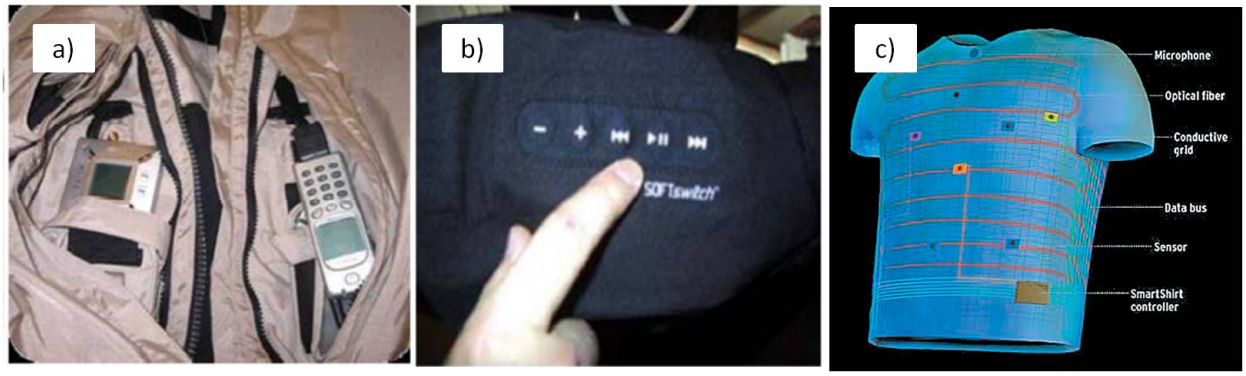

Figure 2.1: Examples of different integration levels between electronics and textiles.

- *wearable electronics*: the subfield of electronics dealing with the study, project and realisation of any integration process between textile and electronics;
- *e-textiles*: any fabric containing electric/electronic components in a textile form (i.e. yarn-shaped);
- *smart clothing*: e-textiles used in order to detect, transform and process signals acquired from a specific environment.

2.2 Wearable electronics: fields of application.

Generally speaking, it has been pointed out that wearable electronics is potentially able to help improve almost any single aspect of people's every day life or work conditions [6].

There are obviously certain applications in which the combination of electronics to textile technology is particularly useful; in more detail, the most important fields of application of wearable electronics may be synthesised in the following list [6] [7]:

- *medical applications for disabled and rehabilitation*: in this case, smart clothes are used to detect physical parameters (such as temperature, heart rate, posture ...) of patients suffering from physical, cognitive or sensory impairment, thus helping the diagnosis and monitoring processes in a simple and non-invasive way;
- *assisting applications in the workplace*: wearable electronics has proved to be able to provide important benefits for people working in dangerous environments, such as the military or the rescue service, because it offers the possibility of real-time monitoring the operators' vital parameters increasing the safety level;
- *entertainment and leisure time applications*: wearable electronic systems have been successfully used for the power supply and data transmission of portable music players and video game consoles.

2.3 Electronic devices for textile applications.

Even though, as stated in the first paragraph of this chapter, the field of wearable electronics is relatively new, many different materials and structures have been proposed and described so far, so that it is not at all easy to identify general prototypes of electronic devices on yarn.

If one is to describe the state of the art of this field the best option is, perhaps, to group these devices into families according to some proper criteria.

Considering the functional activity performed by smart textiles, three different categories may be distinguished:

- *passive smart textiles*: these devices can only sense physical stimuli from the environment. A piezoresistive yarn, able to detect a mechanical stimulus, is a classical example of passive device;
- *active smart textiles*: these devices are not only able to sense physical stimuli but they can also react to the signal they detect, so that they are, at the same time, either sensors and actuators. A photosensitive fibre, able to sense a particular wavelength and also change its colour when that wavelength is detected, is an example of active device;
- *very smart textiles*: like the active devices, very smart textiles are able to both detect stimuli and react to them; moreover, they are able to modulate (i.e. to adapt) their response to the given environmental conditions. A water-permeable fabric stripe, able to detect air moisture and change its form according to both the recorded moisture and, for instance, the environmental temperature could be considered an example of very smart textiles.

Another useful distinction that may be done is the one concerning the chemical nature of the active material used to realise the device. According to this criterion, electronic devices on yarn may be classified into two big categories:

- *inorganic devices*, in which the active layer is not carbon based (silicon and silicon compounds are the most common materials at present);
- *organic devices*, in which the active material is carbon – based (that is, conjugated polymers, oligomers or small molecules).

This paragraph is organised according to this last distinction.

Inorganic electronic devices for textile applications.

The first, simple example of inorganic electronic devices realised in a textile form was the incorporation of electrically conductive yarns into a fabric with the purpose to supply electrical connection to micro-electronic systems attached to the fabric itself [8].

These yarns were either *intrinsically conductive*, that is made of metals, or *extrinsically conductive*, which means made of some polymeric, insulating materials (especially polyester or polyamide) subsequently grafted with metals.

Currently, there are many types of these electrically conductive yarns available on the market and they may be used in ordinary textile machinery to produce electrically conductive substrates.

A further development was done when e-textiles began to be used not only to conduct electricity but also as *sensors*, so that they were able to acquire signals from the environment and transmit them through a textile substrate. A typical example is described by Edmison *et al.* [9] who proposed the insertion of piezoelectric stripes into a fabric (Fig. 2.2) in order to detect mechanical or acoustical stimuli.

A more recent example of a textile electronic system employed in order to monitor both the heart rate and the respiration is the one proposed by Catrysse *et al.* in 2009 [10].

In this paper, the Authors present a complete suit especially designed for the monitoring of the above-mentioned vital parameters of children in a hospital environment. The sensors

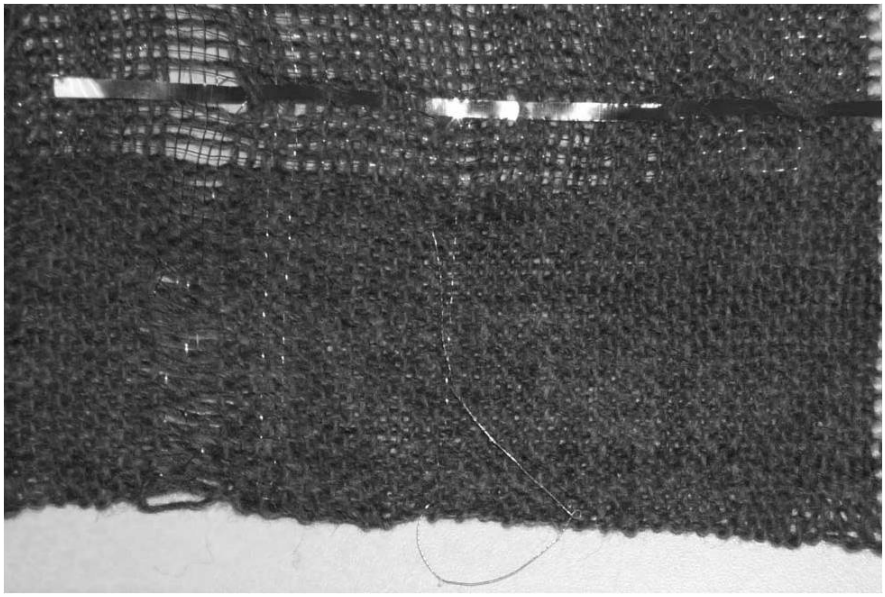

Figure 2.2: Piezoelectric fabric realised by Edmison *et al.*

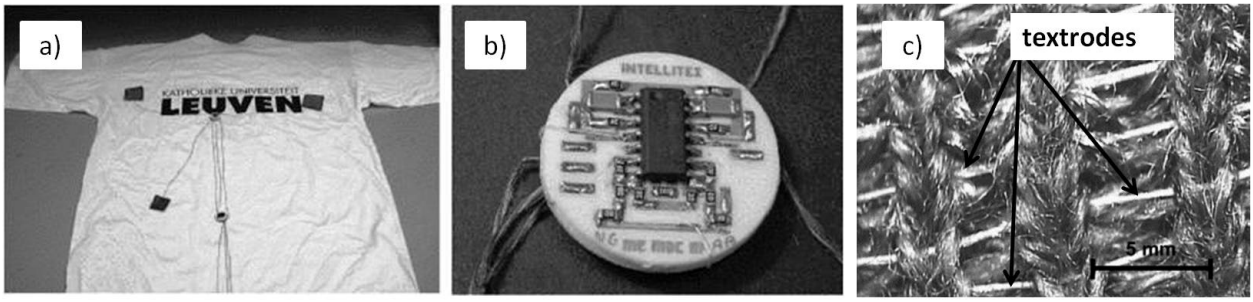

Figure 2.3: Sensorised suit developed by Catrysse *et al.* (a), the electronic interface with some textrodes connected to it (b) and the textrodes woven into the cotton fabric composing the suit.

(specifically called *textrodes*) are all made by means of piezoresistive stainless steel yarns woven into the fabric and therefore completely integrated in the suit.

The electronic interface, responsible for the data handling, storage and transmission electronics, is realised through a microelectronic circuits integrated within a belt connected to the suit. It should be noted, however, that both the electrical interconnections and the transmission antenna are fabricated employing conductive steel yarns woven into the suit.

Fig. 2.3 shows the complete suit (a), a view of the electronic interface with some textrodes connected to it (b) and the textrodes woven into the cotton fabric composing the suit.

Another important problem which can be easily controlled with smart textiles is that of temperature sensing.

Khang *et al.* [11], on behalf of NASA, have recently reported on the realisation of textiles able to detect temperature as well as mechanical strain.

The Authors built a special type of multiwalled carbon nanotubes (CNTs) spun inside a silicon fibre; these CNTs, besides showing piezoelectric properties, are also characterised by temperature-depending conductivity. The sensitivity of these yarns is particularly high: typical variations of ~ 0.01 mA have been recorded in correspondence of temperature variations of 1

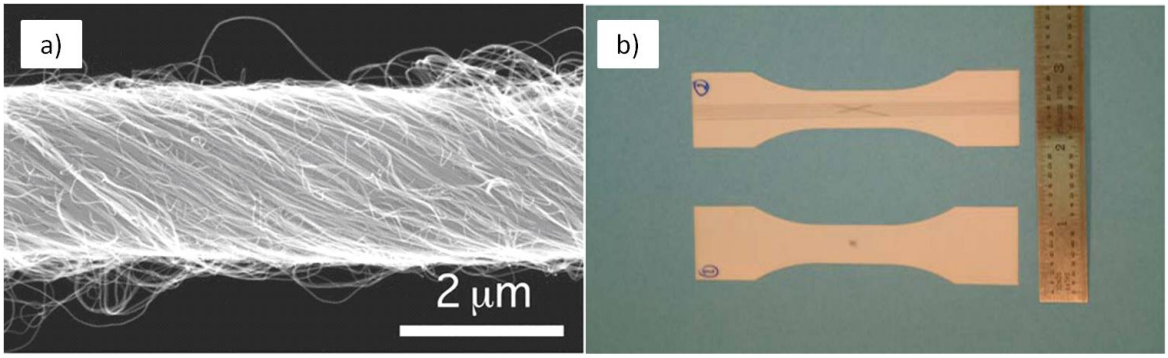

Figure 2.4: CNTs embedded into a silicon fibre (a) and polyester tissue with the sensors developed by Khang *et al.* (b).

°C.

Fig. 2.4 depicts the fibres developed by Khang *et al.* Fig. 2.4 a) shows a Scanning Electron Microscopic (SEM) image of the silicon fibre with the CNTs embedded in it while Fig. 2.4 b) shows two samples of polyester tissue, in which the silicon fibres were woven, which were used for the mechanical and thermal characterisation of the sensors.

Another interesting application, related to what we have defined as *ultra smart textiles*, is that reported by Lee and Kim [12]. The Authors describe a textile system composed of two different parts:

1. conductive yarns able to detect environmental temperature and send it to an electronic control system;

2. a system composed of couples of parallel fibres one of them made of polyethylene covered with polypyrrole (*p-type conduction*), the other made on multiwalled CNTs inserted into a matrix of polyethyleneimine (PEI) (*n-type conduction*).

The temperature-sensitive fibres detect environmental temperature and, when it reaches values outside a specific, pre-defined range, the control system applies a specific voltage to the fibre couples so that an electric current starts flowing through them.

Depending on the sign of the applied voltage, the fibre couples are able to absorb or release heat so that the fabric temperature returns within the set range. This conversion of a voltage drop into a storage/release of heat is usually known as *thermoelectric effect*.

In order to implement more complex electronic functions, such as switching or amplification, more sophisticated electronic devices, such as transistors in a textile form, have to be developed.

The first approach consists of The first example of electrically active e-textile device, namely a Field Effect Transistor (FET), dates back to 2003 and was presented by Bonderover and co-workers [13]. The device is built on polyimide fibres, each 2 mm long. The source, drain and gate contacts were realised with thermally evaporated gold, while silicon nitride was used as gate dielectric. The active layer was made of a 50 nm layer of n-doped amorphous silicon (a–Si).

An example of a textile pattern realised using such devices is shown in Fig. 2.5.

In this fabric, three different types of fibres may be observed: transistor fibres as warps (the two vertical light grey lines), gold-made conductive fibres as wefts (the three horizontal semi-transparent lines) and two insulating fibres (dark vertical lines) which keep the transistors separate. The squares on the transistor fibres represent the gold contact pads.

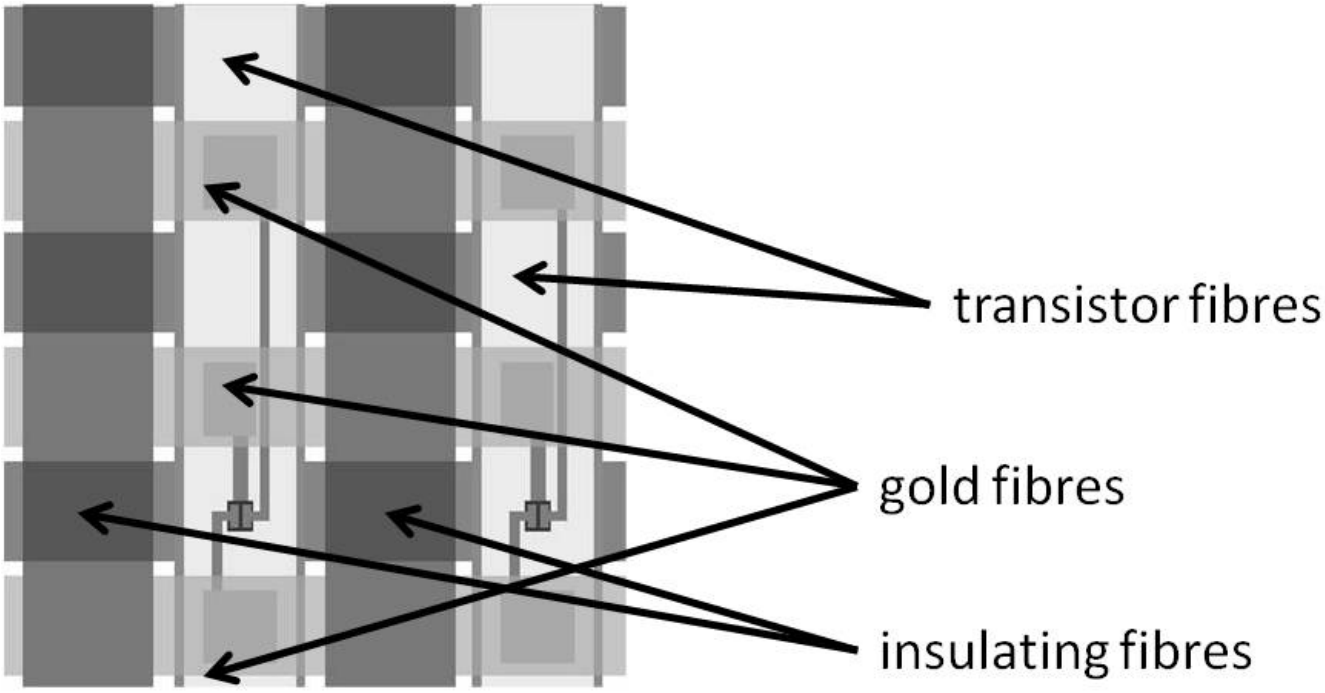

Figure 2.5: Fibre circuit designed by Bonderover *et al.*

The Authors tested this fabric by applying variable pressure onto it and the obtained results showed that the variations in electrical resistance are negligible and do not affect the electrical performances of the transistors.

More recently, Healy *et al.* developed a method to integrate active devices on silicon dioxide fibres (which they called *passive fibres*) [14]. These amorphous glass fibres have a diameter of 125 μm and show very good mechanical properties, such as flexibility and tensile strength. The active layer is made of doped silicon deposited on the fibre by means of a physical vapour deposition (PVD) process.

The contacts are realised with conductive fibres, perpendicular to the passive fibre. The Authors showed that with such a configuration, it is possible to obtain simple active devices, such as p–n diodes (Fig. 2.6), or more complicated circuits, such as ring oscillators.

Very recently (2009), Surve (on behalf of Nike Inc.) [15] was able to reach a very high level of integration of electrical components by means of high resolution (< 0.1 μm) deposition techniques, such as diffusion or ionic implantation. Thanks to these techniques, the Author was able to place a complex circuit, such as an accelerometer, on both natural and synthetic fibres. An example of this circuit is shown in Figure 2.7.

In Fig.2.7, the number 103 indicates the warp fibres (103A is the fibre on which the whole circuit is built), 105 indicates the weft fibres while 107 and 109 refer to the specific devices (in particular, 107 indicates a silicon field-effect transistor (FET) while 109 is a conductive connection line). Clearly, this last application, although exploits single, technologically mature components, is more in the line of a combination between silicon and textile technology with no real material integration between them.

Organic electronic devices for textile applications.

As previously mentioned, the active layer of these devices is carbon–based.

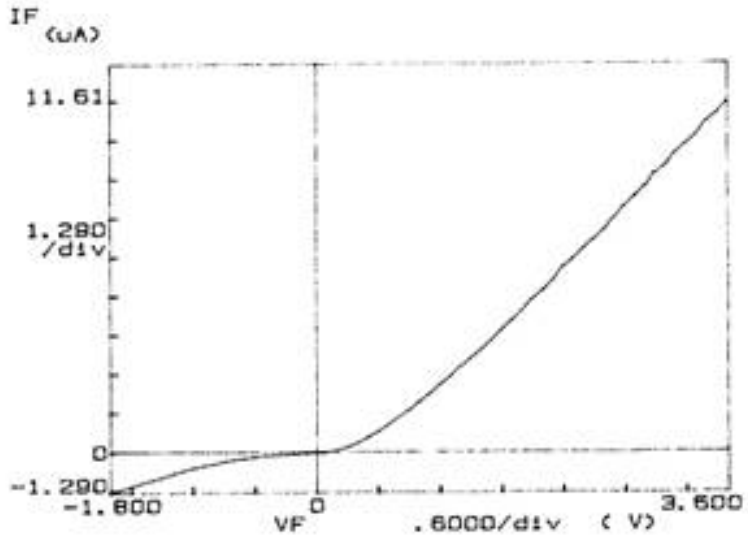

Figure 2.6: Electrical response of a p-n junction on a fibre. [Healy *et al.*]

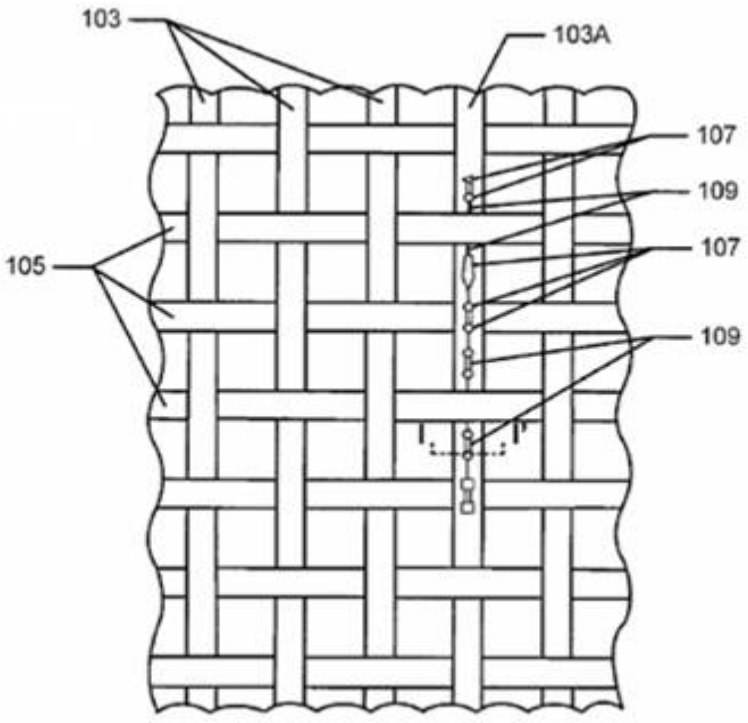

Figure 2.7: Accelerometer on fibres designed by Surve.

Roughly speaking, organic electronic devices specifically designed for textile applications may be grouped into two different categories, according to the specific implemented electronic function:

1. *organic conductive fibres*;
2. *organic transistors on fibrous substrates.*

A further classification related to transistors may be done according to the physical principle which is responsible for the current modulation (see previous chapter for a detailed description about the different types of organic transistors):

- *Organic field–effect transistors (OFETs)*, in which the source–drain current is modulated by varying the charge density in the semiconductor layer through the electric field induced by the gate electrode across an insulating layer;
- *Organic electro–chemical transistors (OECTs)*, in which the source–drain current is modulated by varying the charge density in the semiconductor layer through a reduction-oxidation reaction that occurs between the semiconductor itself and an electrolyte put into contact with the active layer.

Organic conductive fibres.

In accordance with Wallace *et al.*, at present there are two different ways of producing conductive fibres employing organic materials [16].

When the organic (semi)conductor may be easily solved in proper organic solvents, it is possible to use directly traditional spinning methods (such as wet spinning) in order to obtain intrinsically conductive fibres. This is the case, for instance, of materials such polyaniline or thiophene derivatives.

If the spun fibre's conductivity is not good enough, other treatments, such as doping, may be performed on the fibre after it has already been spun [17] in order to improve its electrical behaviour.

In most cases, however, the organic materials cannot be directly employed into the spinning process. In such circumstances, the insulating fibre has to be firstly spun and subsequently coated with a conductive layer. This coating may be realised using different methods, for example by means of in-situ, liquid-phase polymerisation [15] or simply soaking the fibrous substrates in polymeric solutions [19].

At present, conductive coating has been successfully applied to different fibrous substrates, either synthetic [20] (such as nylon) or natural [21] [22] (wool, silk and cotton).

It should be noticed, however, that even if high conductivity (up to 1 S/cm) has been reported [13], these treatments often resulted in an increment of the overall thickness by 30% and, sometimes, in a significant degradation of the fibres' mechanical properties [24].

For this reason, as will be clear in the following chapters of this thesis, I tried to develop methodology on natural cellulosic substrates able to determine a proper increase of conductivity but, at the same time, preserving their excellent wearability and mechanical characteristics.

Organic field effect transistors on fibres.

A first approach in order to build up wearable OFETs consists of fabricating such devices on flexible substrates, from which they can be easily removed, and then transferring them onto a textile substrate.

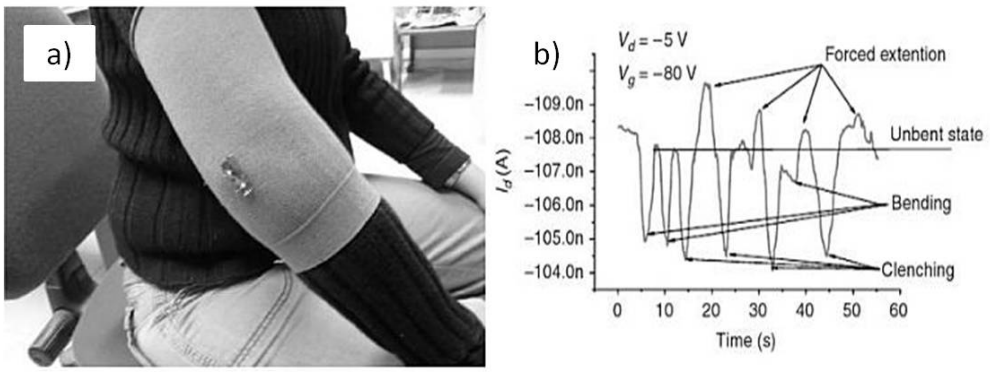

Figure 2.8: Wearable OFET used a strain sensor a) and its electrical response to joint movements b) (Bonfiglio *et al.*.

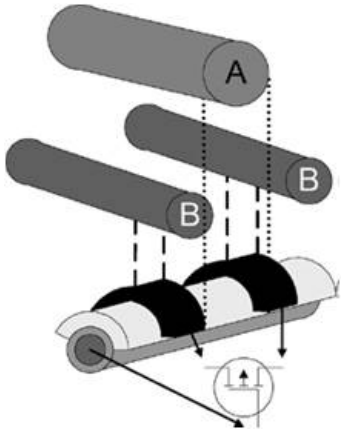

Figure 2.9: Lateral view of the first OFET on yarn showing the different layers and connections [Lee & Subramanian].

Examples of such devices were reported in 2007 by Bonfiglio *et al.* [?]. In this case, the Authors realised pentacene-based OFETs on a flexible substrate made of a thin film of poly(ethyleneterephthalate), acting both as substrate and gate dielectric.

The devices were subsequently transferred onto wearable substrates (such as gloves, belts etc.) and used as sensors in order to monitor physiological parameters of body functions (see Fig. 2.8).

The very first attempt to create organic circuit elements directly in a textile (i.e. yarn-shaped)form may be traced back to 2003, when Lee and Subramanian [25] published the first paper concerning a device on a single yarn showing transistor behaviour.

These transistors were made starting with aluminium wires, on which a thin layer ($\sim$ 250 nm) of low temperature silicon oxide (LTO) was deposited. Pentacene was used as the organic semiconductor and the source and drain contacts were prepared with thermally evaporated gold patterned through a shadow mask. The device structure is shown in Fig. 2.9, in which A represents the gate electrode while B indicates the wires that are the source and drain connections.

The Authors described a method which does not require photolithography patterning and performed a mechanical analysis of their devices, showing that important electrical properties such as mobility and drive current remain almost constant over a wide range of flexion-stress.

In a following paper [33], the same Authors presented a weave patterning process to build simple electronic circuits on fabrics: the circuits are woven into a fabric (according to a pre-

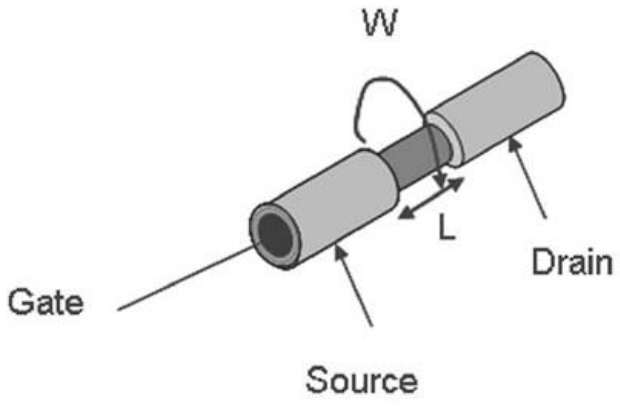

Figure 2.10: Schematic view of the device realised by Maccioni *et al.*

defined circuit pattern), connections between the various devices are realised by means of metal conductive wires while the devices are separated from each other by weaving insulating wires between them. The fabric itself thus acquires a triple function because it holds the circuit structure, connects the devices and isolates FETs from one other.

Another structure was presented by Maccioni *et al.* in 2006 [1]. In this case, the basic fibre consists of a copper wire (45 μm in diameter) uniformly covered with a thin layer of polyimide (1 μm in thickness).

A schematic view of such devices is shown in Fig. 2.10.

Thermally evaporated pentacene was used as the active layer and the source and drain contacts were prepared with both evaporated gold (through a shadow mask) and poly (3,4-ethylenedioxythiophene) poly(styrenesulfonate) (PEDOT PSS, transferred onto the wire using a soft lithography process).

These devices show high mobility and Ion/Ioff ratios higher than 10^3. The same Authors later published a paper [28] in which they proposed a detailed analytical model used to describe the curves of the cylindrical transistors in both the linear and saturation regimes. The experimental results that the authors provided showed that under reasonable hypotheses (i.e. semiconductor and insulator thicknesses are much smaller than the gate radius), their mathematical model is actually able to accurately describe the behaviour of the cylindrical devices and the electrical characteristics.

The same research group also investigated the properties of ambipolar OFETs realised on yarns [49]. Ambipolarity is a very important property of electronic devices which consists of the capability of the device to conduct electricity with both electrons and holes [30]. As a consequence, ambipolar OFETs are able to work for both positive and negative values of V_{DS} (considering, of course, proper values of V_{GS}).

Such a property is usually considered particularly important in the design of electronic circuit, because ambipolar devices may be used in order to build circuits characterised by high robustness, low-power dissipation, higher noise margin and easier circuit design [31].

The substrate was the same as described above (i.e. a copper wire uniformly covered with polyimide), and the active layer was a double–semiconductor layer of thermally evaporated pentacene/C_{60}. The source and drain contacts were prepared with PEDOT:PSS. Relatively high mobilities (up to $7 \cdot 10^{-3}$ cm^2/Vs) were measured in both p and n–type modes. In Fig. 2.11, the n and p type I_{DS}–V_{DS} characteristics are shown.

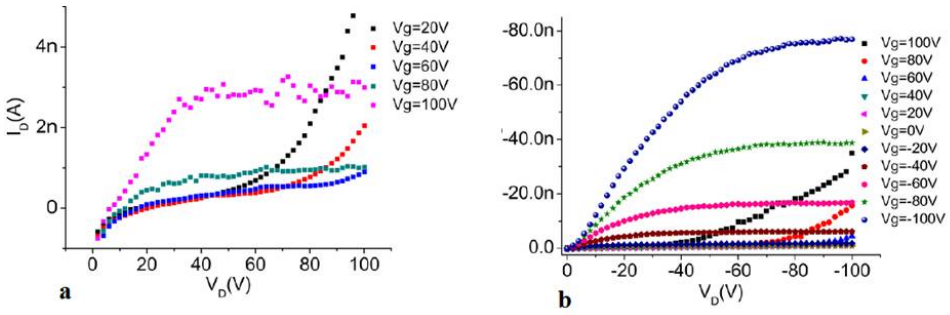

Figure 2.11: a) n-type I_{DS}–V_{DS} b) p-type I_{DS}–V_{DS} [Cosseddu *et al.*].

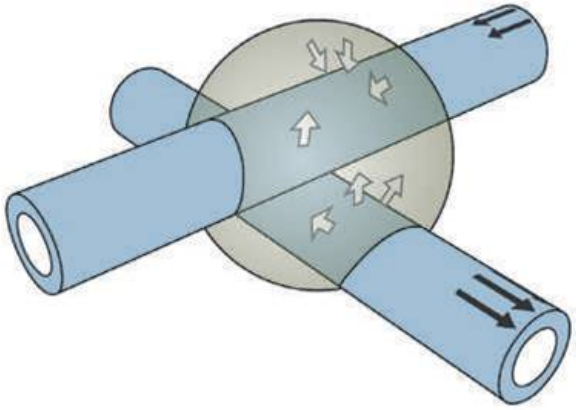

Figure 2.12: Schematic view of the OECT on fibre as proposed by Hamedi *et al.*

Organic electro–chemical transistors on fibres.

The first true example of an organic electrochemical transistor realised on a fibre is that described by Hamedi *et al.* [32]. This device is built on monofilaments made of nylon–6 that is uniformly covered with a high–conductivity type of PEDOT:PSS. The transistor is realised by suspending two coated fibres in a cross geometry and creating an ionic contact by adding a solid polymer electrolyte at the junction of the fibres (Fig. 2.12).

Very recently, the same research group proposed an example of OECT realised on a natural fibre, namely silk filaments [22].

These fibres were treated with a conjugated polyelectrolyte, poly(4-(2,3-dihydrothieno[3,4-b]-[1,4]dioxin-2-yl-methoxy)-1-butanesulfonic acid), known as PEDOT-S; the transistor was realised by placing two treated yarns perpendicularly and joining them by means of a small drop of ionic liquid:polymer ionic liquid (IL:PIL) electrolyte mixture. The final result is shown in Fig. 2.13, where the transistor three electrodes (gate, source and drain) are indicated with the initials G, S and D.

Bibliography

[1] J. Berzowska, *Textile*, **2005**, 3, 58.

[2] D. De Rossi, *Nat. Mater.*, **2007**, 6, 328.

[3] Y. S. Park, M. Shur, W. Tang, *Frontiers in electronics: future chips*, World Scientific, **2002**. ISBN: 9812382224.

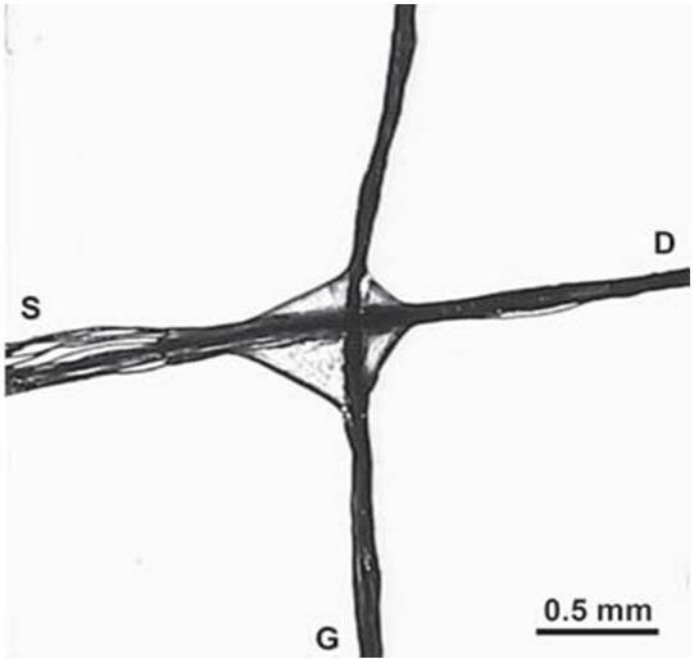

Figure 2.13: Picture of the electrochemical transistor on silk fibres [Müller *et al.*].

[4] B. Quinn, *Textile Futures: Fashion, Design and Technology*, Berg Publishers, **2010**. ISBN: 1845208080.

[5] S. Mann, *ACM Comm.*, **1996**, 39(*8*).

[6] J. Hännikäinen, *Electronic Intelligence Development for Wearable Electronics*, D. Tech. Thesis, Tampere University of Technology, **2006**.

[7] X. Tao, *Wearable electronics and photonics*, Woodhead, **2005**. ISBN: 1855736055.

[8] S. Wagner, E. Bonderover, W. B. Jordan, J. C. Sturn, *Int. J. of High Speed Electronics and Systems*, **2002**, 12(*2*), 391-399.

[9] J. Edmison, M. Jones, Z. Nakad, T. Martin, *Wearable Computers (ISWC)*, **2002**, 41-48.

[10] M. Catrysse, R. Puersa, C. Hertleerb, L. Van Langenhoveb, H. van Egmondc, D. Matthys, *Sensor Actuat. A: Phys.*, **2009**, 114(*2*), p. 302-311.

[11] S. K. Kahng, T. S. Gates, G. D. Jefferson, *40th International SAMPE Conference Proceedings*, 2008.

[12] S. Lee, J. Kim, *J. of Donghua Univ.*,**2006**, 23(*5*).

[13] E. Bonderover, S. Wagner, Z. Suo, *Mater. Res. Soc. Symp. P.*, **2003**, 763, 109-114.

[14] T. Healy, C. Papadas, N. Venios, F. Clemens, M. Wegmann, D. Winker, A. Ullsperger, W. Hartmann, B. O'Neill, J. Donnelly, A. M. Kelleher, J. Alderman, A. Mathewson, *Lect. Notes Comput. Sc.*, **2007**, 210, 255-274.

[15] S. N. Surve, United States Patent Publication No. US 2009/0053950, **2009**.

[16] G. G. Wallace, T. E. Campbell, P. C. Innis, *Fibers and polymers*, **2007**, 8(*2*), p. 135-142.

[17] A. P. Chacko, S. S. Hardaker, R. V. Gregory, R. J. Samuels, *Synthetic Metals*, **1997**, 84, 41.

[18] I. Wistrand, R. Lingstrom, L. Wagberg, *Eur. Polym. J.*, **2007**, 43, 4075-4091.

[19] Y. Ding, M. A. Invernale, G. A. Sotzing, *ACS Appl. Mat. Int.*, **2010**, 2, 1588-1593.

[20] D. Abraham, A. Bharati, A. Subramanyam, *Polymer*, **1996**, 23, 5295.

[21] S. N. Bhadani, S. K. Sen Gupta, G. C. Sahu, M. Kumari, *J. Appl. Polym. Sci.*, **1996**, 61, 207.

[22] S. W. Tan, H. Ge, *Polymer*, **1996**, 37, 965.

[23] X. Liu, H. Chang, Y. Li, W. T. Huck, Z. Zheng, *ACS Appl. Mater. Interfaces*, **2010**, 2(*2*), 529-35.

[24] N. V. Bhat, D. T. Seshadri, M. M. Nate, A. V. Gore, *J. Appl. Polym. Sci.*, **2006**, 102, 4690-4695.

[25] J. B. Lee, V. Subramanian, *IEEE International Electron Device Meeting Technical Digest*, **2003**, 8, 1-4.

[26] J. B. Lee, V. Subramanian, *IEEE T. Electron Dev.*, **2005**, 52(*2*), 269-275.

[27] M. Maccioni, E. Orgiu, P. Cosseddu, S. Locci, A. Bonfiglio, *Appl. Phys. Lett.*, **2006**, 89, 143515:1-3.

[28] S. Locci, M. Maccioni, E. Orgiu, A. Bonfiglio, *IEEE T. Electron Dev.*, **2007**, 54, 2362-2368.

[29] P. Cosseddu, G. Mattana, E. Orgiu, A. Bonfiglio, *Appl. Phys. A*, **2009**, 95, 49-54.

[30] X. Yang, K. Mohanram, *Rice University TREE1002*, **2010**, p.1-5.

[31] J. Wang, B. Wei, J. Zhang, *Semicond. Sci. Technol.*, **2008**, 23, 055003-055007.

[32] M. Hamedi, R. Forchheimer, O. Inganäs, *Nat. Mater.*, **2007**, 6, 357-362.

[33] C. Müller, M. Hamedi, R. Karlsson, R. Jansson, R. Marcilla, M. Hedhammar, O. Inganäs, *Adv. Mater.*, **2011**, *XX*, 1-4.

3

In this Chapter, the experimental part of my research activity will be described in detail.

First of all, the different types of yarns I used to build my devices will be presented.

Then, the different organic/inorganic materials utilised in the fabrication process will be introduced; these materials are listed according to a "functionality " criterion, that means they are divided into functional categories (semiconductors, conductors, dielectrics etc.).

The Chapter concludes with a presentation of the different characterisation techniques employed to evaluate the devices behaviour.

3.1 Materials: the yarns.

The Elektrisola yarn.

The research performed during my doctorate started from a work previously developed in our research group during the course of a M. of Sc. Thesis, whose results were later published [1].

In that work, a special wire produced by Elektrisola KG was used in order to produce a yarn-shaped Organic Field Effect Transistor (OFET).

The Elektrisola yarn is made as follows:

- a metallic (copper) core;
- an outer layer of an insulating polymer (namely polyimide).

Let us analyse in more detail the properties of the materials composing the yarn.

The Elektrisola yarn: metal core.

Copper (chemical symbol Cu) is a chemical element belonging to the group of transition metals; it is rather soft and malleable and, after silver, has the highest electrical and thermal conductivity [2].

The Elektrisola yarn's inner core is a copper wire whose diameter is 45 μm. This metallic core is obtained by a very thin copper yarn on which a further layer of copper is deposited by means of electrolytic deposition, until the yarn reaches the desired diameter; this way it is possible to reduce the quantity of metal employed (and therefore the costs of the final product) without impairing the electrical and mechanical properties of the obtained yarns [3]. It shows very high electrical conductivity (up to $5.85 \cdot 10^7$ S/m).

The Elektrisola yarn: insulating outer layer.

The copper core is covered with a thick layer of polyimide whose *mean* thickness is about 1 μm.

The term "polyimides" is used in Organic Chemistry to refer to a large family of insulating polymers whose monomer (shown in Fig. 3.1) contains an imide group.

The exact electrical behaviour actually depends on the side groups connected to the monomers; in the case of Elektrisola yarn, the relative dielectric constant is 3 (value acquired at 1 MHz) and the electrical resistivity (at 20 °C) is $5.3 \cdot 10^{16}$ Ω/cm.

An image of the cross-section of the Elektrisola yarn (acquired with a Scanning Electron Microscope) is shown in Fig. 3.2. In this picture, the dielectric layer surrounding the metal core is clearly visible between the copper (right) and the expoxy resin (left) in which the wire was embedded.

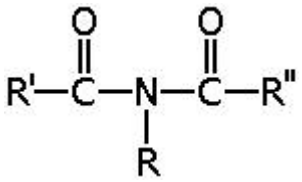

Figure 3.1: Imide monomer.

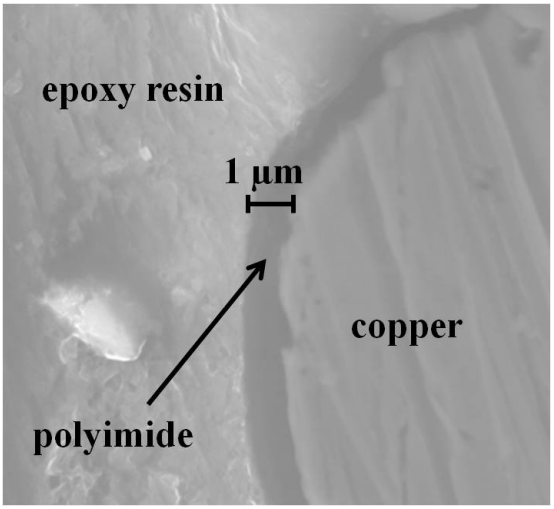

Figure 3.2: SEM cross-section image of the Elektrisola yarn.

Copper yarns.

During the course of my doctorate, I also used a structure similar to the Elektrisola yarns described in the previous paragraph. This second type of yarn is obtained by starting with a copper wire (50 or 150 μm of diameter) produced by Elektrisola on which I deposited a thin film of organic insulator, namely parylene C (see paragraph 3.2).

Cellulose yarns.

As stated at the beginning of the chapter, during the last two years of my doctorate, I focused my attention especially on the utilisation of natural cellulose fibres as substrates for the realisation of organic devices.

In the following sections, the basic physical and chemical properties of cellulose will be described, in order to understand how they can be modified to make it suitable for electronic applications.

Cellulose: chemical structure.

Cellulose is a polymer belonging to the family of *polysaccharides*, that means it is composed of single sugar molecules (monomers) joined by covalent bonds (usually called *glycosidic bonds*) [5].

In the case of cellulose, the monomers are represented by D-glucose molecules connected, above the plane containing the monomers, by means of an ethereal bridge in correspondence with the positions 1 and 4 (β-*glycosidic bond*), as depicted in Fig. 3.3.

Cellulose is the most important component of cell wall of green plants and algae, but also some species of bacteria (for instance, from the genus *Acetobacter*) are able to synthesise it [6].

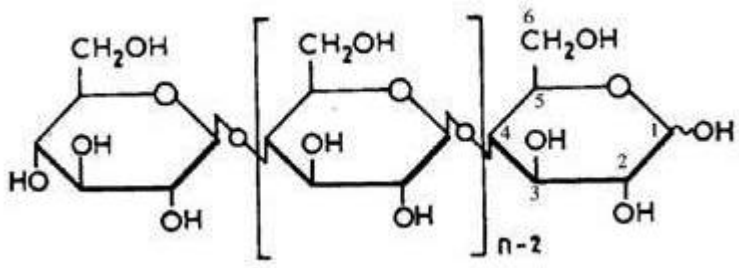

Figure 3.3: Chemical structure of cellulose.

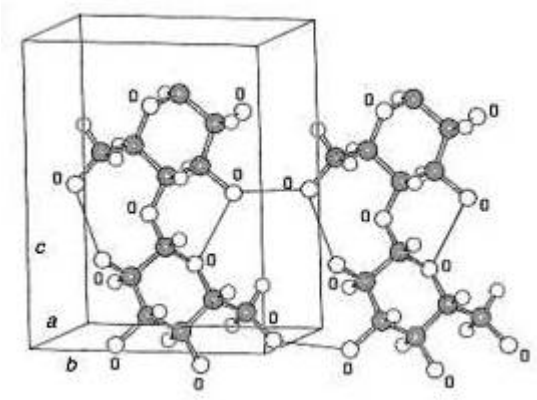

Figure 3.4: I_β cellulose crystal. The crystal axes (a, b and c) are also shown.

From an industrial point of view, cellulose is essential for the production of paper and is also the major constituent of plant fibres used in the textile field such as hemp, linen and cotton.

Cellulose: chemical and physical properties.

Cellulose has a structure quite similar to that of other polysaccharides, such as starch and glycogen, but its special β-glycosidic bonds yield it properties which are almost unique in the world of biopolymers.

The multiple hydroxyl groups on the glucose molecules make cellulose extremely hydrophilic (contact angle of 20-30 °); nonetheless, cellulose is insoluble in water (unlike glycogen and, to a lesser extent, starch) and in most organic solvents. Cellulose can be dissolved only by treating it with highly concentrated aqueous alkali solutions at high temperature [7].

Cellulose is a straight chain polymer (once again, unlike starch and glycogen) and, thanks to the presence of so many hydroxyl groups, very strong inter and intra-molecular hydrogen bonds form between the different polymer chains, holding them firmly together side-by-side. The result is that cellulose arranges in yarn-like structures (called *microfibrils*) characterised by high tensile strength [8].

Several different crystalline structures of cellulose are known, corresponding to the different arrangements of hydrogen bonds. Natural cellulose produced by higher plants usually shows a crystalline form known as I_β, depicted in Fig. 3.4.

Since my work on cellulosic fibres was essentially focused on cotton, in the following section I will briefly describe the mechanical and electrical properties of cotton fibres.

Cotton fibres.

Cotton is the name given to the cellulosic fibres that grow in a protective capsule, around the seeds of cotton plants of the genus *Gossypium*.

Although the exact chemical composition of dry raw cotton depends on the specific variety considered as well as the cultivation conditions, the typical mean values are shown in the following table [10]:

Chemicals	*Composition (%)*
Cellulose	97.0
Proteins	1.0
Oil and wax	0.4
Pectins	0.4
Minerals	0.7
Others	0.5

It can be easily noticed that the cellulose content of cotton fibres is incredibly high; cotton, indeed, is the fibre richest in cellulose.

Before being used for textile applications, cotton is usually treated in order to remove impurities from fibres. After these treatments, fibres show a cellulose content up to 99 %.

Another common treatment performed on raw cotton fibres is *bleaching*, usually by means of peroxides, which changes the yellow-brownish natural colour of cotton into bright white.

The quality of a cotton yarn is usually referred to its behaviour in response to the application of mechanical stimuli. A complete, mechanical characterisation of a textile fibre requires the measurement of several, different parameters (Hodgkinson lists at least *ten* [11]).

However, the most important mechanical parameters used to describe the properties of natural fibres are those extracted from the stress-strain curves [12]. In a stress-strain test, the samples extremities are fixed to two clamps, able to apply a controlled force parallel to the sample longitudinal axis.

A stress-strain curve is a graphical representation of the relationship between stress, derived from measuring the load applied on the sample, and strain, derived from measuring the deformation of the sample, i.e. elongation, compression, or distortion.

Measurement usually ends when the sample gets physically ruptured.

An example of stress-strain curve is shown in Fig. 3.5.

From a stress-strain curve, the following parameters (essential to evaluate the mechanical properties of the fibre) may be extracted:

- *Young's modulus*: usually defined as the slope of the stress-strain curve in the initial (quasi)-linear trait. Being the ratio between the stress and the corresponding elongation, it should be expressed as [Stress]/[Elongation]; however, since elongation is a dimensionless quantity, Young's modulus is formally measured using the same units for the stress. It means that, in SI units, it is measured in Pa (more commonly using its multiples, such as MPa or GPa). Young's modulus is a measure of the yarn's resistance to elastic deformation; high values of this parameter indicate that the yarn requires the application of intense forces in order to be deformed (elongated);

- *Stress at break*: the mechanical stress applied in correspondence with the sample's physical rupture. In SI units, it is measured in Pa (more commonly using its multiples, such as

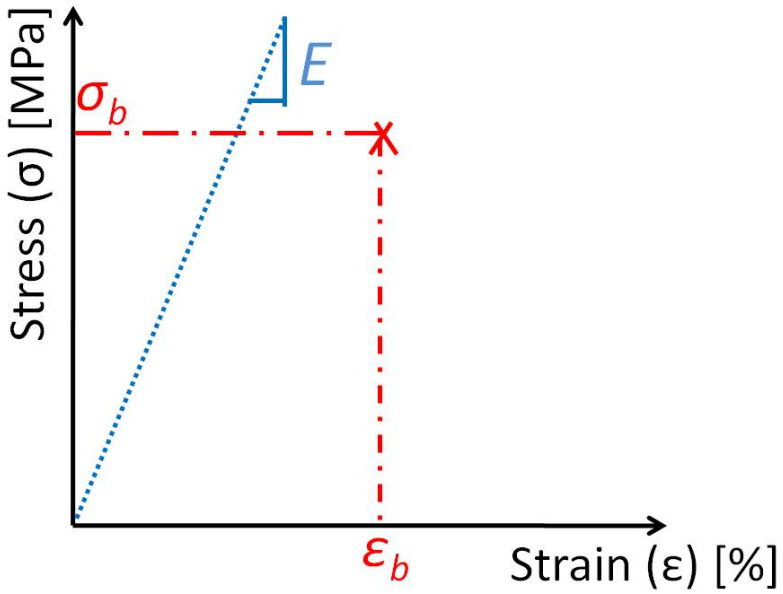

Figure 3.5: Example of a stress-strain curve on a cellulosic fibre.

MPa or GPa). Stress at breaks refers to the capability of the yarn to resist breaking under tensile stress;

- *Elongation at break*: elongation recorded at the moment of rupture of the specimen, often expressed as a percentage of the original length. It is a dimensionless quantity. It refers to the capability of the yarn to elongate, when subjected to tensile stress, before breaking. Some fibres will break immediately without showing any significant elongation (low elongation at break), others will elongate much and eventually break (high elongation at break).

If the yarn's physical breaking occurs in the linear trait of the stress-strain curve, then the relationship between the three quantities mentioned above may be expressed as follows:

$$\sigma_b = E \cdot \epsilon_b \tag{3.1}$$

where σ_b is the stress at break, E is Young's modulus and ϵ_b is the elongation at break. The typical values of these three parameter for cotton fibres are given in the table below [13]:

Quantity	*Value*	*Unit*
Young's modulus	5300 - 8000	MPa
Stress at break	400 - 850	MPa
Elongation	3 - 8	%

Besides their mechanical properties, in view of potential applications in the field of wearable electronics, natural cellulosic fibres may be also characterised by examining their electrical behaviour.

Even though electrical resistance of cotton fibres depends on several environmental parameters, such as air moisture and temperature, as well as the geometrical characteristics of the yarns, its mean values are always around 10^9 Ω/cm: cotton (like all other cellulosic fibres) is therefore intrinsically insulating [13].

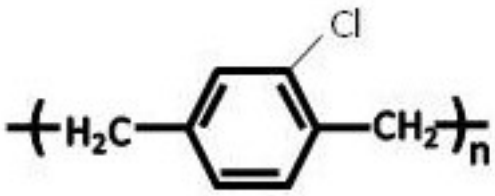

Figure 3.6: Monomer of parylene C.

3.2 Materials: Organic dielectrics (parylene).

"Parylene" is actually a trade name commonly used to indicate a family of polymers known as poly(para-xylylenes) according to IUPAC nomenclature [4]. These polymers are usually obtained starting from a certain amount of dimer which is treated and deposited by means of a Chemical Vapour Deposition (CVD) process (for details on the procedure see paragraph 3.6).

The specific type of parylene used in my research is called *parylene C*. Its monomer is made of a benzene ring to which two -CH_2- groups are connected in para position, while a chlorine atom (hence the name parylene *C*) is connected in ortho position (Fig. 3.6).

Parylene films are characterised by the following interesting properties [14]:

- high crystallinity;
- high molecular weight;
- extreme resistance to chemical attacks (and therefore high compatibility with most of the solvents commonly used in the cleaning and processing of electronic circuits and systems);
- excellent dielectric properties (if thick enough, parylene films are almost pore-free);
- (relatively) uniform thickness;
- capability to form layers perfectly conformal to the substrate.

Along with the characteristic described above, parylene C also exhibits the features listed below [14] [15]:

- extremely low permeability to gases and moisture;
- very high elongation to break;
- biocompatibility.

Parylene C is characterised by a relative dielectric constant value of 3.15 (value acquired at 60 Hz), while its electrical resistivity (at 20 °C) is $6 \cdot 10^{16}$ Ω/cm [16].

3.3 Materials: Organic semiconductors.

Pentacene.

Pentacene is an organic molecule (chemical formula: $C_{22}H_{14}$) belonging to the family of *polyacenes*, it is therefore a planar molecule composed of five linearly fused benzene rings (Fig. 3.7).

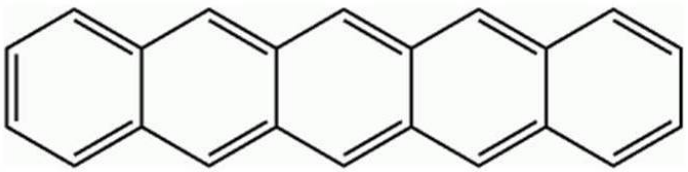

Figure 3.7: Pentacene molecule.

At ambient conditions, pentacene appears as a bright, purple powder; due to its insolubility in most of common organic solvents, it us usually deposited by means of thermal evaporation.

As stated in Chapter 1, the morphology of a polymeric solid strongly depends on the deposition technique and conditions, but usually thermally evaporated pentacene forms polycrystalline films, even though different crystal structures and morphologies have been observed [17].

In the scientific literature, many various structures and methods to measure the "band gap" of pentacene (i.e. the energy difference between HOMO and LUMO) have been proposed. The results obtained depend on many factors, for instance:

- pentacene morphology;
- materials used in combination with pentacene;
- techniques employed in order to measure the gap.

That being said, the value measured is consistently ~ 2 eV[18] [5]: pentacene is therefore a semiconductor.

Fullerene [C_{60}]

According to IUPAC definitions, *fullerenes* are organic compounds composed solely of an even number of carbon atoms, which form a cage-like fused-ring polycyclic systems [4].

The most important fullerene, from the point of view of Organic Electronics, is without doubt the *buckminsterfullerene*, with the formula C_{60}. This molecule is a truncated icosahedron made of 20 hexagons and 12 pentagons, with a carbon atom at the vertices of each polygon and a bond along each polygon edge (Fig. 3.8).

C_{60} is an extremely hydrophobic molecule, but it exhibits a good solubility in non-polar solvents, such as benzene and its derivatives [20]. In order to improve its solubility in polar solvents, in particular water, various derivatives have been synthesised and characterised [21].

The most common method used at present to obtain high quality C_{60} thin film is thermal evaporation in high vacuum [22].

Thermally evaporated buckminsterfullerene usually forms polycrystalline films [23]; spectroscopic studies performed on such films have shown that its band gap is ~ 2.2 eV.

Probably the most important property of C_{60} and its derivatives is that, in combination with commonly used materials (such as, for instance, Au and SiO_2) they usually exhibit an electron-type, rather than hole-type, conduction [24]; fullerene may be therefore considered as one of the few n-type organic semiconductors (even though ambipolar behaviour has been also demonstrated [25]; see also paragraph 1.5.1 of Chapter 1 for remarks on the concept of n-type and p-type in organic FETs).

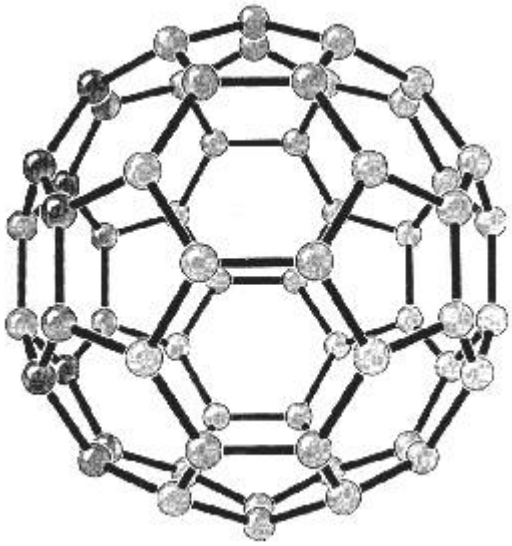

Figure 3.8: Buckminsterfullerene molecule.

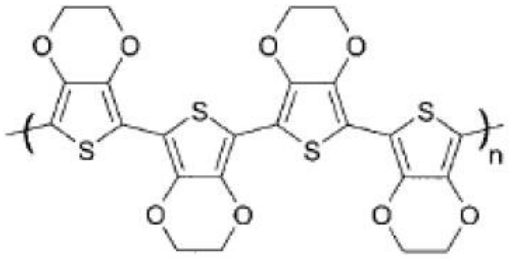

Figure 3.9: PEDOT chain.

Poly(3,4-ethylenedioxythiophene) and its derivatives.

Poly(3,4-ethylenedioxythiophene)[PEDOT] is an organic polymer belonging to the family of *polythiophenes*. Its monomer is composed of an aromatic thiophene ring with the carbon atoms in position 3 and 4 connected by means of a double ethereal bridge (Fig. 3.9).

PEDOT was synthesised for the first time in 1988 by Jonas and co-workers in Bayer AG Labs [26] [27].

Although initially conceived to be an easily soluble polymer, PEDOT turned out to be insoluble in many common organic solvents. Notwithstanding this, it exhibits some very interesting properties. First of all, it is characterised by very high conductivity (up to $\sim$ 200 S/cm). In addition to that, PEDOT shows very high chemical stability in its oxidised state and thin films of oxidised PEDOT are found to be almost transparent [28].

The problem related to the very low solubility was solved by doping PEDOT with other chemicals. The following sections will deal with the two PEDOT derivatives used in the experimental activity performed in the course of my doctorate.

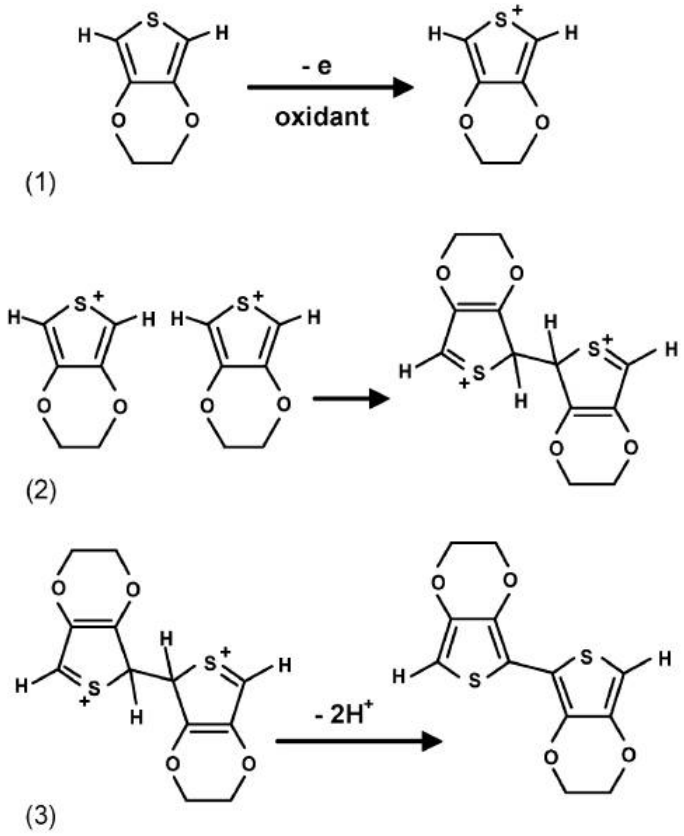

Figure 3.10: Formation of PEDOT chains in VVP polymerisation process.

PEDOT:tosylate.

This PEDOT derivative is produced by means of a Vacuum Vapour Phase (VVP) polymerisation process starting from the monomer (EDOT) in its vapour phase by means of an oxidising agent.

A three-step polymerisation process was proposed by Fabretto *et al.* in order to explain the formation of PEDOT derivatives in presence of oxidising agents [29]. This process may be schematically described as follows (Fig. 3.10):

1. the oxidant oxidises the monomer;

2. couples of oxidised monomers combine to form positively charged dimers;

3. protons are removed from dimers (probably by residual water vapours contained into the vaporisation chamber) and then stabilise;

4. the oxidation process is repeated starting from dimers, which combine to form tetramers and so on.

In the case of PEDOT:tosylate, the oxidant used to start the polymerisation process is iron tosylate (Fe(III):p-toluenesulphonate), an iron salt of p-toluensulphonic acid depicted in Fig. 3.11.

Morphological studies based mainly on spectroscopic techniques [30] have shown that VVP-deposited PEDOT:tosylate films are essentially polycrystalline. The crystals are composed of

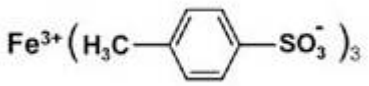

Figure 3.11: Chemical structure of iron tosylate.

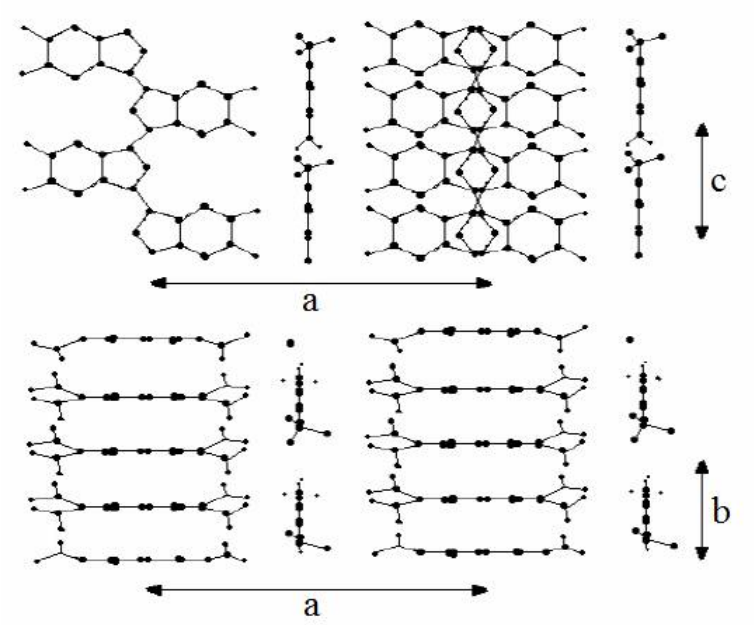

Figure 3.12: Unit cell of PEDOT:tosylate crystals.

pseudo-orthorhombic unit cell with four monomers and one tosylate ion per cell, as pictured in Fig. 3.12.

PEDOT:tosylate thin film may exhibit very high conductivity (up to 10^3 S/cm); in such films, the measured band gap is rather low (< 1.5 eV) [31].

PEDOT:PSS.

In this particular case, PEDOT is doped by a water-soluble polyelectrolyte, namely poly(styrene sulphonic acid) [PSS]. PSS, in analogy with tosylate anions, acts as an oxidant and removes electrons from thiophene rings of PEDOT. The result is that PEDOT chains become positively charged while, on the other hand, PSS chains acquire negative charges so that an electrostatic attraction develops between the two (Fig. 3.13).

The doping of PEDOT with PSS results in many modifications of PEDOT behaviour.

First of all, PSS anions act as emulsifiers for PEDOT, so that the PEDOT:PSS blend is soluble in water and in many other organic solvents [32], which makes PEDOT:PSS very easy to use and process.

On the other hand, it is also true that PEDOT:PSS usually shows a conductivity lower than that of pristine PEDOT. This is usually explained as follows: notwithstanding the doping, which should normally result in a conductivity increment (see Chapter 1), PSS forms large insulating regions surrounding conductive PEDOT spots [33]. As a consequence, many PEDOT:PSS preparations available on the market usually exhibit conductivities lower than 1 S/cm [34].

In order to increase PEDOT:PSS conductivity, several chemical treatments have been proposed [32].

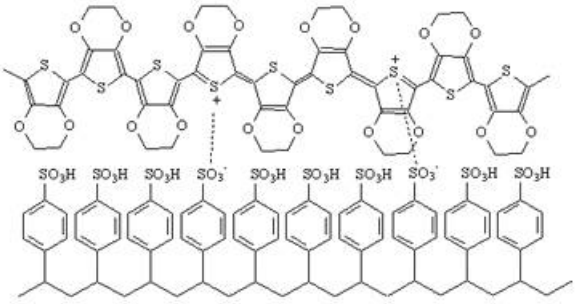

Figure 3.13: Structure of PEDOT:PSS.

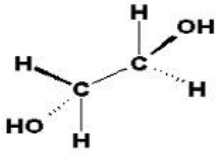

Figure 3.14: Structure of ethylene glycol.

In 2002, it was reported by some research group that conductivity of PEDOT:PSS could be increased more than two orders of magnitude if the semiconductor was properly treated with certain organic compounds [35] [9].

Many of the different compounds used in these studies belong to the family of *polyalcohols*, which means that they have two or more hydroxyl groups bonded to sp^3-hybridised carbon atoms.

Among polyalcohols, a special role is played by ethylene glycol (EG), whose chemical structure is depicted in Fig. 3.14.

The goals achieved with EG treatment are [37]:

- conductivity is increased up to 200 times;
- PEDOT:PSS becomes insoluble in water.

The combination of these two results is particularly important in those applications (for instance, in the electrochemical field) where PEDOT:PSS films have to be put in touch with water-based solutions. Indeed, PEDOT:PSS may be initially processed by simple methods such as spin coating and then treated with EG in order to increase its conductivity and, at the same time, make it insoluble in water and other solvents.

The exact mechanism responsible for such modifications is still unknown. However, Ouyang *et al.*, on the basis of spectroscopic experiments, speculate [37] that treatment with EG transforms PEDOT from benzoid (i.e. aromatic) to quinoid (i.e. non aromatic) (Fig. 3.15). Quinoid PEDOT is able to form very long, linear chains characterised by extremely strong interchain interactions which determine both the increase in conductivity and insolubility.

3.4 Materials: metal nanoparticles.

At present, there is no accepted international consensus on what a nanoparticle exactly is, however it is usually recognised that any particle smaller than 100 nm may be defined as a nanoparticle [39].

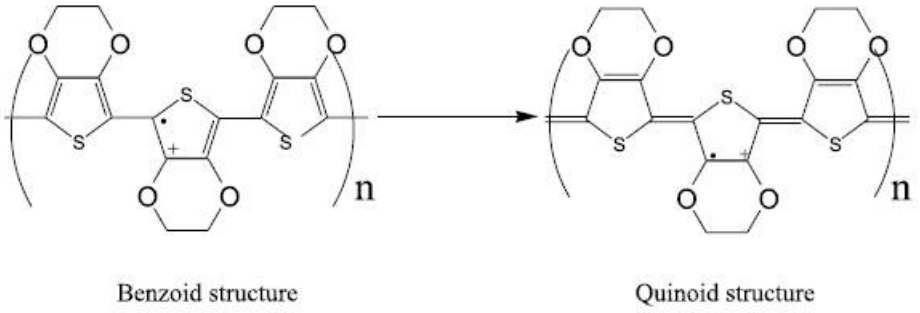

Figure 3.15: Transition of PEDOT:PSS from benzoid to quinoid structure induced by EG treatment.

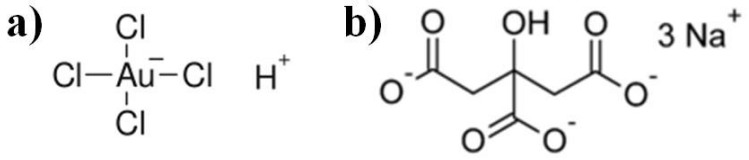

Figure 3.16: Chemical structure of a) chloroauric acid b) trisodium citrate.

Although several methods for the synthesis of metal nanoparticles have been proposed, the one introduced by Turkevich *et al.* [40] almost sixty years ago remains the most common and, perhaps, the simplest ever described.

Using this method, spherical metal nanoparticles (average diameter $\sim$ 30 nm) can be produced, in the form of a water-based colloid.

Our attention will be essentially focused on the production of gold nanoparticles, but similar considerations may be made for other metals.

The Turkevich method is based on a reduction-oxidation reaction occurring between a metallic chloride and a reducing agent. In the case of gold nanoparticles, chloroauric acid ($HAuCl_4$)is used as a source of gold chlorides while sodium citrate (for instance, trisodium citrate, $Na_3C_6H_5O_7$) is used as a reducing agent [41]; the chemical structure of these two chemicals is shown in Fig. 3.16.

In a schematic way, the formation of gold nanoparticles may be explained as follows. Firstly, a small amount of chloroauric acid is dissolve in water and dissociates as shown in equation 3.2:

$$HAuCl_4 \rightarrow H^+ + (AuCl)_4^- \tag{3.2}$$

Then, sodium citrate is added to the solution, under heating and vigorous stirring. The function of sodium citrate is twofold [42]:

- reduce gold from its oxidised Au(III) state to its neutral metallic state;
- surround metallic gold and prevent aggregation of nanoparticles.

Fig. 3.17 shows a schematic view of a single gold nanoparticle surrounded by citrate anions (left) and a TEM image of gold nanoparticles in a colloid drop (right).

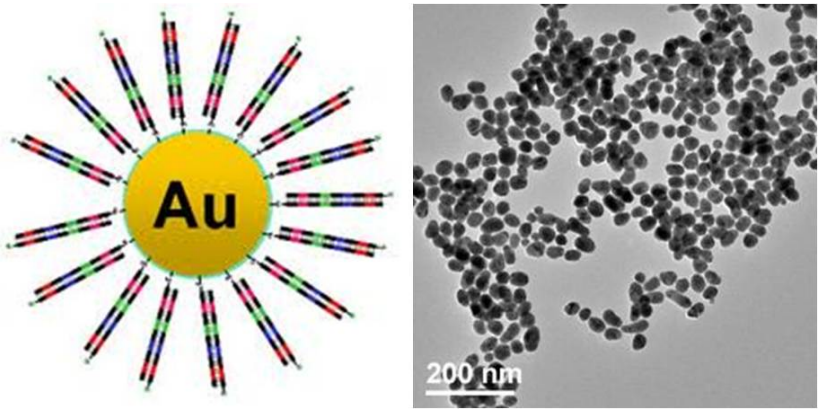

Figure 3.17: Au nanoparticles: schematic view (left) and TEM image (right).

3.5 Methods: vacuum thermal evaporation.

The vacuum thermal evaporation deposition technique is used in order to deposit thin films of solid materials on a substrate (typically, but not exclusively, a planar substrate).

This technique consists in heating the material to be deposited until its evaporation or sublimation occurs [43].

The material vapour finally condenses in form of thin film on the cold substrate surface and on the vacuum chamber walls.

Usually low pressures are used, about 10^{-6} or 10^{-5} Torr, in order to avoid chemical or physical interactions between the vapour and the residual atmosphere. At these low pressures, the vapour atoms are able to move through the vacuum chamber in straight lines from the evaporation source towards the substrate. This originates 'shadowing' phenomena with 3D objects, especially in those regions not directly accessible from the evaporation source (crucible).

In the evaporation deposition technique, the material is deposited into a small metallic or glass container, called *crucible*. The crucible heating may be performed by means of several techniques; the equipment in our laboratory utilises, in particular, the *Joule effect*, which means that heat is generated by an electrical current passing through a filament surrounding or composing the crucible.

For this reason, the metal employed for the realisation of the crucible must have a very high fusion temperature. A typical metal used as heating resistance is therefore tungsten (W) (T_{fusion} = 3422 °C).

A schematic view of the vacuum equipment used in the laboratory is showed in Fig. 3.18.

In my research activity, thermal evaporation was used to deposit pentacene (sublimation temperature $\sim$ 145 °C) [44] and C_{60} (sublimation temperature $\sim$ 650 °C) [45] for the realisation of OFETs on yarn.

3.6 Methods: Chemical Vapour Deposition of parylene.

Parylene C is deposited on samples by means of a Chemical Vapour Deposition (CVD) process.

A schematic view of the equipment used for this CVD is provided in Fig. 3.19.

As already stated in paragraph 3.2, the deposition of parylene [46] starts placing the samples to be covered with parylene into the polymerisation chamber and a certain amount (usually a few grammes) into the vaporisation chamber.

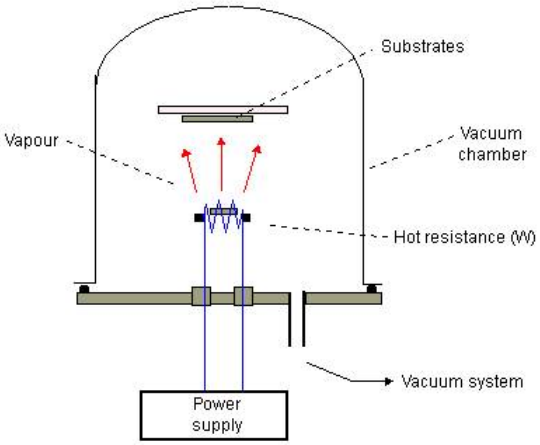

Figure 3.18: Schematic view of a vacuum thermal evaporation system.

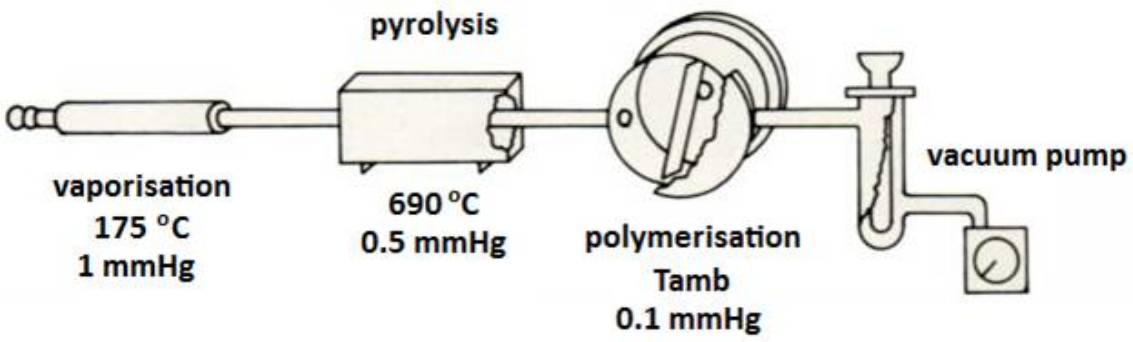

Figure 3.19: Schematic view of the CVD system used for the deposition of parylene.

The vacuum pump is then switched on and until a pressure of $\sim$ 1 mmHg is reached. Temperature of the vaporisation chamber is then gradually increased so that the dimer contained in it begins to sublimate.

Dimer vapours then reach the pyrolysis chamber in which, at a pressure of $\sim$ 0.5 mmHg, a temperature of 690 °C is maintained. Such a high temperature decomposes each dimer molecule into its two constituent monomers.

Monomer vapours (extremely unstable, from a chemical point of view) are eventually pumped into the polymerisation chamber where, at ambient temperature and at a pressure of $\sim$ 0.1 mmHg, they start to polymerise by forming covalent bonds between one another.

When polymer chains are long enough, they are driven by gravity towards the substrate, conformally coating it.

In my experimental research, parylene C was used as gate dielectric of OFETs realised on both metallic and cotton yarns.

3.7 Methods: spin coating.

Spin coating is a simple method used in order to deposit a liquid onto a planar substrate.

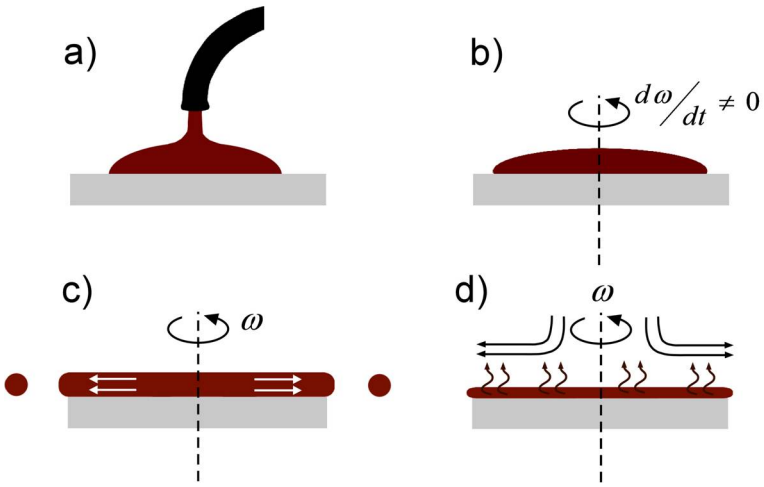

Figure 3.20: Phases of the spin coating process.

In a spin coating process, the sample is fixed at the centre of a spinning substrate, usually shaped as a disc. Then a certain amount of the liquid materials to be deposited on the sample is put on the sample's surface. The substrate is then spun round (the rotation speed depends on several parameters) so that the fluid is spread uniformly by centrifugal force and the liquid excess is expelled from the sample [47].

The thickness and morphology of spin coated layers depend on several factors [48]:

- chemical composition of the deposited liquid;
- chemical and physical properties of the solvents employed to make the solution;
- rotation speed and rotation time;
- optional substrate heating.

The different phases of the spin coating process (a) deposition of the liquid, b) acceleration of the substrate, c) formation of the thin film, d) evaporation of the solvent) are schematically described in Fig. 3.20.

In my experimental activity, spin coating was used to deposit a thin layer of PEDOT:PSS on small pieces of plastic substrates (mainly polydimethylsiloxane substrates). These substrates were then used as "stamps " with the purpose to contact the yarns' outer surface during the measurements on OFETs.

3.8 Samples preparation: logic inverters on Elektrisola yarns.

My experimental activity started with the construction of logic inverters realised starting from pentacene-based Organic Field Effect Transistors (OFETs) on Elektrisola yarns (described in section 3.1.1).

Each transistor is realised depositing a thin pentacene (nominal thickness 50 nm) film at pressure below $2 \cdot 10^{-5}$ mbar, at a constant rate of ~ 4 Å/min.

These transistors were completely characterised during a M. of Science Thesis carried out before my doctorate [1]; their structure is shown in Fig. 3.21.

In order to obtain a logic inverter, the *saturated-load* configuration was chosen; the two different transistors were fixed on a plastic (namely, PET) substrate and the connections were made by means of thermally evaporated gold. The final circuit is shown in Fig. 3.22.

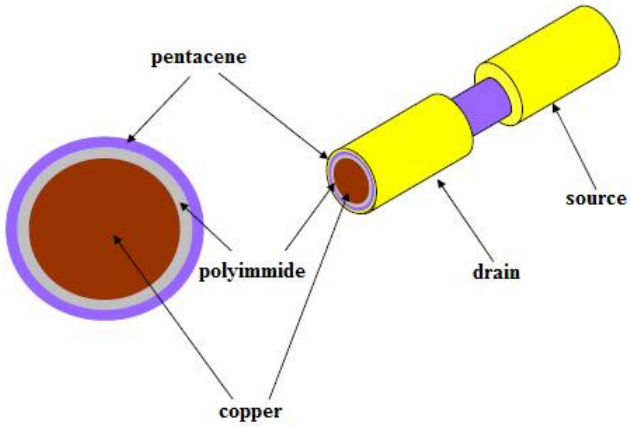

Figure 3.21: Schematic view of pentacene-based OFET.

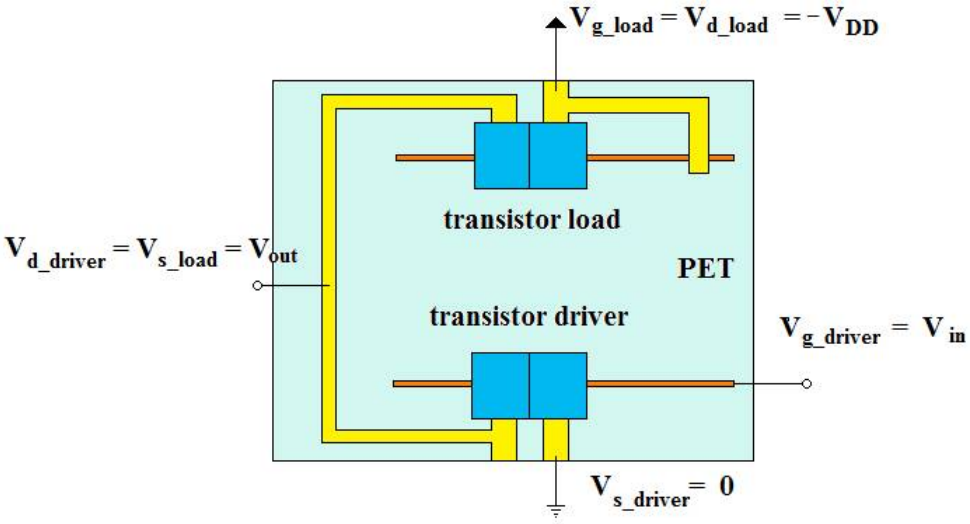

Figure 3.22: Schematic view of pentacene-based logic inverter.

3.9 Samples preparation: ambipolar OFETs on Elektrisola yarns.

These ambipolar devices on yarn [49] were realised by depositing, by vacuum thermal evaporation, on the Elektrisola yarn a first layer of pentacene (nominal thickness: 20 nm) and, on the top of it, a second layer of fullerene C_{60} (nominal thickness: 35 nm).

Both deposition processes occurred at pressure below $2 \cdot 10^{-5}$ mbar, at a constant rate of $\sim$ 5 Å/min.

A polydimethylsiloxane (PDMS) stamp, reproducing source and drain geometry, was coated with a very thin PEDOT:PSS film, and finally the yarn was sandwiched between a cover slide where two gold electrodes had been previously deposited and the PEDOT:PSS coated PDMS stamp. In this way source and drain electrodes can be easily accessed and a stable contact is therefore realised.

The device is illustrated in Fig. 3.23.

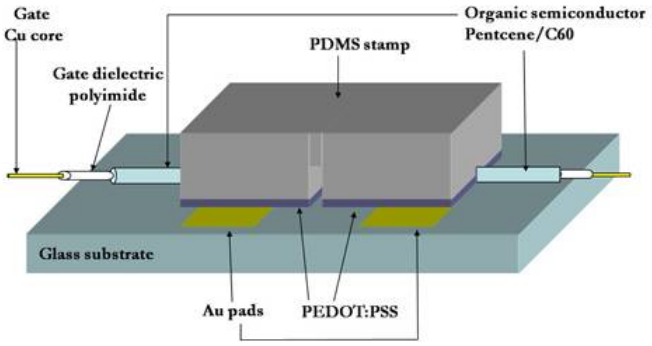

Figure 3.23: Schematic representation of ambipolar organic OFETs on yarn.

3.10 Samples preparation: p-channel OFETs on copper yarns.

The core of these devices is the copper yarn described in paragraph 3.1.2., acting as the transistor gate electrode.

All around these yarns, parylene C was deposited (nominal thickness: 2 μm) and, on the top of the dielectric, pentacene was thermally evaporated, with the usual conditions (pressure below $2 \cdot 10^{-5}$ mbar, at a constant rate of $\sim$ 4 Å/min).

Finally, the source and drain contacts were realised by means of a PEDOT:PSS coated PDMS stamp, as described in the previous section.

3.11 Samples preparation: conductive cotton yarns.

In order to obtain conductive yarns starting from cotton wires, two different procedures were followed. They are treated separately in the following two sections.

Conductive cotton yarns: Au nanoparticles and PEDOT:tosylate deposition.

As a first step, cotton yarns were rendered cationic, which means that cellulose was chemically modified so that the yarns were uniformly covered with a layer of positive charges.

To do that, I followed a procedure already reported by Hinestroza and co-workers [50].

The cationic solution is composed as described hereafter: 100 g of (3 – chloro – 2 – hydroxypropyl)trimethylammonium chloride (CHTAC, 65% solution in water) and 45.5 g of NaOH were mixed into 200 ml of deionised water. Yarns were firstly dipped in the solution at 50 °C for 30 min then dried at 120 °for 15 min, rinsed several times with deionised water and dried again at 60 °for 30 minutes.

A schematic view of cationic cellulose is given in Fig. 3.24.

The cationic samples were then decorated with Au nanoparticles using the procedure described by Hinestroza *et al.* [50].

The procedure for the preparation of Au nanoparticles solution may be summarised as follows. An aqueous solution of hydrogen tetrachloroaurate trihydrate (0.05 g in 45 mL of deionised water) was heated at 90 °C for 10 min. An aqueous solution of sodium citrate tribasic dihydrate (0.02 g in 5 mL of deionised water) was introduced to the gold salt solution under vigorous stirring and heated for 1 h at 90 °C till the solution became uniform wine-red colour.

Pieces of the cationic cotton yarns were then immersed into a beaker containing 50 mL solution of Au nanoparticles so that these nanoparticles could form an electrostatic bond with cationic cellulose. After 48 h of soaking, the cotton specimens were removed from the container

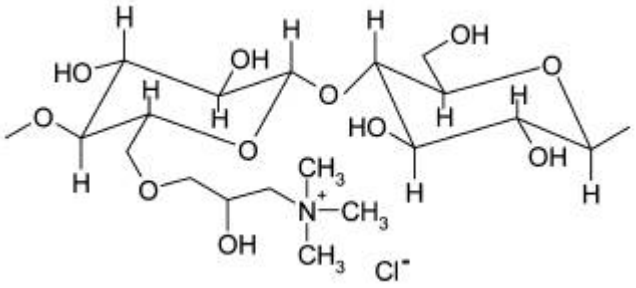

Figure 3.24: Molecular structure of cationic cellulose.

and rinsed thoroughly with deionised water, in order to remove loosely bound metal nanoparticles. The coated yarns were then dried in an oven at 60 °C for 30 min.

The second step of our process is the deposition of PEDOT:tosylate on our Au nanoparticles decorated yarns.

To do that, first of all one has to prepare the oxidising agent necessary to catalyse the polymerisation process. The catalyst is represented by a solution of 125:25:1 % wt of isopropanol:Fe(III)-tosylate:pyridine, made by dissolving 0.785 g of Fe(III)-tosylate in 5 mL of isopropanol and adding 32.1 μL of pyridine under vigorous stirring. The solution was filtered using a 0.45 μm PTFE filter. The cotton yarns were immersed into a beaker containing the Fe(III):tosylate solution. After 10 minutes of soaking, the yarns were removed from the beaker and dried on a hot plate at 80 °C for 3 min.

A vapour phase polymerisation (VPP) chamber was used to polymerise the EDOT into PEDOT. The cotton fibres, after the treatment with Fe(III):tosylate, were placed into the vacuum chamber and kept at 35°C while a crucible containing $\sim$ 100 μL EDOT was heated up to 80 °C. Pressure during polymerisation was around 100 Torr. Polymerisation time was approximately of 30 min. After polymerisation, the samples were dried in an oven at 50 °C for 30 min. Then they were soaked into ethanol for 10 min, in order to remove the iron. The samples were finally dried in a vacuum oven at room temperature for 12 hours.

It is worth noting that the deposition of PEDOT:tosylate may also occur on plain cotton yarns, so that a comparison in terms of conductivity may be performed between those yarns treated with both PEDOT:tosylate and Au nanoparticles and those covered only with PEDOT:tosylate.

Conductive cotton yarns: PEDOT:PSS deposition and treatment with ethylene glycol.

Another type of conductive cotton yarns was prepared using PEDOT:PSS.

The cotton yarns were soaked in an aqueous dispersion of PEDOT:PSS (CLEVIOS^{TM} PH 500, purchased from H.C. Starck and used as received) for 48 h at 6 °C.

Samples were then baked on a hotplate at 145 °C for 60 min.

After baking, samples were soaked in ethylene glycol (EG) (anhydrous, 99.8 %, purchased from Sigma Aldrich and used as received) for 3 min at room temperature. Then they were baked on a hotplate at 145 °C for 60 minutes.

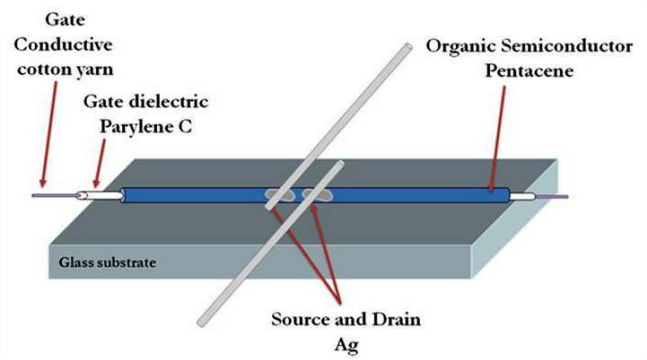

Figure 3.25: Schematic view of the cotton-based OFET.

3.12 Sample preparation: assembly of cotton-based Organic Field Effect Transistors.

The core of the cotton-based Organic Thin Film Transistors (OTFTs) is the yarn treated with PEDOT:PSS/EG described above, which acts as the gate electrode of the final device.

The gate dielectric layer has been realised by depositing a thin Parylene C film (nominal thickness 1.5 μm) on the entire yarn surface. After that, a thin pentacene (nominal thickness 50 nm) film has been deposited by thermal evaporation at pressure below $2 \cdot 10^{-5}$ mbar, at a constant rate of ~ 4 Å/min.

Source and drain electrodes have been realised by depositing two drops of conductive silver paint on the previously realised structure. The silver paint drops have been placed by means of a very sharp needle, in this way, a typical channel length of approximately 200 ± 50 μm have been obtained, whereas channel width is usually given by the average circumference of the employed yarn.

The device is illustrated in Fig. 3.25.

3.13 Sample preparation: assembly of cotton-based Organic ElectroChemical Transistors.

The core of the cotton-based Organic ElectroChemical Transistors (OECTs) is, once again, the yarn treated with PEDOT:PSS/EG.

In order to obtain a transistor, it was necessary to prepare a semi-solid electrolyte solution (electrolyte gel). To do that, the procedure described hereafter was followed. First, a 250 mM solution of KCl (potassium chloride) in deionised water was prepared. As a gelling agent, Bacto^{TM} Agar (purchased from DIFCO Microbiology, used as received) was employed. 0.75 g of Bacto^{TM} Agar were dissolved in 20 g of KCl aqueous solution (3.75 % in weight). The solution was then heated up at 90 °C and vigorously stirred for 60 min. After that, the gel was poured into a Petri dish and let cool down at room temperature until complete solidification occurred. To improve solidification, the gel was then stored at 6 °C for at least 24 h before being used.

The cotton-based OECTs were assembled as follows. A piece of PEDOT:PSS/EG treated yarn (1 cm) was inserted into the centre of a small parallelepiped of electrolyte gel (approximately: 6 mm^3) with the help of a needle. Two conductive cotton yarns (2 cm long), treated with Au nanoparticles and PEDOT:tosylate, were fixed at the end of the transistor with a simple knot and acted as source and drain electrodes. Another Au nanoparticles and PEDOT:tosylate treated yarn was fixed on the top of the electrolyte gel block and used as the gate electrode.

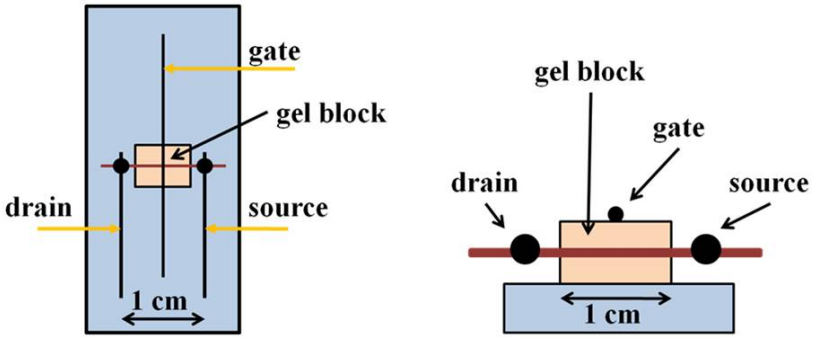

Figure 3.26: Schematic view of the cotton-based OECT, seen from above(left) and from one side (right).

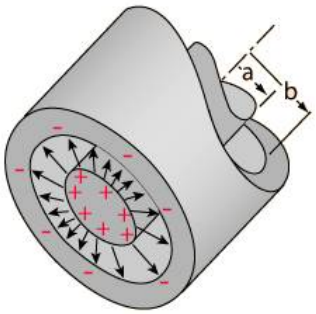

Figure 3.27: Structure of a cylindrical capacitor.

The final device is illustrated in Fig. 3.26.

3.14 Samples characterisation: capacitive measurements.

In order to extract physical parameters from current-voltage characteristics of OFETs it is essential to know the insulating layer capacitance.

If the dielectric used is completely characterised (i.e. its dielectric constant has already been determined) and if the capacitor geometry is known, the calculation of capacitance may be done quickly by applying simple formulae.

Sometimes, however, the capacitor geometry is not known; in that case capacitance has to be measured directly and geometry may be reconstructed by means of inverse formulae.

Since devices I studied are characterised by a cylindrical geometry, the base of this discussion is, of course, the structure of a cylindrical capacitor.

A capacitor is a passive electronic component consisting of two conductive surfaces (the *plates*) separated by a non-conductor (dielectric); when a voltage is applied between the two plates, a static electric field is generated across the dielectric and charges are accumulated on the plates surface [51].

The ratio between the charge stored on the plates surface and the applied voltage is called *capacitance* and is, ideally, a constant.

A cylindrical capacitor is composed of two conductive cylinders. One of them is inserted into the other and they are separate by an insulating layer (see Fig. 3.27).

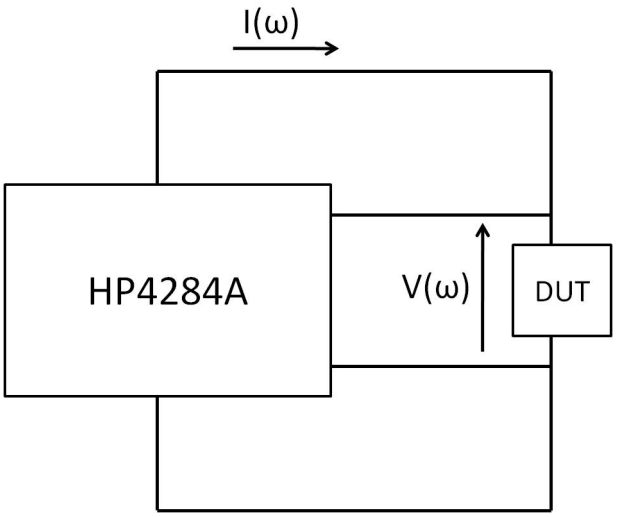

Figure 3.28: Scheme of capacitive measurements.

A cylindrical capacitor is therefore characterised by two geometrical parameters: the radius of the inner cylinder (a in Fig. 3.27) and the radius of the outer cylinder (b in Fig. 3.27). The dielectric thickness is, of course, (b - a).

The capacitance of a cylindrical capacitor is given by the following formula [52]:

$$C = L \cdot \frac{2\pi\epsilon_0\epsilon_r}{\ln\frac{b}{a}} \tag{3.3}$$

where L is the capacitor length, ϵ_0 is vacuum permittivity ($\sim 8.85 \cdot 10^{-14}$ F/cm) and ϵ_r is the dielectric relative permittivity.

Considering that a cylinder, with radius b and height L, has a lateral surface of $2\pi b\ L$, the capacitance per unit area of such capacitor is defined as:

$$\frac{C}{A} = \frac{\epsilon_0\epsilon_r}{b \cdot \ln\frac{b}{a}} \tag{3.4}$$

During my experimental activity, capacitance values were measured using an LCR Meter, namely the Hewlett Packard HP4284A.

This instrument is actually able to measure the complex impedance (as a function of frequency) of the device under test (DUT), as illustrated in Fig. 3.28.

As shown in Fig. 3.28, capacitive measurements require the presence of four probes. Two of them inject a variable current *I(ω)* while the other two (connected closer to the sample) measure the corresponding voltage drop *V(ω)*. The separation of current injection from voltage measurement is actually very important because this way it is possible to neglect the contribution of contact resistances [53].

The quantity actually measured by the HP4284A is a complex impedance *Z(ω)*, defined as follows:

$$Z(\omega) = \frac{V(\omega)}{I(\omega)} \tag{3.5}$$

This impedance is then associated to a circuit model properly selected by the user among a list provided by the instrument. For capacitors with organic dielectrics, it has been demon-

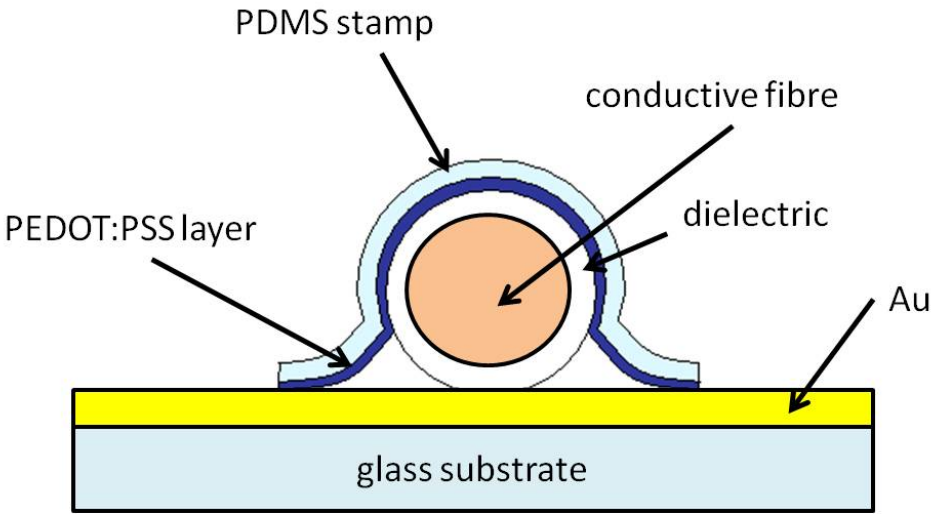

Figure 3.29: View of cylindrical capacitors.

strated that a good equivalent circuit is represented by a parallel RC circuit, where the parallel capacitance C_p represents the capacitive coupling of the two plates and the parallel resistance R_p describes the leakage current flowing through the dielectric [16].

The impedance of a parallel RC circuit is expressed by the following formula [55]:

$$Z(\omega) = \frac{R_p}{1 + j\omega R_p C_p} \tag{3.6}$$

Thanks to equation 3.5, the HP4284A is able to calculate the values of C_p and R_p for any specific value of frequency.

In the course of my measurements I chose a frequency range relatively low (frequency sweep from 30 Hz to 1 MHz); this is essentially due to the fact that the OFETs I realised are polarised with continuous voltages and also that the parallel RC circuit model becomes much less accurate at high frequencies.

For each frequency, the instrument acquires a certain number of samples and the result provided is a mean of these values. In order to increase the accuracy of measurements, I set the HP4284A so that 16 samples for each frequency were obtained.

Lastly, it should be noticed that capacitance measurements were performed by sandwiching the yarn between a PEDOT:PSS coated PDMS stamp and a gold covered glass, as shown in Fig. 3.29. In this picture, it can be seen that the inner conductor is represented by the dark blue conductive yarn while the outer electrode is represented by the PEDOT:PSS layer surrounding (in the worst case) half of the yarn; the potential to the outer conductor may be applied connecting the electrode directly to the gold layer, which is short-circuited to the PEDOT:PSS layer surrounding the fibre.

As a consequence, the dielectric was not completely surrounded by a second conductive layer. Strictly speaking, therefore, our structures cannot be considered perfect cylindrical capacitors; however, assuming that PEDOT:PSS surrounds at least half of the yarn, we can consider an area which is approximately half of the lateral surface of a cylinder, that is πb, if the capacitor has a length L of 1 cm.

Under these hypotheses, the capacitance and the dielectric thickness may be represented as follows:

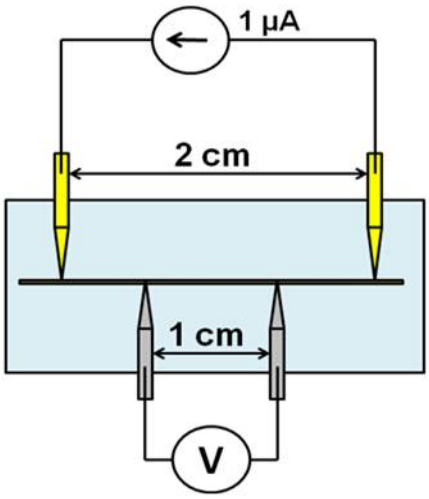

Figure 3.30: Resistance measurements on yarns.

$$C = (\pi b) \cdot \frac{\epsilon_0 \epsilon_r}{2b \cdot \ln \frac{b}{a}} \implies (b-a) = a\left(e^{\left(\frac{\pi \epsilon_0 \epsilon_r}{2 \cdot C}\right)} - 1\right) \tag{3.7}$$

3.15 Samples characterisation: resistance measurements.

In order to measure the resistance (per unit length) of our samples, the standard four probe method was chosen.

As already stated in the previous paragraph, with this method the current injection and voltage measurement are made by means of two different couples of electrodes, so that contact resistances of the voltmeter may be neglected.

The measurement system scheme is shown in Fig. 3.30.

It can be seen from Fig. 3.30 that the outer couple of electrodes was used in order to inject a current in the yarn (usually, the current value was 1 μA), while the inner couple of electrodes was used in order to measure the corresponding voltage drop.

For resistance measurements, a couple of Keithley 2612 Semiconductor Parameter Analysers was used (one as current source, the other as voltmeter).

3.16 Samples characterisation: OFETs current-voltage characteristics.

It has been stated in paragraph 1.5.1 that to power an OFET two different voltages have to be applied, namely the drain voltage V_{DS} and the gate voltage V_{GS} (the source is usually connected to the circuit ground).

The electrical characterisation of the transistor requires the acquisition of two different types of curve:

- I_{DS} - V_{DS} curves, in which the gate voltage is kept constant while drain voltage is swept in a proper range;

- I_{DS} - V_{GS} curves, in which the drain voltage is kept constant while gate voltage is swept in a proper range.

The protocol commonly followed for the characterisation of OFETs on yarns (both metal and cotton yarns) is summarised hereafter:

- I_{DS} - V_{DS} curves: V_{DS} swept in the range [0 ÷ -60] V with step of - 1 V, while V_{GS} varied in the range [+20 ÷ -100] V with steps of -10 V;
- I_{DS} - V_{GS} curves: V_{DS} was kept at -60 V while V_{GS} was swept in the range [+100 ÷ -100] with steps of -2 V.

3.17 Samples characterisation: OECTs current-voltage characteristics.

In order to polarise OECTs, two voltages are also required: the drain voltage V_{DS} and the gate voltage V_{GS} (once again, the source is usually connected to the circuit ground).

OECTs are usually characterised by means of I_{DS} - V_{DS} curves. In our devices V_{DS} varied from 0.5 V to –0.5 V with steps of -0.01 V (*forward curve*) and then again from –0.5 V to 0.5 V with steps of 0.01 V (*backward curve*).

OECTs may be also characterised by monitoring the I_{DS} in a certain time interval, while V_{DS} is kept constant and V_{GS} varies abruptly in order to determine an alternative on-off switch of the OECT. In our case, V_{DS} was fixed at -0.5 V while V_{GS} varied abruptly from 0 to 0.4 V (square wave) every 30 s.

For measurements on both OECTs and OFETs, a couple of Keithley 2612 Semiconductor Parameter Analysers was used (one as V_{DS} source, to measure the current I_{DS}, the other as V_{GS} source, to measure the I_{GS} leakage current).

3.18 Samples characterisation: Transmission Electron Microscopy.

In order to evaluate the morphology of cotton fibres treated with PEDOT:tosyalte and Au nanoparticles, a Transmission Electron Microscopy (TEM) analysis was performed on the cross sections of those samples.

In a conventional TEM analysis, a very thin slice (tens of nm of thickness) of the sample is irradiated with an electron beam of uniform current. These electrons are emitted into the *electron gun* by means of different physical phenomena (thermionic, Schottky or field emission are the sources commonly used) [56].

Once emitted, the electrons are accelerated by a high voltage field ($\sim$ 200 - 500 kV) and after having crossed a three or four-stage condenser-lens system they hit the sample, usually placed on a small copper grid.

An image is formed from the interaction of the electrons transmitted through the specimen; the transmitted electrons are magnified and focused onto an imaging device, very often a CCD camera [56].

The whole structure of this type of microscope is illustrated in Fig. 3.31.

Since electrons are characterised by an extremely small De Broglie length ($\sim$ 1 nm), the resolution achievable with a TEM system is higher than other microscopes, especially light microscopes. At present, TEMs are able to have atomic resolution (a couple of Å) [57].

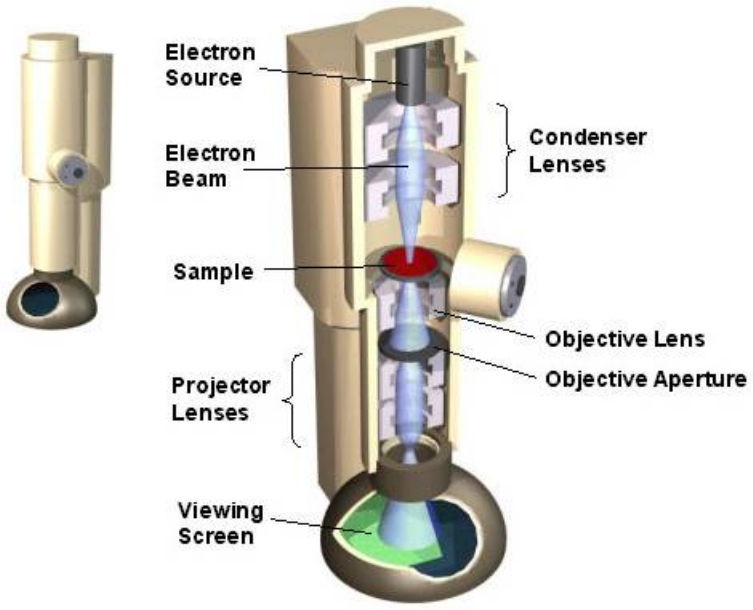

Figure 3.31: Scheme of a TEM microscope.

The information which one can obtain performing a TEM analysis may be grouped into three main categories [57]:

- *morphological information*: the size, shape and arrangement of the particles which make up the specimen as well as their relationship to each other on the scale of atomic diameters;
- *crystallographic information*: the arrangement of atoms in the specimen and their degree of order, detection of atomic-scale defects in areas a few nm in diameter;
- *compositional information* (if the microscope is so equipped): the elements and compounds the sample is composed of and their relative ratios, in areas a few nm in diameter.

Microscopic analysis on cotton samples was performed with the aid of a FEI Tecnai F20 high resolution TEM/STEM Microscope, available at the Nanoscale Facility Center at Cornell University (Ithaca, NY, USA); this microscope is also equipped with a Gatan tridium spectrometer for electron energy loss spectroscopy spectra at high energy resolution (< 0.2 eV).

3.19 Samples characterisation: mechanical analysis of conductive cotton fibres.

The cotton samples treated with PEDOT:tosylate and Au nanoparticles were mechanically characterised through the acquisition of stress-strain curves using a TA Instruments DMA Q800 Dynamic Mechanical Thermal Analyser, available at Materials Research Center, Cornell University (Ithaca, NY, USA).

Samples (4 cm long) were fixed at the end of two metallic clamps then a variable tensile stress, within the range $[0.1 \div 20]$N (step: 0.3 N), was applied to each sample until physical rupture occurred.

Fig. 3.32 illustrates the equipment (Fig. 3.32 a) and a detail of the fibre being tested already inserted between the two metallic clamps (Fig. 3.32 b).

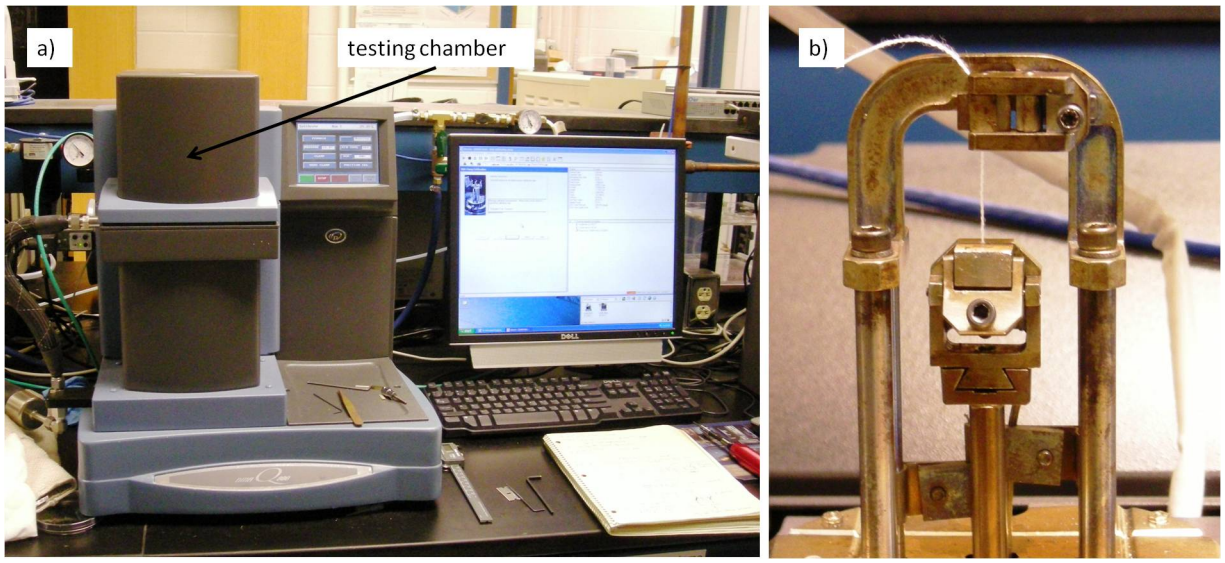

Figure 3.32: Picture of the Dynamical Mechanical Thermal Analyser a) and a detail of a cotton fibre about to be tested b).

A photodiode-based optical system was used in order measure the sample elongation.

During testing, temperature was kept constant at 25 °C; all tests were performed in nitrogen atmosphere.

Bibliography

[1] M. Maccioni, E. Orgiu, P. Cosseddu, S. Locci, A. Bonfiglio, *Appl. Phys. Lett.*, **2006**, 89, 143515:1-3.

[2] D. R. Lide, *Handbook of Chemistry and Physics*, CRC Press, **2000**. ISBN: 9780849304811.

[3] F. Endres, D. MacFarlane, A. Abbott, *Electrodeposition from ionic liquids*, Wiley-VHC, **2008**. ISBN: 3527315659.

[4] A. D. McNaught, A. WilkinsonIUPAC, *Compendium of Chemical Terminology, 2nd ed. (the "Gold Book")*, Blackwell Scientific Publications, **1997**. ISBN 0967855098.

[5] G. Karp, *Cell and Molecular Biology: Concepts and Experiments*, John Wiley & Sons, **2009**. ISBN: 0470483377.

[6] B. H. A. Rehm, *Microbial production of biopolymers and polymer precursors: applications and perspectives*, Horizon Scientific Press, **2009**. ISBN: 1904455360.

[7] K. Kamide, *Cellulose and cellulose derivatives: molecular characterization and its applications*, Elsevier, **2005**. ISBN: 0444822542.

[8] C. T. Brett, *Int. Rev. Cytol.*, **2000**, 199, 161-199.

[9] S. Park, J. O. Baker, M. E. Himmel, P. A. Parilla, D. K. Johnson, *Biotech. for Biofuels*, **2010**, 3(*1*), 10.

[10] M. Lewin, *Handbook of fibre chemistry*, CRC/Taylor & Francis, **2007**. ISBN: 0824725654.

[11] J. M. Hodgkinson, *Mechanical testing of advanced fibre composites*, Woodhead Publishing, **2000**. ISBN: 1855733129.

[12] K. P. Mieck, T. Reussmann, A. Nechwatal, *Mat.-wiss. u. Werkstofftech.*, **2003**, 34, 285–289.

[13] J. W. S. Hearle, W. E. Morton, *Physical properties of textile fibres*, Woodhead Publishing in association with the Textile Institute, **2008**. ISBN: 1845692209.

[14] C. A. Harper, E. M. Petrie, *Plastics materials and processes: a concise encyclopaedia*, John Wiley & Sons, **2003**. ISBN: 0471456039.

[15] C. Kärnfelt, C. Tegnander, J. Rudnicki, J. P. Starski, A. Emrich, *IEEE T. Microw. Theory*, **2006**, 54(*8*), 3417-3425.

[16] J. J. Licari, *Coating materials for electronic applications: polymers, processes, reliability, testing*, William Andrew, **2003**. ISBN: 0815514921.

[17] H. Yanagisawa, T. Tamaki, M. Nakamura, K. Kudo, *Thin Solid Films*, **2004**, 464, 398-402.

[18] O. L. Griffith, J. E. Anthony, A. G. Jones, D. L. Lichtenberger, *J. Am. Chem. Soc.*, **2010**, 132, 580–586.

[19] J. Lee, D. Hwang, C. Park, S. Kim, S. Im, *Thin Solid Films*, **2004**, 12, 421-452.

[20] R. S. Ruoff, D. S. Tse, R. Malhotra, D. C. Lorents, *J. Phys. Chem.*, **1993**, 97, 3379-3383.

[21] A. M. López, A. M. Alonso, M. Prato, *J. Mater. Chem.*, **2011**, 21, 1305-1318.

[22] P. Kovacik, G. Sforazzini, A. G. Cook, S. M. Willis, P. S. Grant, H. E. Assender, A. A. R. Watt, *ACS Appl. Mater. & Inter.*, **2011**, 3(*1*), 11–15.

[23] H. Zhang, C. Wu, L. Liang, Y. Chen, Y. He, Y. Zhu, N. Ke, J. B. Xu, S. P. Wong,A. Wei, S. Peng, *J. Phys. Condens. Matter*, **2001**, 13, 2883–2889.

[24] T. Ono, K. Hirose, *Phys. Rev. Lett.*, **2007**, 98(*2*), 026804.

[25] T. Nishikawa, S. Kobayashi, T. Nakanowatari, T. Mitani, T. Shimoda, Y. Kubozono, G. Yamamoto, H. Ishii, M. Niwano, Y. Iwasa, *J. Appl. Phys.*, **2005**, 97, 104509.

[26] Bayer AG, *Eur. Patent* 339 340

[27] F. Jonas, L. Schrader, *Synth. Met.*, **1991**, 821, 41-43.

[28] M. Dietrich, J. Heinze, G. Heywang, F. Jonas, *J. Electroanal. Chem.*, **1994**, 87, 369.

[29] M. Fabretto, K. Zuber, C. Hall, P. Murphy, *Macromol. Rapid Commun.*, **2008**, 29, 1403–1409.

[30] K. E. Aasmundtveit, E. J. Samuelsen, O. Inganäs, L. A. A. Pettersson, T. Johansson, S. Ferrer, *Synth. Met.*, **2000**, 113, 93.

[31] Y. Wang, *J. Phys. Conf. Ser.*, **2009**, 152.

[32] L. Groenendaal, F. Jonas, D. Freitag, H. Pielartzik, J. R. Reynolds, *Adv. Mater.*, **2000**, 12(*7*), 481-494.

[33] H. J. Lee, J. Lee, S. Park, *J. Phys. Chem. B*, **2010**, 114, 2660–2666.

[34] Y. Xia, J. Ouyang, *ACS Appl. Mater. & Inter.*, **20010**, 2(*2*), 474-483.

[35] L.A.A. Pettersson, S. Ghosh, O. Inganäs, *Org. Electron.*, **2002**, 3, 143.

[36] J. Y. Kim, J. H. Jung, D. E. Lee, J. Joo, *Synth. Met.*, **2002**, 126, 311.

[37] J. Ouyang, Q. Xua, C. Chua, Y. Yang, G. Li, J. Shinar, *Polymer*, **2004**, 45, 8443–8450.

[38] D. A. Bernards, G. G. Malliaras, textitOrganic semiconductors in sensor applications, Springer, **2008**. ISBN: 3540763139.

[39] R.J. Aitken, K.S. Creely, C.L. Tran, *Nanoparticles: An occupational hygiene review*, Document prepared by the Institute of Occupational Medicine for the Health and Safety Executive, Edinburgh, **2004**.

[40] J. Turkevich, *J. Am. Chem. Soc.*, **1963**, 85, 3317.

[41] J. Kimling, M. Maier, B. Okenve, V. Kotaidis, H. Ballot, A. Plech, *J. Phys. Chem. B*, **2006**, 110, 15700-15707.

[42] L. A. Dykman, V. A. Bogatyrev, *Russ. Chem. Rev.*, **2007**, 76(*2*), 181-194.

[43] G. L. Weissler, R. Warner Carlson, *Vacuum physics and technology*, Academic Press, **1979**. ISBN: 0124759149.

[44] M. Fanetti, L. Gavioli, M. Sancrotti, M. G. Betti, *Appl. Surf. Sci.*, **2006**, 252(*15*), 5568-5571.

[45] H. Rausch, T. Braun, *Chem. Phys. Lett.*, **2001**, 350, 15-18.

[46] J. B. Fortin, T. Lu, *Chemical vapour deposition polymerisation: the growth and properties of parylene thin films*, Springer, **2003**. ISBN: 1402076886.

[47] R. W. Kelsall, I. W. Hamley, M. Geoghegan, *Nanoscale science and technology*, John Wiley & Sons, **2005**. ISBN: 0470850868.

[48] W. S. Wong, A. Salleo, *Electronic materials: science & technology*, Springer, **2009**. ISBN: 0387743626.

[49] P. Cosseddu, G. Mattana1, E. Orgiu, A. Bonfiglio, *Appl. Phys. A - Mater.*, **2009**, 95(*1*), 49-54.

[50] H. Dong, J. P. Hinestroza, *ACS Appl. Mater. Inter.*, **2009**, 1(*4*), 797-803.

[51] R. L. Meade, R. Diffenderfer, *Foundations of electronics, circuits and devices*, Cengage Learning, **2002**. ISBN: 0766840263.

[52] M. Fogiel, *The Essentials of Physics, Volume II*, Research & Education Assoc., **1987**. ISBN: 0878916199.

[53] A. V. Bakshi, U. A. Bakshi, *Electronic Measurements and Instrumentation*, Technical Publications, **2008**. ISBN: 8189411241.

[54] W. Brütting, *Physics of organic semiconductors*, Wiley-VHC, **2005**. ISBN: 352740550X.

[55] S. L. Herman, *Dalmar's standard book of electricity*, Cengage Learning, **2003**. ISBN: 1401825656.

[56] L. Reimer, H. Kohl, *Transmission electron microscopy: physics of image formation*, Springer, **2008**. ISBN: 0387400931.

[57] E. Fischer, *Materials science for engineering students*, Academic Press, **2009**, ISBN:0123735874.

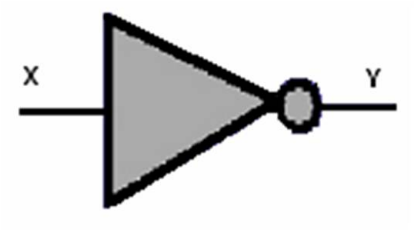

X	Y
1	0
0	1

Figure 4.1: Circuit symbol (left) and truth table (right) of a logic inverter.

4

In this chapter, the main experimental results obtained on the structures described in Chapter 3 will be illustrated.

We will begin with a short introduction about the main concepts concerning logic inverters, with special emphasis on the specific type of inverter realised with OFETs built on Elektrisola yarns, namely the so-called *saturated-load inverter*.

Then, the results obtained on the cotton-based organic devices will be presented.

First of all, the electrical and mechanical behaviour of conductive cotton yarns will be analysed; then it will be shown how these conductive yarns may be employed in order to build all cotton-made transistors.

4.1 Logic inverters realised by means of OFETs on yarns.

Before starting the presentation of these results, it would be better to introduce briefly the concept of logic inverter and its electronic implementation.

A *logic inverter* is an electronic circuit able to change the logic level of a binary input to its opposite level [1].

In terms of bits, if the input is "0" then the output is "1" and, vice versa, if the input is "1" then the output is "0" .

Fig. 4.1 illustrates both the circuit symbol for a logic inverter as well as a truth table summarising its logic function.

It has been shown that several different circuit configurations are possible in order to implement a logic inverter [2].

In our case, we realised a circuit employing only p-channel OFETs made on Elektrisola yarns (see paragraph 3.8) in a configuration known as *saturated-load inverter*, schematically shown in Fig. 4.2.

It can be clearly seen from Fig. 4.2 that the inverter is composed of two (ideally) identical transistors, named *driver* and *load*. More in detail, the driver source is connected to the ground and its drain is short-circuited with the load source. The load drain is short-circuited with its own gate; this special connection is called *diode connection* and its function is to keep the load transistor constantly in saturation mode (see below). The load drain (and its gate, the two being short-cut) is connected to the system bias, called $-V_{DD}$; the minus sign indicates that, the circuit being composed of p-channel transistors, it is necessary to use a negative voltage.

For the sake of simplicity, let us assume that the two transistors are perfectly identical, so that they are characterised by having the same threshold voltage $|V_T|$.

The input signal is applied to the driver gate while the output is read in correspondence with the driver drain - load source short circuit.

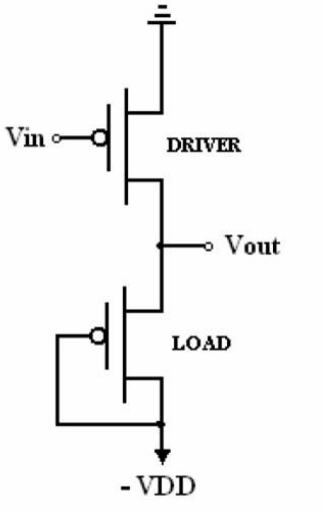

Figure 4.2: Circuit configuration of the saturated-load inverter.

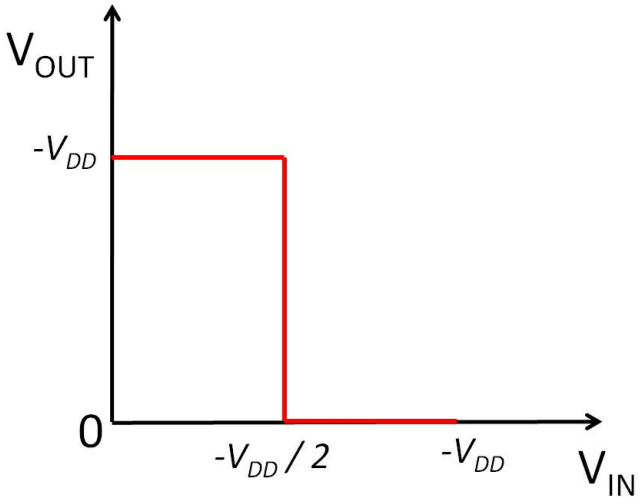

Figure 4.3: Ideal transfer characteristic of a logic inverter.

In order to explain the working principle of the circuit, it should be noted that binary signals are actually represented by particular voltage values. Usually, the logic value "1" is associated to *high* voltages (i.e. values close to -V_{DD}) while the logic value "0" is associated to *low* voltages (i.e. values close to 0); this usage is known as *positive logic*. The input voltage value in correspondence of which the transition from low to high input values occurs is called *logic threshold* and ideally corresponds to -V_{DD}/2.

The curve representing the relationship between V_{IN} and V_{OUT} is generally indicated as *transfer curve*; its ideal representation is provided in Fig. 4.3.

The logic inverters we are really able to implement are, of course, just approximations of the ideal behaviour described above. A real transfer characteristic is illustrated in Fig. 4.4.

If we analyse Fig. 4.4, we can identify some important voltage values [3], listed hereafter:

- V_{OL} = Voltage Output Low = maximum output voltage for a valid "0" ;
- V_{OH} = Voltage Output High = minimum output voltage for a valid "1" ;

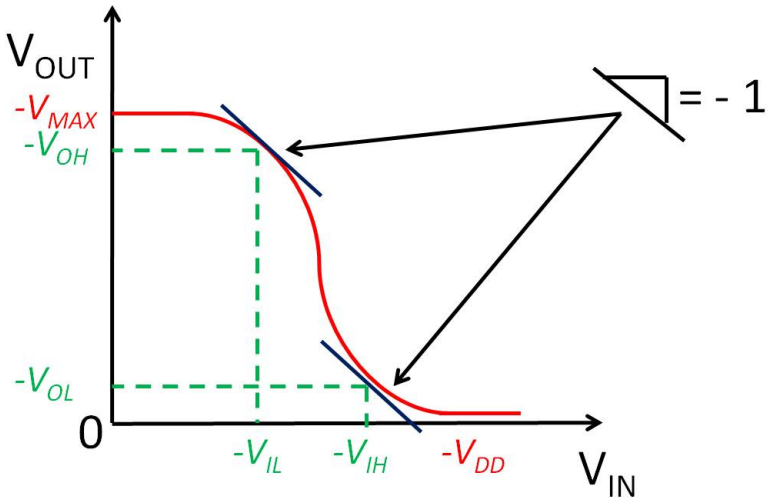

Figure 4.4: Real transfer characteristic of a logic inverter.

- V_{IL} = Voltage Input Low = smaller input voltage where slope equals -1;
- V_{IH} = Voltage Input High = larger input voltage where slope equals -1;
- $V_{MAX} = V_{OUT}$ for $V_{IN} = 0$ V;

Two very important parameters which may be calculated from the transfer curve are the *noise margins*. Mathematically speaking, they are defined as follows:

$$\begin{array}{rl} NM_H \equiv |V_{OH} - V_{IH}| & \text{high noise margin} \\ NM_L \equiv |V_{IL} - V_{OL}| & \text{low noise margin} \end{array} \tag{4.1}$$

the noise margin is the amount by which the signal exceeds the threshold for a proper ”0” or ”1” . Noise margins as high as possible are important in order to guarantee robustness against noise.

Another important parameter is the *indecision region*. It is defined as follows:

$$\Delta V \equiv |V_{IH} - V_{IL}| \tag{4.2}$$

The indecision region is a range of input voltage values for which the system cannot decide if they are to be intended as high or low logic values. A good logic inverter should have, therefore, the smallest possible indecision region.

That being said, the saturated-load circuit working principle may be explained as follows [4].

First of all, as previously mentioned, the diode connection makes the load transistor operate in saturation regime. Indeed (let us consider an n-type MOSFET):

$$\text{G} \equiv \text{D} \implies V_{GS} \equiv V_{DS} \implies \not{N}_{DS} \geq (\not{N}_{GS} - V_T) \implies 0 \geq -V_T \tag{4.3}$$

The condition expressed by equation 4.3 is always satisfied, which implies that the load transistor always operates in saturation mode.

Two different situations may then occur:

- $V_{IN} < V_{IL}$: then the drive transistor is its OFF state and V_{OUT} is approximately - $|V_{DD} - V_T|$;

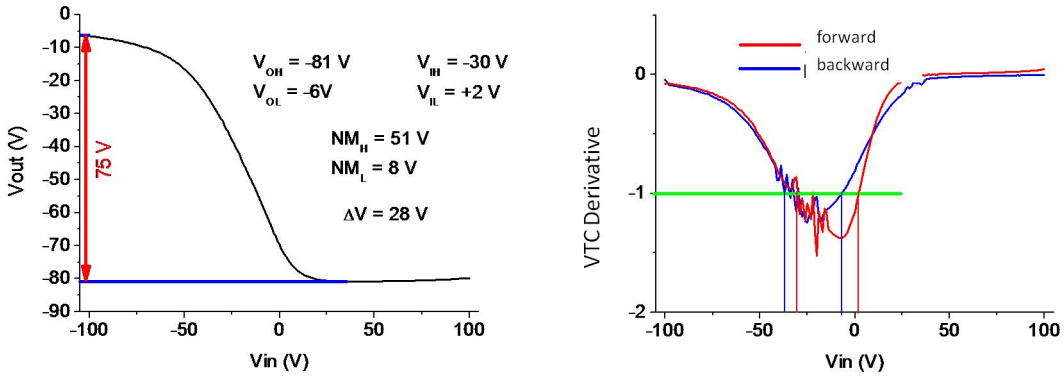

Figure 4.5: Elektrisola yarn-based inverter transfer characteristic.

- $V_{IN} > V_{IH}$: then the drive transistor is its ON state and V_{OUT} is approximately - $|V_T|$.

The driver and load transistors are usually designed so that $V_T \simeq 0$ V, so that the two output logic values "0" and "1" may be as close as possible to 0 V and - V_{DD}, respectively.

The scheme of an Elektrisola yarn-based saturated-load inverter has already been shown in Chapter 3.

Fig. 4.5 shows a typical transfer characteristic (together with its derivative) of such inverters (V_{DD} = -100 V); measurements were performed in air in the dark.

Ten saturated-load inverters were realised and characterised; for each physical parameter, mean values and standard deviations are indicated in the following table:

$V_{T\text{-load}}$ [V]	$V_{T\text{-drive}}$ [V]	NM_H [V]	NM_L [V]	ΔV [V]
-3 ± 3	-5 ± 6	40 ± 9	51 ± 7	26 ± 10

It is not at all easy to compare these results to those reported in the literature. At present, the only example of pentacene-based OFET inverter on fibres is that reported by Lee *et al.* [5] but, unfortunately, the Authors do not provide much data about the performance of their device.

For this reason, we decided to tentatively compare the performances of our inverters with other pentacene-based OFET inverters realised on a planar substrate; it should be clear, however, that the two different structures (the planar and cylindrical) are not strictly comparable because of the following factors:

- the capacitive coupling between semiconductor and gate electrode is much higher in coaxial capacitors than it is in planar structures [6];
- pentacene growth on cylindrical substrate exhibits, at same deposition conditions, a different morphology with respect to pentacene deposited on planar substrates [1];
- the most important electrical parameters of the transistors composing the inverters (such as the threshold voltage) heavily depend on the dielectric and the metals chosen to form the MIS structure as well as the drain and source contacts.

These remarks being made, when we compare the behaviour of our saturated-load inverters to that of other inverters presented in the literature [7] [8] [9] [10] [11], we can notice that our devices actually show better performances in terms of noise margins and symmetry of the transfer characteristic.

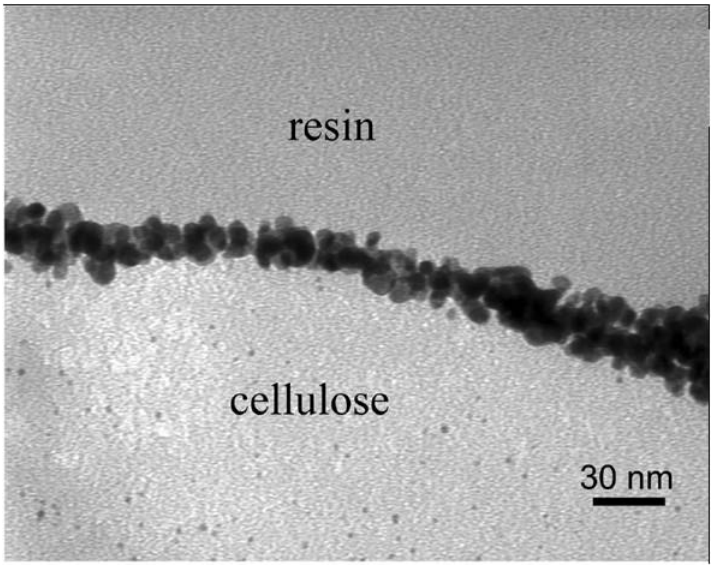

Figure 4.6: TEM image acquired on a cross-section of a yarn treated with Au nanoparticles.

The indecision region, however, appears to be wider than that reported by other Authors; this might be due to the fact that our driver transistors show an I_{ON}/I_{OFF} ration which is lower (up to two orders of magnitude) with respect to the values described for other inverters, which means that the transition between the ON and OFF state requires higher input voltages to be performed. That may result in a widening of the indecision region.

4.2 Cotton-based devices: conductive yarns.

Yarns treated with PEDOT:tosylate.

In this case, four different types of devices were realised and characterised:

- plain cotton yarns;
- cotton yarns covered with Au nanoparticles;
- cotton yarns covered with PEDOT:tosylate;
- cotton yarns treated with Au nanoparticles and subsequently covered with PEDOT:tosylate.

First of all, a transmission electron microscopic analysis was performed on the cross-section of the different yarns typologies in order to evaluate the effects of the various treatments.

Three representative TEM images of the treated yarns are shown in Figs. 4.6, 4.7 and 4.8.

Let us analyse in more detail the results illustrated in Fig. 4.6.

Fig. 4.6 is a Dark-Field TEM image acquired on a cross section of a cationic cotton fibre uniformly coated with Au nanoparticles. It clearly illustrates that nanoparticles adhere to the outer surface of the cotton yarn forming a film whose mean thickness is ~ 30 nm.

Fig. 4.7 is a Bright-Field TEM image acquired on a cross section of a cotton fibre coated with PEDOT:tosylate. The cotton fibre's natural channels are visible on the left of the image while the electronically uniform embedding resin appears on the right. The white layer (and therefore more conductive material) separating the two materials corresponds to the conductive

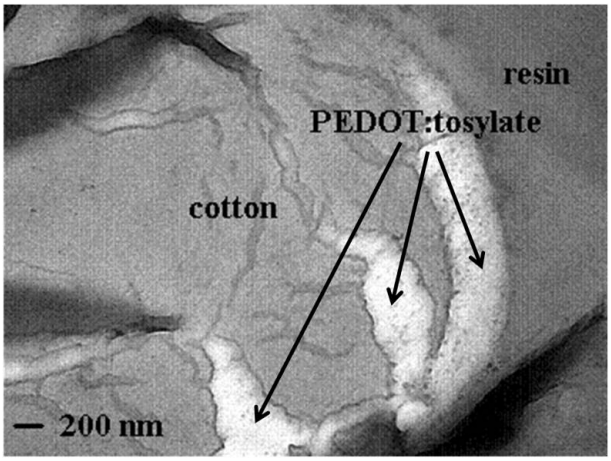

Figure 4.7: TEM image acquired on a cross-section of a yarn treated with PEDOT:tosylate.

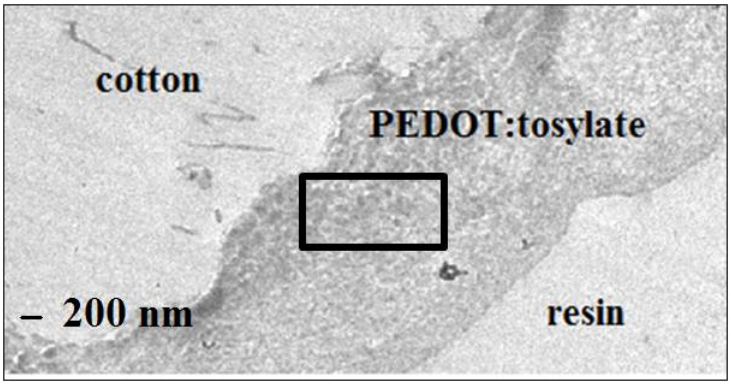

Figure 4.8: TEM image acquired yarns treated with both Au nanoparticles and PEDOT:tosylate; the black rectangle represents the area where the EDS spectrum was acquired.

polymer PEDOT. The thickness of the PEDOT layer is not uniform possibly because the cotton microfibres composing the yarn are, by themselves, irregularly shaped.

Fig. 4.8 is a Dark-Field TEM image acquired on a cross section of a fibre treated with Au nanoparticles and subsequently covered with a layer of PEDOT:tosylate. The cotton fibre is visible on the left side of the image while the electronically uniform embedding resin appears on the right. The two materials are separated by a grey, conductive layer, which appears darker (and therefore more conductive) in close proximity to the cotton fibre. In this image, a rectangle in the conductive layer can be clearly noticed. That indicates the area in which an Energy-Dispersive X-ray Spectroscopic (EDS) analysis was performed. The spectrum obtained is shown in Fig. 4.7.

The spectrum peaks illustrated in Fig. 4.9 demonstrate that the conductive layer surrounding the yarn's outer surface is rich in gold (indicative of the presence of Au nanoparticles) and sulphur (indicative of PEDOT:tosylate). This analysis confirms that the conductive layer is actually composed of Au nanoparticles and PEDOT:tosylate. The large copper peak is related to the copper microgrid on which the sample was placed.

It is worth noting that, as shown in Fig. 4.7, PEDOT:tosylate is not confined to the yarn's external surface but penetrates among the yarn's inner fibres in a very irregular way. For this reason, it was not possible to obtain a precise measurement of the samples' cross–sectional conductive area and the electrical performance of the different fibres has been therefore compared

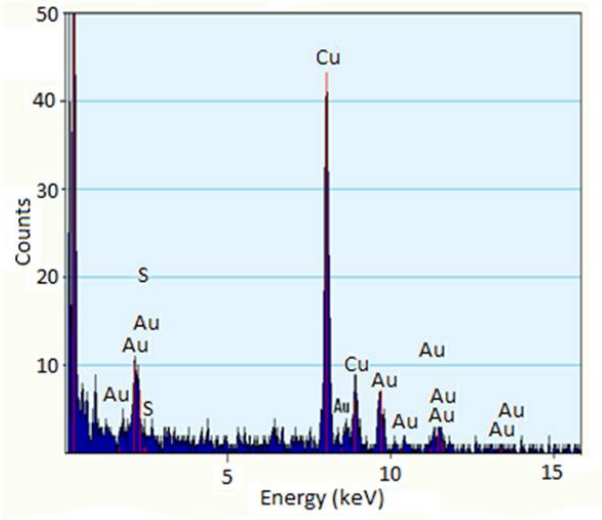

Figure 4.9: Spectroscopic analysis performed on a cotton yarn treated with Au nanoparticles and subsequently coated with PEDOT: tosylate.

in terms of resistance per unit length.

Electrical characterisation.

As stated in paragraph 3.15, all samples were electrically characterized with a four-point probe method in order to eliminate possible contributions of contact resistances.

For each sample typology, ten samples (1 cm long) were measured; the mean values of the electrical resistance of all samples types are reported in the following table and summarised in Fig. 4.10. The most conductive samples are those treated with both Au nanoparticles and PEDOT:tosylate.

Sample Typology	Resistance/length [Ω/cm]
Plain Cotton	$3.08 \pm 0.09 \cdot 10^8$
Cotton + Au nanoparticles	$1.12 \pm 0.01 \cdot 10^8$
Cotton + PEDOT:tosylate	$186.83 \pm 0.02 \cdot 10^3$
Cotton + Au nanoparticles + PEDOT:tosylate	$24.73 \pm 0.03 \cdot 10^3$

On the yarns treated with PEDOT:tosylate (with and without Au nanoparticles), washing tests were also performed; these tests are particularly important for devices with potential applications in the textile field, considering that fabrics and clothes usually require to be immersed in water for their cleaning.

Washing tests were realised soaking treated yarns in deionised water at room temperature for 30 min. Yarns were then removed and placed on a hotplate at 100 °C to allow solvent evaporation. The yarns (10 samples, 2 cm long) were electrically characterised using a four probe method, resistance per unit length values were acquired before and after the washing tests.

The results are summarised in the following table:

Sample Typology	Resistance/length [Ω/cm]
Cotton PEDOT:tosylate (before washing)	$186.83 \pm 0.02 \cdot 10^3$
Cotton PEDOT:tosylate (after washing)	$3.08 \pm 0.06 \cdot 10^8$
Cotton + Au nanoparticles + PEDOT:tosylate (before washing)	$24.73 \pm 0.03 \cdot 10^3$
Cotton + Au nanoparticles + PEDOT:tosylate (after washing)	$2.87 \pm 0.04 \cdot 10^8$

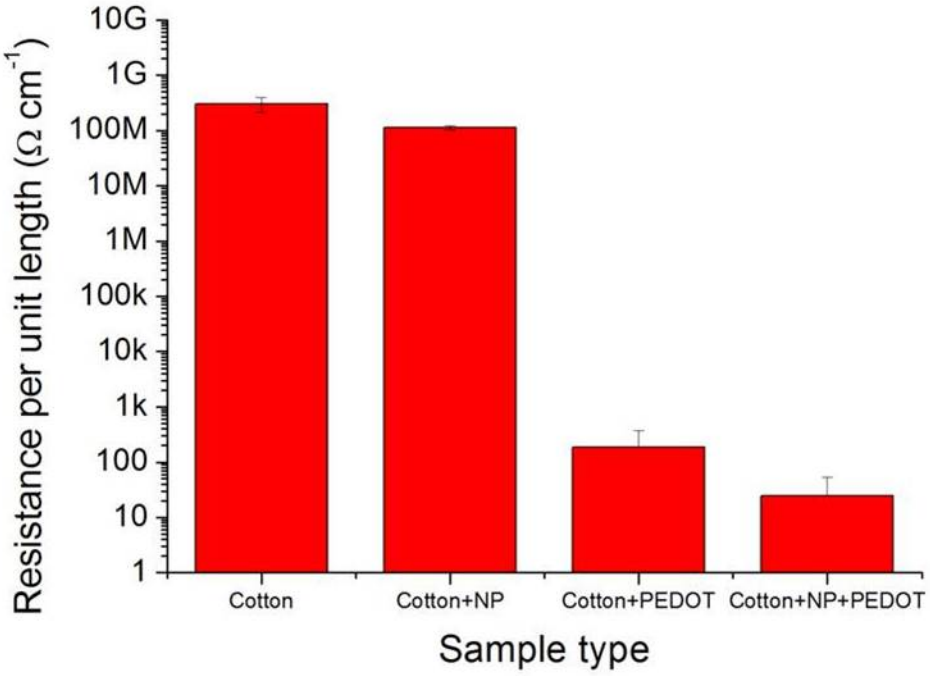

Figure 4.10: Resistance per unit length vs treatment (Au nanoparticles, PEDOT:tosylate and both).

These results clearly show that, unfortunately, in both cases, the yarns treated with PEDOT:tosylate are not water-resistant. This result was not completely unexpected. Even though, to our knowledge, the solubility of PEDOT:tosylate in water has not been investigated in detail yet, contact angle measurements of water droplets on PEDOT:tosylate films suggest that this organic compound is moderately hydrophilic (contact angle ~ 58 °) [12] so that dissolution of the polymer into water is not at all unlikely.

Mechanical characterisation.

The treated yarns were also mechanically characterised by measuring static stress vs. strain curves, three main parameters were calculated, namely Young's modulus (E), stress at break (σ), elongation at break ($\epsilon_{\%}$).

For each yarn typology, ten samples (4 cm long) were tested. The following table shows mean values and standard deviations.

Sample Typology	E [MPa]	σ [MPa]	$\epsilon_{\%}$ [%]
Plain Cotton	342 ± 75	10.3 ± 3.3	4.4 ± 1.8
Cotton + Au NPs	140 ± 60	8.2 ± 1.9	11.0 ± 5.3
Cotton + PEDOT:tos	331 ± 82	3.0 ± 1.3	2.5 ± 1.0
Cotton + Au NPs + PEDOT:tos	142 ± 18	4.3 ± 1.0	4.4 ± 0.9

For the sake of clarity, the results presented in the previous table are also represented in Fig. 4.11, 4.12 and 4.13. Young's modulus was calculated as the slope of stress-strain curve in the linear regime, the stress to break is the stress corresponding to the sample's physical rupture

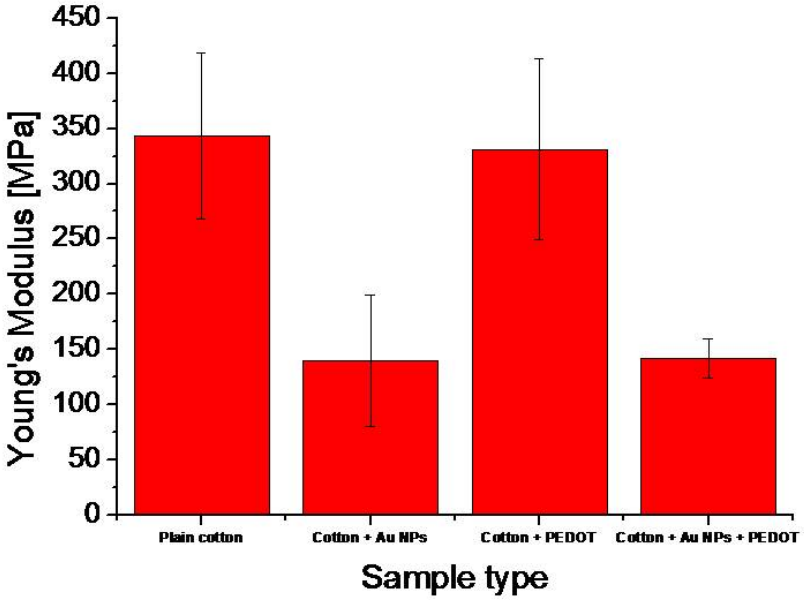

Figure 4.11: Young's modulus vs treatment on conductive cotton fibres.

and the elongation to break is the percentage elongation corresponding to the sample's breaking (with respect to the original length, that is 4 cm).

It can be noticed from the data reported in the table that the deposition of PEDOT:tosylate alone does not affect Young's modulus very much, while the mean value of this parameter is reduced of approximately 60% when gold nanoparticles are deposited on the yarns.

As for the stress at break, it is possible to see that the treatment with both gold nanoparticles and PEDOT:tosylate decreases the value of this parameter of the 58% with respect to the value measured for plain cotton yarns. The stress at break of yarns treated with only gold nanoparticles or only PEDOT:tosylate is also lower than the value measured for plain cotton yarns of, respectively, the 20 and 61%.

As for the variations of elongation to break caused by the different treatments, the yarns which received both the treatments with gold nanoparticles and PEDOT:tosylate have almost the same mean value of elongation to break of plain cotton yarns (4.42% and 4.36% respectively). Interestingly enough, when only gold nanoparticles are deposited on cotton yarns the elongation to break increases up to 11.01% while it is reduced to 2.47% when only PEDOT:tosylate is deposited on cotton yarns.

Fig. 4.14 depicts a typical stress–strain curve of a Au nanoparticles + PEDOT:tosylate yarn compared to a curve acquired on a plain cotton yarn.

Considering the results shown in Fig. 4.14, two main observations can be made: first the maximum elongation before breaking appears to be similar for both samples, thus indicating that the main mechanical property of interest for evaluating the ability of the yarn to be woven or knit are preserved in treated yarns.

Secondly, the treated yarn can reach larger strain values before starting to experience elongational stress. This unusual effect, that was observed only in nanoparticles-treated samples (with and without PEDOT:tosylate) may be tentatively attributed to a "lubricant " effect due to the conformal nature of the nanoparticles coating which seems to enable them to slide on one another following the application of the mechanical stimulus (see Fig. 4.15 where a schematic

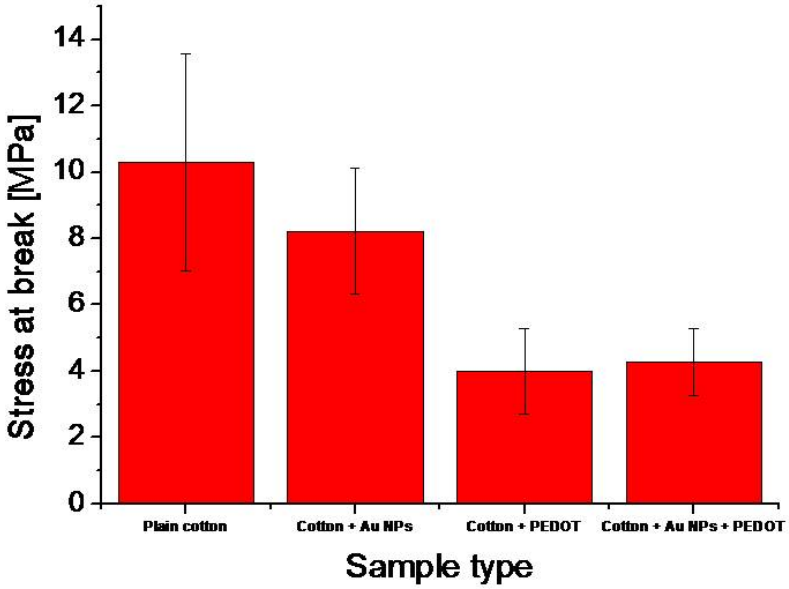

Figure 4.12: Stress at break vs treatment on conductive cotton fibres.

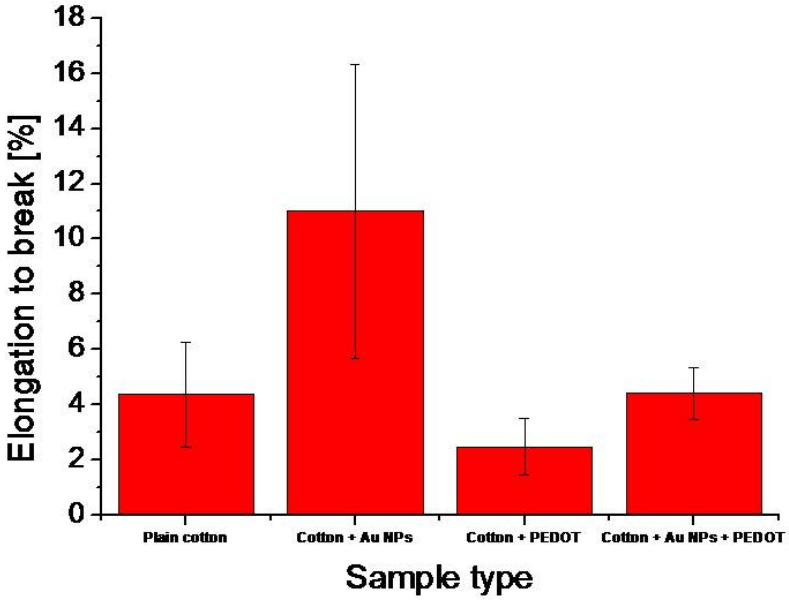

Figure 4.13: Elongation at break vs treatment on conductive cotton fibres.

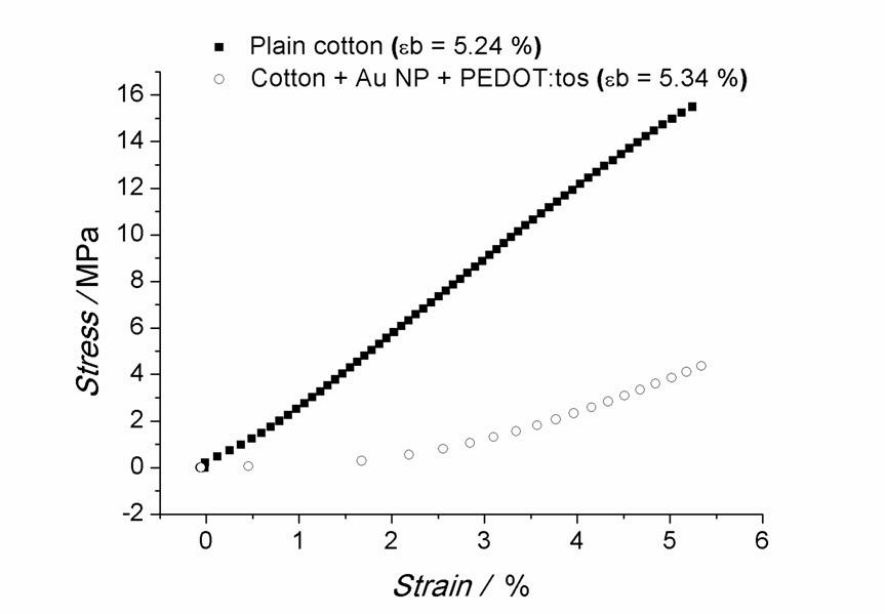

Figure 4.14: Stress-strain curves acquired on a plain cotton yarn (black squares) and a cotton yarn treated with Au nanoparticles and subsequently coated with PEDOT:tosylate (white circles).

representation of this effect is given).

These observations demonstrate anyway that the proposed treatment does not stiffen the cotton yarns.

Yarns treated with PEDOT:PSS.

Resistance per unit length values as a function of samples' typology and washing treatment as measured using the four probe method.

The measured voltage drop referred to 2 cm long samples. For each yarn typology, ten resistance values were acquired; the following graph shows the mean values and the error bars (standard deviation).

The obtained results are summarised in the following table.

	Cotton + PEDOT:PSS	Cotton + PEDOT:PSS + EG
Before washing	1.7 ± 0.4 MΩ/cm	2.2 ± 0.6 kΩ/cm
After washing	951 ± 57 MΩ/cm	2.3 ± 1.1 kΩ/cm

The deposition of ethylene glycole (EG) over previously PEDOT:PSS-treated cotton yarns is responsible for a decrease of resistance of up to three orders of magnitude, with respect to untreated cotton yarns and is not significantly affected by washing in deionised water (at room temperature for 30 min).

The table shows that treatment with EG is not only able to prevent PEDOT:PSS from dissolution in water but also increase conductivity of three additional orders of magnitude.

The results shown in the previous table are graphically represented in Fig. 4.16. Unwashed samples are labelled with *UW*, washed samples with *W*.

Comparing the performance of our yarns with other results regarding conductive cotton fibres recently published [13] [14] [15], the following considerations may be made:

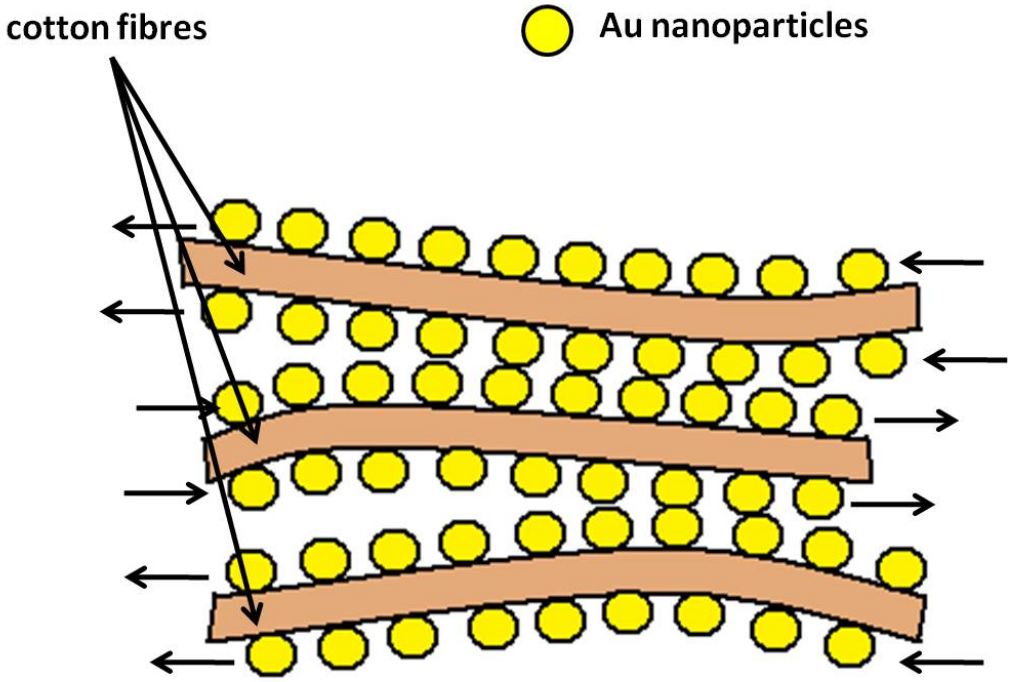

Figure 4.15: Schematic model of the microfibres composing the cotton yarns treated with Au nanoparticles (yellow circles). Nanoparticles may allow the microfibres to slide on one another, which results in an increment of the elongation at break.

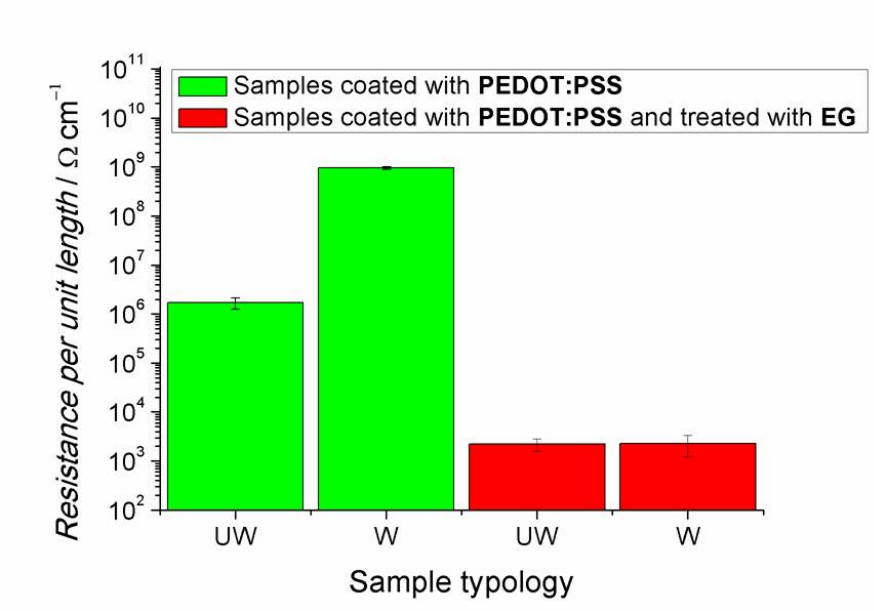

Figure 4.16: Resistance per unit length vs washing of samples treated with PEDOT:PSS.

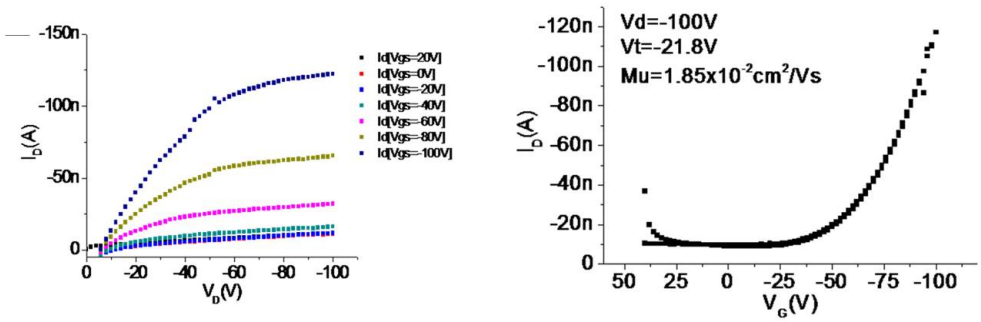

Figure 4.17: Typical I_{DS}-V_{DS} (left) and I_{DS}-V_{GS} (right).

- other methods resulted in lower resistance values (up to 0.5 Ω/cm), this is due to the fact that higher conductivity materials, such as metals [13], carbon nanotubes (CNTs) [14] or poly(allyl amine) [15], have been employed;

- it should be noticed that the treatments proposed by other Authors determine a degradation of the mechanical properties (especially on the elongation at break) of the treated yarns [13] [15], or make the yarn harder and difficult to bend [14] while, as stated previously, our yarns treated with PEDOT:tosylate and Au NPs are not, from a mechanical point of view, negatively affected by the treatment.

We can conclude, therefore, that thanks to the method we have proposed it is possible to obtain conductive cotton yarns representing a good compromise between satisfactory conductivity and sufficiently good mechanical properties.

4.3 Cotton-based devices: OFETs.

First of all, samples were characterised by means of capacitive measurements in order to determine the proper capacitance value to be used to extract the physical parameters of transistors.

Ten cylindrical capacitors, realised on a cotton yarn treated with PEDOT:PSS and EG covered with parylene C (3.3 g of dimers were used), were realised and measured.

The resulting mean capacitance per unit length is 0.34 ± 0.03 nF/cm (value acquired for a frequency of 60 Hz).

If we assume that both the channel length and width are ∼ 500 μm (so that W/L ≃ 1), then the capacitance per unit area is ∼ 2.17 F/cm^2.

Fig. 4.17 shows typical I_{DS}-V_{DS} and I_{DS}-V_{GS} curves acquired on such transistors.

In this case, twenty different transistors were realised. The mean values of mobility and threshold voltages are reported in the table below.

Threshold voltage [V]	Mobility [cm^2/Vs]
- 24.5 ± 5.4	1.3 ± 1.0 · 10^{-2}

The values we obtained are within the range commonly measured for pentacene-based transistors [16].

Higher mobilities on pentacene-based OFETs on yarns, up to 0.5 cm^2/Vs, were actually reported in 2005 by Lee *et al.* [5]; it should be noticed, however, that:

- the Authors built their transistors on metallic (aluminium or steel) yarns; being much more conductive than our cotton fibres, these metallic gates are better capacitively coupled with the semiconductor thus increasing the MIS capacitance, which has been demonstrated to result in higher field effect mobilities [17] [18];
- such high mobilities are obtained on yarn-shaped OFETs whose dielectric layer is made of cross-linked poly-4-vinylphenol (PVP). PVP has a higher dielectric constant (4.3 at 1 kHz) [19] than parylene-C (3.1 at 1 KHz) which, once again, increases the MIS capacitance.

Our non-optimal I_{ON}-I_{OFF} ratio ($\sim 10^2$ - 10^3 vs the more common 10^4) may be due to the fact that, despite the dielectric covering, the external surface of our yarns is characterised by the presence of many conductive "micro hairs" which are responsible for the creation of a parasitic conductive path between source and drain.

From the observation made above, we can therefore conclude that the performance of our devices could be probably greatly improved by reducing the hairiness of the external surface of our yarns and using gate insulators with higher dielectric constants.

4.4 Cotton-based devices: OECTs.

In order to test the feasibility of realising an electrochemical transistor on cotton yarn, our first trials consisted of a very simple structure made of a single cotton yarn soaked in PEDOT:PSS for 48 h at 6 °C and then baked on a hotplate at 145 °C for 1 h.

The PEDOT:PSS deposited on these yarns acted as active layer; the three electrodes (source, drain and gate), in this first phase on my reseearch, were represented by three metal contacts. The electrolyte used was an aqueous solution (500 mM) of potassium chloride KCl.

The yarns were, first of all, inserted into a small PDMS parallelepiped in which the electrolytic solution was subsequently inserted. Each yarn was then fixed on a clean glass substrate and the source and drain contacts were placed directly onto it at a distance of 1 cm. A small drop of electrolytic solution ($\sim$ 1 mm^3) was put into the PDMS parallelepiped and the gate electrode was then inserted into the solution.

More than twenty samples were realised and measured but just one of them actually showed a transistor behaviour. Fig. 4.18 a) shows a picture of this device, while its I_{DS}-V_{DS} characteristics are shown in Fig. 4.18 b).

Even though this device showed a transistor behaviour, a very high failure rate (i.e. number of non-working devices) was observed. That can be attributed to two facts:

1. cotton yarns are actually very hydrophilic and tend to absorb water quickly; once the yarn is drenched with electrolyte solution and a source-drain voltage is applied, current is determined prevalently by ionic conduction through the yarn (rather than hole conduction through the PEDOT:PSS layer);
2. PEDOT:PSS, without any further treatment, is water soluble so that it is very likely that when the yarn is put in touch with the electrolytic solution, the semiconductive layer dissolves and no transistor effect can therefore be observed.

Our strategy to face these problems was twofold:

- on one hand, we treated the PEDOT:PSS coated cotton yarns with ethylene glycol (see Chapter 3 for more details) in order to make the semiconductor insoluble in water;
- on the other hand, we decided to use solid electrolyte instead of aqueous solution in order to reduce the quantity of water in touch with the semiconductive layer.

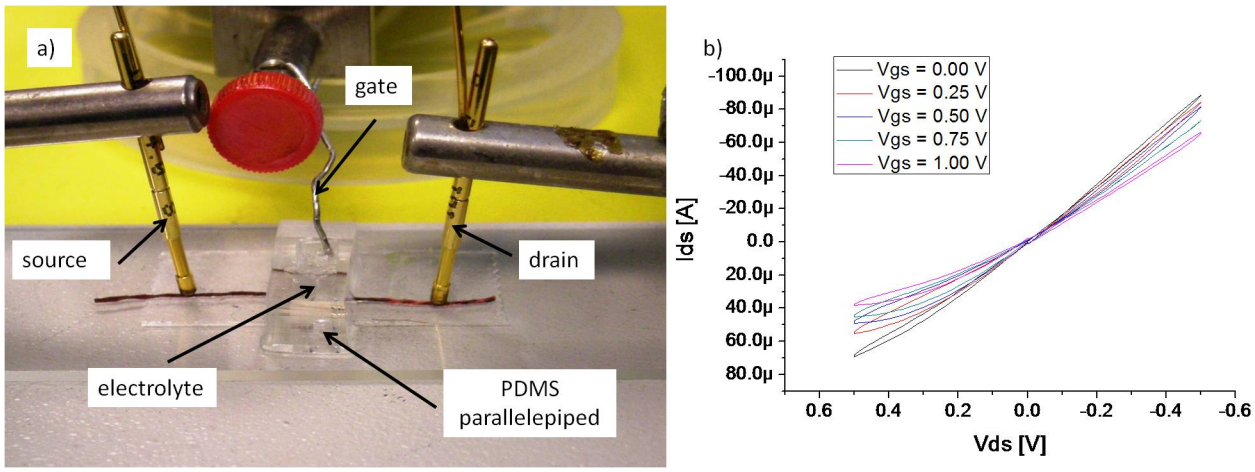

Figure 4.18: OECT on a cotton yarn a) the same transistor's output characteristics b).

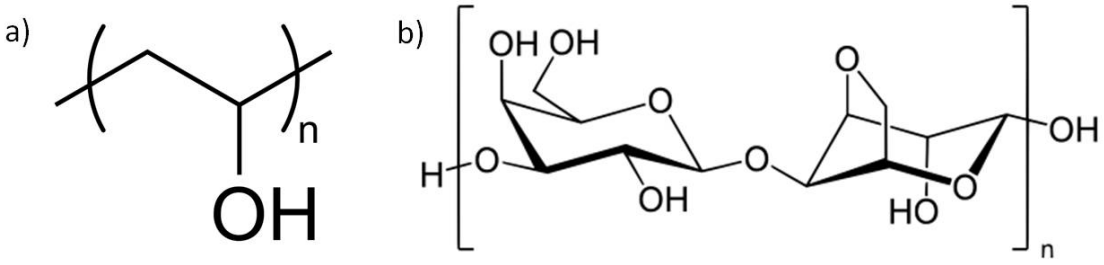

Figure 4.19: Chemical structure of the gelling agents used in the production of electrolytic gels: polyvinyl alcohol (PVA) a) and agarose b).

Regarding this last point, two different electrolytic gels were tested:

1. polyvinyl alcohol (PVA, see Fig. 4.19 a) saline gel [20] (9% wt, using the same 500 mM KCl electrolytic aqueous solution);

2. agarose (see Fig. 4,19 b) based saline gel [21] (3.75 % wt, using the same 500 mM KCl electrolytic aqueous solution).

Both gels were used for the OECTs realisation. We have to say that, despite the high concentration of PVA, the polyvinyl alcohol gel was still very liquid, so that when it was put in touch with yarns they got drenched: no transistor effect could be measured using PVA-based electrolytic gel.

On the other hand, the addition of agarose as gelling agent to the electrolytic solution produced quite a solid gel.

The different behaviour of the two electrolytic gels can be easily seen in Fig. 4.20. Fig. 4.20 a shows a drop of the PVA-based gel on a glass slide: it can be noticed that the "gel " almost behaves as a liquid. Fig. 4.20 b shows, on the other hand, that agarose-based electrolytic gel was solid enough that it could be cut in small parallelepipeds which could be easily held with a pair of tweezers.

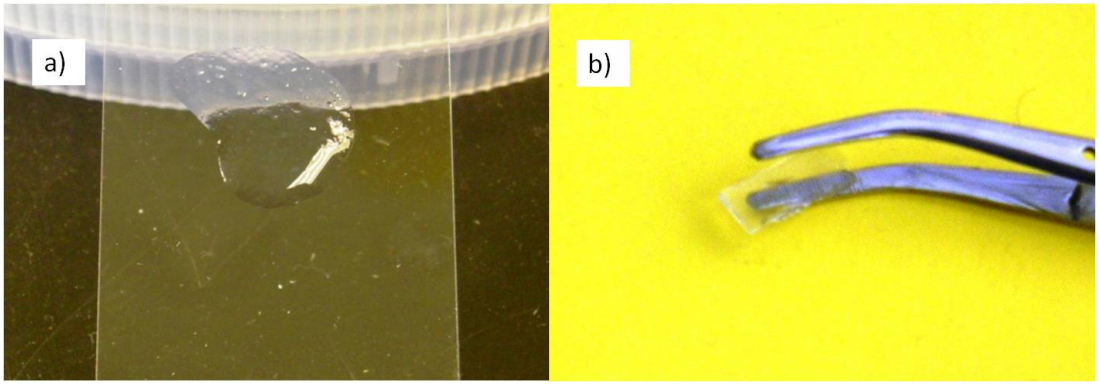

Figure 4.20: A drop of the PVA-based electrolytic gel a) and a small parallelepiped of agarose-based gel held by tweezers b).

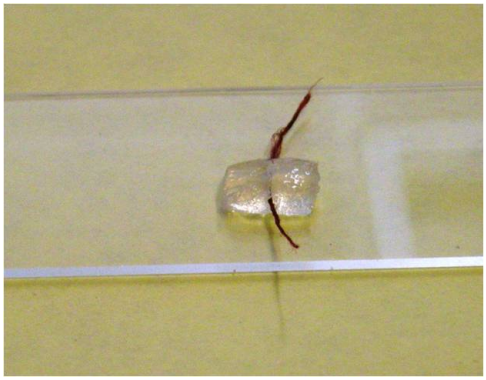

Figure 4.21: PEDOT:PSS/EG treated yarn inserted into an agarose-based electrolyte block, ready for measurement.

The yarn treatment with ethylene glycol, together with the agarose-based electrolytic gel, enabled us to measure a transistor effect on more than ten samples; in such transistors, each yarn was placed in the middle of the electrolyte block with the help of a needle.

Fig. 4.21 shows a PEDOT:PSS/EG treated yarn inserted into an agarose-based electrolyte block, ready for measurement.

In order to obtain an all cotton-made OECT transistor, we eventually replaced the metallic electrodes with conductive cotton yarns (see Chapter 3 for a complete description of the assembly of such devices). A picture of one of these devices in shown in Fig. 4.22.

Fig. 4.23 shows atypical I_{DS}-V_{DS} characteristics (left) and a I_{DS}-*time* curve for our all cotton-made electrochemical transistors.

It can be clearly noticed that, despite the non-optimal I_{ON}-I_{OFF} ratio, the transistor effect is clearly achieved.

At present, just another research group has published results concerning OECTs on a natural fibre (namely, a silk fibre) [22]. When compared to these silk-based transistors, first of all our devices appear to be characterised by higher currents, as shown in the following table:

	V_{DS}	V_{GS}	I_{DS}
Silk OECT	-1 V	0 V	$\sim$ - 7.25 μA
Cotton OECT	-0.5 V	0 V	$\sim$ **- 14 μA**

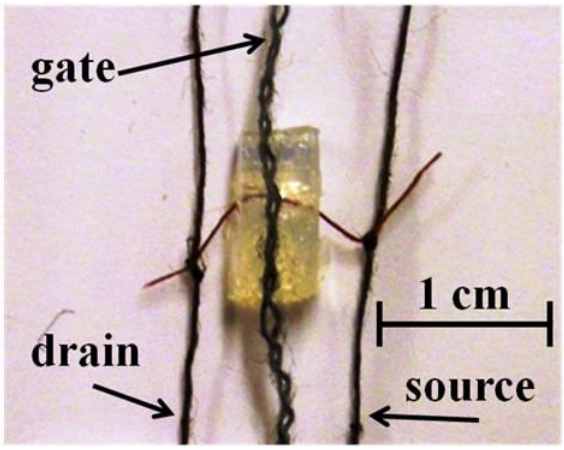

Figure 4.22: All cotton-made OECT, ready for measurement.

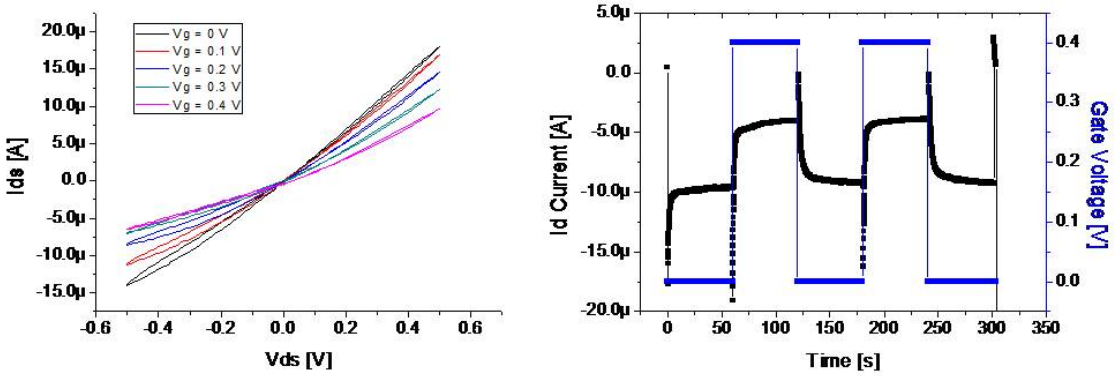

Figure 4.23: Typical I_{DS}-V_{DS} (left) and I_{DS}-*time* (right) characteristics of an all cotton-made OECT.

Moreover, the switching speed of our cotton OECT ($\sim$ 50 s) is slightly higher than that reported by Müller *et al.* ($\sim$ 60 s).

Bibliography

[1] A. P. Godse, D. A. Godse, *Digital Logic Circuits*, Technical Publications, **2009**. ISBN: 8184317603.

[2] A. K. Maini, *Digital electronics: principles, devices and applications*, John Wiley & Sons, **2007**. ISBN: 0470032146.

[3] A. S. Sedra, K. Carless Smith, *Microelectronic circuits*, Oxford University Press, **2004**. ISBN: 0195142519.

[4] R. C. Jaeger, T. Blalock, *Microelectronic Circuit Design*, McGraw-Hill Companies,Inc., **2010**. ISBN: 0073380458.

[5] J. B. Lee, V. Subramanian, *IEEE T. Electron Dev.*, **2005**, 52(*2*), 269-275.

[6] J. Guo, S. Goasguen, M. Lundstrom, S. Datta, *Appl. Phys. Lett.*, **2002**, 81(*8*), 1486-1488.

[7] J. B. Koo, C. H. Ku, J. W. Lim, S. H. Kim, *Org. Electron.*, **2007**, 8, 552-558.

[8] J. Jeon, B. Murmann, Z. Bao, *IEEE Electr. Device L.*, **2010**, 31(*12*), 1488-1490.

[9] S. H. Kim, J. Jang, H. Jeon, W. M. Yun, S. Nam, C. E. Park, *Appl. Phys. Lett.*, **2008**, 92(*18*), 183306.

[10] Y. Watanabe, H. Iechi, K. Kudo, *IEICE Trans. Electron.*, **2006**, E89-C(*12*), 1777-1778.

[11] H. Klauk, M. Halik, U. Zschieschang, F. Eder, G. Schmid, C. Dehm, *Appl. Phys. Lett.*, **2003**, 82(*23*), 4175.

[12] R. Shinar, J. Shinar, *Organic electronics in sensors and biotechnology*, McGraw Hill Professional, **2009**, ISBN: 0071596755.

[13] X. Liu, H. Chang, Y. Li, W. T. S. Huck, Z. Zheng, *ACS Appl. Mater. Interf.*, **2009**, 2(*2*), 529-535.

[14] B. S. Shim, W. Chen, C. Doty, C. Xu, N. A. Kotov, *ACS Nano Lett.*, **2008**, 8(*12*), 4151-4157.

[15] I. Wistrand, R. Lingström, L. Wågberg, *Eur. Poly. J.*, **2007**, 43, 4075-4091.

[16] W. Brütting, *Physics of organic semiconductors*, Wiley-VHC, **2005**. ISBN: 352740550X.

[17] L. A. Majewski, R. Schroeder, M. Grell, *Synthetic Met.*, **2004**, 144, 97-100.

[18] W. Xu, S. Rhee, *Org. Electron.*, **2009**, 11(*6*), 996-1004.

[19] F. Chen, C. Chuang, Y. Lin, L. Kung, T. Chen, H. D. Shieh, *Org. Electron.*, **2006**, 7(*5*), 435-439.

[20] Y. Pan, D. Xiong, R. Ma, *J. Cent. South. Univ. T.*, **2006**, 13(*1*), 27-31.

[21] B. G. Johansson, *Scand. J. Clin. Lab. Inv.*, **1972**, 29(*124*), 7-19.

[22] C. Müller, M. Hamedi, R. Karlsson, R. Jansson, R. Marcilla, M. Hedhammar, O. Inganäs, *Adv. Mater.*, **2011**, XX, 1-4.

Conclusions.

First of all, let us summarise briefly the main results achieved with the experimental activity performed during my doctorate:

- starting from a previously designed structure (an OFET on a metal yarn) I demonstrated that it is possible to combine these devices in order to obtain more complex electronic circuits, which show a better performances than other analogous circuits already described in the scientific literature;
- I showed two new procedures to obtain conductive yarns starting from ordinary cotton fibres;
- starting from the conductive cotton yarns, I showed that it is possible to obtain active devices such as two different types of transistors.

My personal opinion is that the results obtained and presented in this Thesis clearly show that organic materials may be successfully used in order to realise electronic devices with many prospective applications in the textile field.

As shown with the realisation of logic inverters, it is possible to assemble simple electronic circuits using yarn-shaped OFETs, thus demonstrating the practical feasibility and implementation of essential logic functions.

Another important goal was achieved with the organic electronic devices built on a cellulosic substrate. Thanks to these results, I have proved that it is actually possible to combine the excellent comfort and wearability properties of cotton with the characteristics of organic materials so that cotton fibres with electrical functionalities, but still maintaining good mechanical qualities, can be realised with relatively simple methods.

Obviously, much work has to be done yet. Some crucial problems have to faced yet, for instance:

- the insertion of the devices I presented into a fabric;
- washability;
- resistance to usage;
- restistance to weather conditions;

just to name the most important ones.

That being said, I strongly believe that the results explained in this thesis may be a good point from which to start in order to develop a complete integration of Organic Electronics into the textile field with very interesting potential applications from both the industrial and scientific point of view.

Acknowledgements.

First and foremost, I would like to thank my parents. They have always been my first supporters, they have always believed in me, even (or should I say especially?) when I was the first one not to rely on myself. Thank you, Dad and Mum, for the love and support, I will always be grateful to you.

I would also like to thank my wonderful sister and my two brothers (together with my brother and sisters-in-law) because they have always encouraged me, helped me whenever I was in time of need and kept my chin up every single time (no exceptions) I was feeling down.

Valentina, Alessandra, Mattia... what can I say about you? I love you so much... whenever I am with you I instantly become happy and forget all my daily troubles.

I am lucky enough to have many good friends in my life, but there's a very special one I would like to mention here. Matteo, you are my third brother, you know me like very few other people do. Thank you for your constant presence and for always giving me the good advice at the right time.

A big "thank you" goes to my scientific advisor, Prof. Annalisa Bonfiglio, for giving me the opportunity to live such a wonderful experience of getting a doctorate and for always being a source of learning and inspiration.

I am also deeply grateful to my (ex or present) colleagues: Emanuele, Laura, Piero, Monia and the two "new entries" Stefano and Alberto. Guys, you can't imagine how much I enjoyed spending these years with you. Nothing I did could have been possible without your help, support and encouragement.

Now, let us address to those who live on the other side of the Atlantic Ocean.

I would like to thank Prof. George Malliaras and Prof. Juan Hinestroza for giving me the chance to work with them during the months I spent at Cornell. Thank you for being so kind, teaching me so much and helping me to feel comfortable when I was so far away from home.

When I was in the US, I met so many extraordinary people... I don't actually know where to start with my thank-you list!

First of all, I would like to thank my colleagues at CU for always being so kind and helpful.

I'd also like to thank Richard (LB) and his mates (Dan, Keith, Rot-knee, Andy, Aaron, Mike, Mark, Robbie...) and Mr K & Monsieur M for being the best possible people I could ever meet. You made my stay in Ithaca a wonderful experience, you can't imagine how much I learnt from each of you.

Last, but not least, I would like to thank all those people who tried to make my life harder and worse. Because of you, I learnt the difference between good and bad people, I am sorry to inform you that I'm still a happy person.